

FUZZY LOGIC CONTROL OF A NATURAL CONVECTION LOOP

A Thesis

Presented to

the Faculty of the Department of Mechanical Engineering

California State University, Los Angeles

In Partial Fulfillment

of the Requirements for the Degree

Master of Science

in

Mechanical Engineering

By

Daniel S. Lopez

August 2022

© 2022

Daniel S. Lopez

ALL RIGHTS RESERVED

The thesis of Daniel S. Lopez is approved.

Dr. Arturo Pacheco-Vega, Thesis Director

Dr. Jim Kuo, Committee Member

Dr. Scott R. Ploen, Committee Member

Dr. Nancy Warter-Perez, Department Chair

California State University, Los Angeles

August 2022

## ABSTRACT

### Fuzzy Logic Control of a Natural Convection Loop

By

Daniel S. Lopez

In this work, three different fuzzy controllers were developed to investigate their ability to stabilize flow and temperature of a single-phase fluid in a natural convection loop. The toroidal convective loop is filled with an incompressible fluid that exchanges energy throughout it. Half of the loop has a known heat input, while the other half has a known heat output. Normally, buoyancy forces – produced by temperature differences within the fluid – drive the fluid flow inside the thermosyphon, generating three possible flow scenarios: stable, oscillatory and chaotic behavior. For the analysis, one-dimensional models are first developed from the momentum and energy equations using the Boussinesq approximation, and by assuming averaged values of velocity and temperature over the cross-section of the torus. The resulting system of differential equations are then converted to a nonlinear dynamical system and solved under various operating conditions. The controllers are built using fuzzy logic, which has the ability to describe complex systems in terms of linguistic variables, following expert-based if-then rules to make inferences about their behavior. Quantification of the linguistic variables is done via triangular and trapezoidal membership functions, and the rules are built from numerical data under different operating conditions from the mathematical model. Since the tilt angle for the loop and the heat flux are used as the parameters characterizing its dynamic behavior, these are the manipulated variables, whereas the control variables are

average fluid velocity and temperatures inside the loop. SIMULINK is used to implement the fuzzy controllers, along with the corresponding control actions, while numerical experiments are conducted to assess their relative performance. Results demonstrate the following: 1) all three controllers were successfully able to maintain stability and fluid flow in this system with constant heat flux 2) the tested controller was able to maintain stability and fluid flow in the system with a variable heat flux by also varying the set-point of the feedback loop, and 3) the more information that is given to the controller the better can perform.

## ACKNOWLEDGMENTS

This accomplishment was by no means an individual effort, but the culmination of support from academic and professional colleagues, family, and friends. Without you all, this would simply not be possible.

I would like to thank my thesis advisor Dr. Pacheco-Vega for his patience and guidance through this journey. He has helped me learn to navigate my way through the research process and overcome various obstacles both inside and outside of lab. I appreciate all of it. I would like to thank Dr. Kuo and Dr. Ploen for being a part of my thesis committee and all of the great feedback. I would like to thank and acknowledge the CREST CEaS of the National Science Foundation-award number HRD 1547723. I would also like to thank Professor Daniel Patrick Anderson who taught me how to be a great student, how to be an great engineer, and more importantly, how to enjoy it.

I would like to thank SoCalGas management and colleagues for investing in me and all the support over the last few years. They allowed me to pursue both my professional and academic goals.

I would like to thank my wife Melissa for all her love and support over these years and throughout this long journey. She has been my rock through all of this. I would like to thank my parents for all the love and support as well and always investing in my education from an early age. I am very fortunate to be surrounded with countless family and friends who have been supportive through all of this as well. To every single one of you, thank you.

## TABLE OF CONTENTS

ABSTRACT . . . . .	iv
ACKNOWLEDGMENTS . . . . .	vi
LIST OF TABLES . . . . .	x
LIST OF FIGURES . . . . .	xi
NOMENCLATURE . . . . .	xiii
1 Introduction . . . . .	1
1.1 Natural Convection Loops . . . . .	2
1.2 Review of System Dynamics . . . . .	5
1.3 Review of Fuzzy Logic Control . . . . .	7
1.4 Objectives . . . . .	10
1.5 Thesis Overview . . . . .	10
2 Problem Description and Mathematical Model . . . . .	12
2.1 Description . . . . .	12
2.2 Mathematical Model . . . . .	13
2.2.1 Mass Balance . . . . .	14
2.2.2 Momentum Balance . . . . .	15
2.2.3 Energy Balance . . . . .	21
2.3 System of Ordinary Differential Equations . . . . .	23

3	Steady State and Dynamic Stability Analysis . . . . .	26
3.1	Integration Methods . . . . .	26
3.2	Steady State Analysis . . . . .	26
3.3	Linear Stability Analysis . . . . .	28
3.4	Stable, Oscillatory, and Chaos Dynamics . . . . .	35
4	Introduction to Fuzzy Logic . . . . .	40
4.1	Background on Fuzzy Logic . . . . .	40
4.1.1	Crisp Sets, Fuzzy Sets and Membership Functions . . . . .	42
4.1.2	Inference Systems and Knowledge Base . . . . .	47
4.1.3	Defuzzification . . . . .	49
5	System and Stability Analysis . . . . .	52
5.1	System Behavior without a Controller . . . . .	52
5.2	Fuzzy Logic Controller Development and Strategy . . . . .	54
5.2.1	Fuzzy Logic Controller 1 . . . . .	56
5.2.2	Fuzzy Logic Controller 2 . . . . .	59
5.2.3	Fuzzy Logic Controller 3 . . . . .	61
5.3	Stability Results . . . . .	63
5.3.1	Controller Functionality . . . . .	64
5.3.2	Disturbance Rejection Method 1 . . . . .	69
5.3.3	Disturbance Rejection Method 2 . . . . .	73
6	Conclusion and Future Work . . . . .	77

6.1	Conclusions . . . . .	77
6.2	Future Work . . . . .	77
	REFERENCES . . . . .	79
A	Development of Dynamical System . . . . .	83
B	Linear Stability Analysis using the Routh-Hurwitz Stability Criterion . . . . .	98
C	Custom MATLAB Solver for a Three Equation Dynamical System . . . . .	105

## LIST OF TABLES

3.1	Routh-Hurwitz stabilization criterion table. . . . .	32
4.1	General example of a truth table. . . . .	48
5.1	Quantitative measures of the dynamic behavior for the fluid velocity, $x$ . . . . .	53
5.2	Decision table for tilt angle andjustment, FLC 1. . . . .	57
5.3	Decision table for tilt angle andjustment, FLC 2. . . . .	61
5.4	Decision table for tilt angle andjustment, FLC 3. . . . .	63
5.5	Stability results for different FL controller configurations. . . . .	66
5.6	Corresponding values of $Q$ , $\alpha$ , and $\bar{x}$ . . . . .	70

## LIST OF FIGURES

1.1	Sample engineering applications of natural convection. . . . .	3
1.2	Different thermosyphon configurations. . . . .	4
1.3	Elements and membership in crisp and fuzzy sets. . . . .	8
2.1	Toroidal thermosyphon. . . . .	13
2.2	Differential element of the thermosyphon. . . . .	16
2.3	Differential element, momentum balance. . . . .	17
2.4	Differential element, energy balance. . . . .	21
3.1	Linear stability curve. . . . .	34
3.2	Stable behavior for $Q = 5, \alpha = 60^\circ$ . . . . .	36
3.3	Oscillatory behavior at the neutral stability curve for $Q = 5, \alpha = 58^\circ$ . . . . .	37
3.4	Limit cycle behavior with chaos parameters for $Q = 5, \alpha = 50^\circ$ . . . . .	38
3.5	Chaos behavior for $Q = 5, \alpha = 30^\circ$ . . . . .	39
4.1	Universe X, set A, and elements $x_1$ and $x_2$ . . . . .	42
4.2	Common types of membership functions. . . . .	45
4.3	Fuzzy logic inference engine diagram. . . . .	46
4.4	Logic operators; union, intersection, and complement. . . . .	46
4.5	Example of membership functions for cold, warm, and hot water. . . . .	48
4.6	Mamdani inference method and centroid defuzzification method. . . . .	50
5.1	Baseline system behavior without a controller. . . . .	53
5.2	Feedback loops with different number of inputs. . . . .	55

5.3	FLC 1 design parameters. . . . .	58
5.4	Feedback loop for the FLC 1. . . . .	59
5.5	FLC 2 design parameters. . . . .	60
5.6	Feedback loop for the FLC 2. . . . .	61
5.7	FLC 3 design parameters. . . . .	62
5.8	Feedback loop for the FLC 3. . . . .	63
5.9	Thermal stability results of FLC 1. . . . .	65
5.10	Stability correlation between $x$ , $y$ , and $z$ . . . . .	66
5.11	Thermal stability comparison for FLC 1, FLC2, and FLC 3. . . . .	67
5.12	Controlled system behavior on the stability graph. . . . .	68
5.13	Critical points $\bar{x}$ as a function of $Q$ and $\alpha$ . . . . .	69
5.14	Disturbance rejection results with a change of $Q$ from 5 to 3. . . . .	70
5.15	Disturbance rejection results with a change of $Q$ from 5 to 4. . . . .	71
5.16	Disturbance rejection results with a change of $Q$ from 5 to 6. . . . .	72
5.17	Disturbance rejection results with a change of $Q$ from 5 to 7. . . . .	73
5.18	Disturbance rejection results with a change of $Q$ (5 to 3) and $x_{ref}$ (1.59 to 1.31). . . . .	74
5.19	Disturbance rejection results with a change of $Q$ (5 to 4) and $x_{ref}$ (1.59 to 1.46). . . . .	75
5.20	Disturbance rejection results with a change of $Q$ (5 to 6) and $x_{ref}$ (1.59 to 1.70). . . . .	75
5.21	Disturbance rejection results with a change of $Q$ (5 to 7) and $x_{ref}$ (1.59 to 1.80). . . . .	76

## NOMENCLATURE

$A$	cross sectional area [ $m^2$ ]
$A_{st}$	Accumulates terms
$a$	Acceleration [ $m/s^2$ ]
$C_p$	specific heat [ $J/kg \cdot K$ ]
$d$	Diameter[m]
$E$	Inlet terms
$E_{\delta x}$	Error signal
$F$	Force [N]
$F_g$	Gravitational force [N]
$F_p$	Pressure force [N]
$F_v$	Viscous force [N]
$G$	Generation terms
$g$	gravitational constant [ $m/s^2$ ]
$\tilde{g}$	local gravitational constant [ $m/s^2$ ]
$h$	Heat transfer coefficient [ $W/m^3 \cdot K$ ]
$K_f$	Friction coefficient [ $Ns/m^3$ ]
$k$	Thermal conductivity [ $W/K \cdot m$ ]
$L$	Length of tube [m]
$m$	Mass [kg]
$\dot{m}$	Mass flowrate [kg/s]
$\hat{n}$	Normal direction

$P$	Pressure [Pa]
$P_1, P_2$	Critical points
$P_p$	Perimeter [m]
$Q$	External heat rate[J/m·s]
$Q_s$	Heat rate transported by fluid flow[J/m·s]
$q$	Heat [J/m]
$q^*$	Heat, dimensionless
$R$	Radius [m]
Re	Reynolds number
$r$	Radius [m]
$S$	Outlet terms
$s$	Cartesian spatial coordinate [m]
$T$	Temperature [K]
$T_0$	Reference temperature [K]
$T^*$	Fluid temperature, dimensionless
$T_m^{*c}$	Fluid temperature, Fourier cosine coefficient, dimensionless
$T_m^{*s}$	Fluid temperature, sin coefficient, dimensionless
$t$	Time [s]
$t^*$	Time, dimensionless
$u$	Fluid velocity [m/s]
$u^*$	Fluid velocity, dimensionless
$X$	Universe of discourse

$x$	Fluid velocity, dimensionless
$x'$	Perturbation, dimensionless
$\bar{x}$	Steady state fluid velocity, dimensionless
$y$	Fluid temperature, Fourier cosine coefficient, dimensionless
$y'$	Perturbation, dimensionless
$\bar{y}$	Steady state fluid temperature, Fourier cosine coefficient, dimensionless
$z$	Fluid temperature, Fourier sin coefficient, dimensionless
$z'$	Perturbation, dimensionless
$\bar{z}$	Steady state fluid temperature, Fourier sin coefficient, dimensionless

*Greek symbols*

$\alpha$	Tilt angle [ $^{\circ}$ ]
$\beta$	Thermal expansion coefficient [ $\text{K}^{-1}$ ]
$\lambda$	Eigenvalue
$\mu$	Dynamic viscosity [ $\text{Ns}/\text{m}^2$ ]
$\mu_A$	Membership function
$\rho$	Density [ $\text{kg}/\text{m}^3$ ]
$\rho_0$	Density at reference temperature [ $\text{kg}/\text{m}^3$ ]
$\sigma$	Standard deviation
$\tau_w$	Shear stress [ $\text{Pa}$ ]
$\theta$	Angular coordinate [ $^{\circ}$ ]

*Subscripts and superscripts*

$s$	Surface
$0$	Initial value
$*$	Nondimensional value

## CHAPTER 1

### Introduction

A thermodynamic system is a device or environment that contains elements to be studied in the context of energy exchange within the system and between the system and the environment. One key mechanism of energy exchange in this system is heat transfer. Heat transfer is defined as the exchange of thermal energy due to a difference in temperature. These systems can be observed in nature when the sun heats up the shoreline or when hot springs are heated from below the earth's surface. They can also be found in many human made applications such as air conditioners and furnaces. There are three different modes in which heat transfer can occur: conduction, convection, or thermal radiation.

Conduction is the transfer of heat through a stationary medium, which can be a solid or fluid. This occurs due to the interaction between particles with more energy, and particles with less energy. Convection is the transfer of heat between a surface and a moving fluid, when there is a difference in temperature. The energy is transferred in part from random molecular motion (diffusion), and in part from the bulk motion of the moving fluid (advection). Radiation is a bit more complex. All matter above absolute zero emit energy in the form of electromagnetic waves. When two surfaces are at different temperatures, and lack a connecting medium, a net exchange of energy will occur. This heat transfer is called thermal radiation. This study will primarily focus on convective heat transfer within a fluid.

Convection can be classified by the driving force of its flow. Forced convection uses an auxiliary device, usually a pump or a fan, to induce flow in a system. This requires

additional energy to operate that device. Free (natural) convection depends on temperature changes within a fluid, which create density changes, and in turn create buoyant forces that will drive the fluid flow [1]. This does not require additional energy and advancements in technology have allowed this type of convection to be used in both large and small scale engineering applications.

An example of natural convection is a geothermal power plant, which is shown in Fig. 1.1(a). In this large-scale engineering system, wells are dug deep below the earth's surface and filled with a fluid, which is then heated up by its surroundings. This causes the fluid to rise and turn into steam, which then operates a turbine for electric power. The steam then condenses and returns into the ground. A more straightforward example is a simple heat sink used on electronics and small engines as shown in Fig. 1.1(b). The cooling fins absorb heat from the base causing their temperature to rise. The fins then transfer that energy to adjacent air. With an increase in temperature, and decrease in density, that air begins to rise and displace the cooler air above it. This less dense and cooler air now falls and replaces the hotter air adjacent to the fins and the cycle continues. This cycle of moving fluid is the principle behind a natural convection loop.

## **1.1 Natural Convection Loops**

A natural convection loop, also known as thermosyphon, is a thermal device that circulates fluid in a closed pipe. This loop contains a fixed section that receives heat and a fixed section that releases heat, generally through a heat exchanger or heated coil. The location of these fixed sections vary by thermosyphon design. The pipe is filled with a fluid, usually water for single phase or a refrigerant for multiphase studies. The purpose

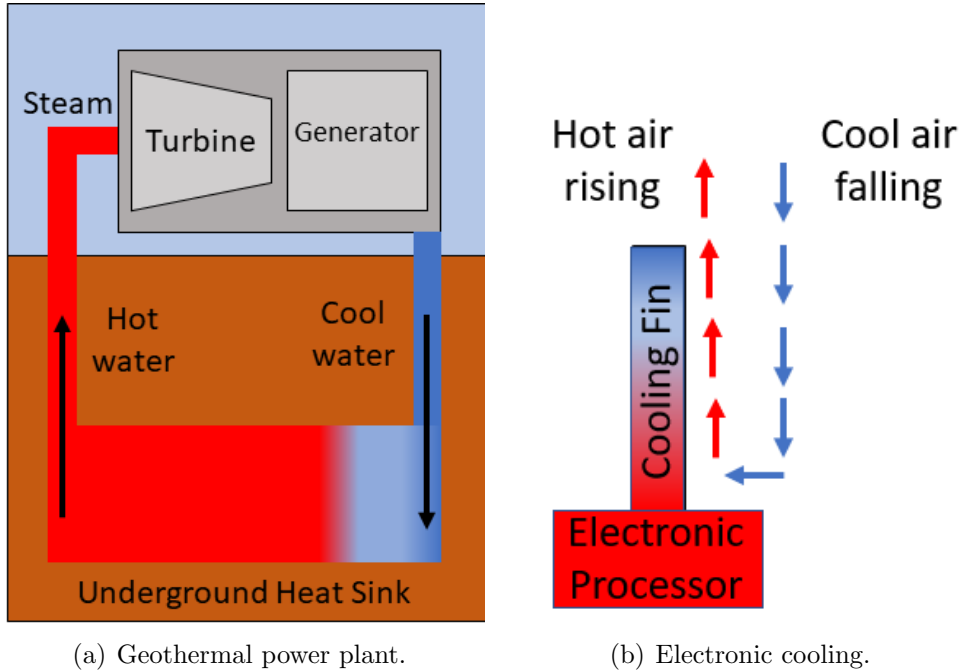


Figure 1.1: Sample engineering applications of natural convection.

of a thermosyphon is to transfer heat from one place to another via buoyancy driven fluid flow instead of using an auxiliary pump. For example, in the geothermal system the heat from the earth is transferred to the fluid which rises and produces work in the turbine. In the heat sink system, the heat generated from the electric part is transferred to the cooling fins, then to the surrounding air. The ability to control the transfer of heat in a thermal system is a critical tool in a wide variety of engineering applications and disciplines. The analysis of heat transfer in small scale systems and simulations can provide valuable insight to develop strategies for larger and more complex applications.

In 1973, Japiske [2] provided an excellent review of heat transfer within a natural convection loop. The work covers many variations including open loop, closed loop, single phase, and two-phase systems. Extensive research in fluid flow behavior within natural convection loops have since been studied [3]-[11]. These studies have looked at

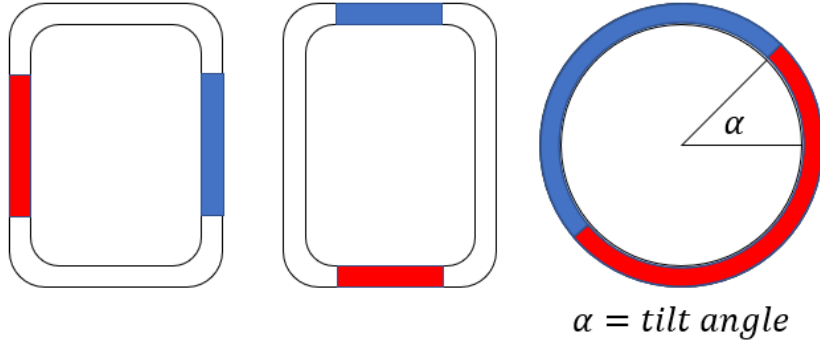


Figure 1.2: Different thermosyphon configurations.

the different fluid dynamic characteristics that affect flow and stability including the Graetz, Prandtl, and Reynolds numbers, in addition to different configurations of the heated/cooled sections. Examples of these different heat input and output locations, colored red and blue respectively, are shown in Fig. 1.2. The last configuration in the figure is a toroidal thermosyphon that rotates about its center, allowing the heated and cooled section to move with a given tilt angle  $\alpha$ . This particular configuration has been studied by several authors [6]-[11] and will be the subject of this study. The toroidal thermosyphon in this study has two variable parameters. The first variable parameter is tilt angle  $\alpha$ , which maps the location of the heated/cooled sections as they rotate about the center. The second is the amount of heat,  $Q$ , added or removed from the system. The right combination of those two parameters can induce flow by creating a temperature and density differential in the fluid, which creates buoyant forces. This study does that by having the heat input section near the bottom of the system, and the heat output section near the top. As the fluid near the bottom is heated, its temperature increases and its density decreases, causing it to rise and displace the fluid at the top.

As the fluid near the top is cooled, its temperature decreases and its density increases, causing it to fall and replace the fluid at the bottom. In addition to these heat input and output conditions, the thermosyphon can also be rotated with a certain degree of tilt to manipulate the buoyant forces and fluid flow. The right combination of tilt and heat input can induce fluid flow in the tube without the need for an auxiliary pump, which can reduce energy consumption of the system. This energy savings can be scaled for a variety of engineering applications from computer electronics to residential solar water heaters to nuclear cooling. Several studies have looked at its detailed application in solar heater applications [12] - [14]. Fluid flow stability is critical to maintain efficient heat transfer in this system and will be investigated thoroughly in this research.

## **1.2 Review of System Dynamics**

To investigate stability of the system, one-dimensional models have been used extensively, and a number of reports exist in the literature, as described in this section. Creveling et al. [3] investigated the effects of the tilt angle on the stability of a toroidal thermosyphon with the heated/cooled sections rotated about its center. Their analysis focused on the influence of both friction factor and Reynolds number upon the fluid flow stability. The study compared the one-dimensional analytical data with experimental data. Damerell and Schoenhals [4] studied a similar setup that compared analytical and experimental data. Fluid oscillations and direction reversals were observed and it was concluded that stability was not achievable at certain heat input rates. In addition, analytical and experimental results did not agree at all tilt angles. Grief et al. [5] studied transient velocity and temperature stability using the tilted model with fixed heated and cooled

sections. From this, fluid velocity and temperature profiles were obtained. Mertol et al. [6] used a two-dimensional analysis and concluded there are significant velocity variations in the radial and axial directions that are not considered in one-dimension. Effects from the heat transfer coefficient and Graetz number were also considered. Lavine et al. [7] did a three-dimensional analysis on this system with a variable tilt angle. Streamwise flow reversals and secondary motion at the wall were observed. The flow reversals reduced wall friction and buoyancy forces which significantly affected the averaged fluid velocity. Graetz, Prandtl, and Reynolds number were considered in addition to tilt angle. Their study discovered key flow phenomena that are not shown in one-dimensional or two-dimensional analyses. Lavine et al. [8] continued this research by investigating the effects of Grashof number in a three-dimensional analysis. Bernier and Baliga [9] used a thermosyphon that used heated and cooled sections on the left and right side instead of top and bottom. The work investigated mixed convection effects and the experimental results agreed with the numerical ones in both one and two-dimensional analysis. Bernier and Baliga [15] continued their work to use higher Grashof numbers. They concluded the one-dimensional models suffered in accuracy due to the distortion of velocity and temperature profiles. Pacheco-Vega et al. [10] analyzed the one-dimensional toroidal thermosyphon with heated and cooled section at the bottom and top sides with an adjustable tilt angle about the center. His research looked at three different combination of heat conditions: known heat flux around the loop, known temperature around the loop, and a mixture of these conditions. Stability was analyzed with the tilt angle and heat input as the variable inputs. A 4th order Runge-Kutta numerical simulation was used for the non-dimensional analytical analysis and a set of three nonlinear equations

were developed to model the system behavior. Three distinct stability behaviors were produced from a steady state analysis as a function of the two input parameters: stable flow, limit cycle flow, and chaotic flow. Understanding flow stability is key in the design of a natural convection loop system to ensure efficient heat transfer. If it can be understood well enough it can also be controlled.

### **1.3 Review of Fuzzy Logic Control**

Thermal systems are designed to move heat from one place to another. To do this efficiently, a robust controller must be implemented. The control of thermal systems is particularly difficult due to the dynamic nature of the fluid flow and convective heat transfer [11]. These applications can range from heat exchangers to residential cooling to HVAC (heating ventilation air-conditioning) systems in multi-level commercial buildings. System controllers for most thermal systems operate on some combination of a temperature feedback loop. It will have a setpoint, a controller, a plant (experimental or simulation) and a summation block to compare the existing value to setpoint value. In most applications PID (proportional integral derivative) controllers are used but they leave a lot to be desired. The need for constant retuning can lead to poor performance, which can lead to an increase in energy costs. There is a need for a more efficient control strategy that will provide the robustness and efficiency these systems require. There have been many studies done on the application of fuzzy logic to control thermal systems.

Fuzzy logic (FL) uses linguistic terms to develop rules based on previous knowledge. It uses membership functions which create fuzzy sets, allowing it to control systems with vague or imprecise data [16]. What distinguishes FL from traditional control is the fuzzy

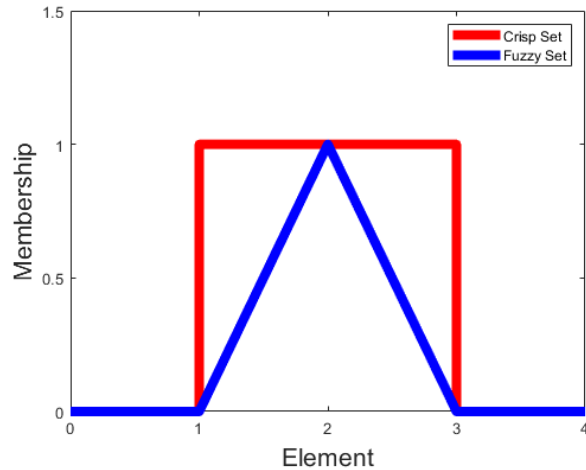


Figure 1.3: Elements and membership in crisp and fuzzy sets.

sets, which allow the elements to belong or partially belong to a set or sets. This contrasts the binary logic of a crisp set which says an element either belongs or does not belong.

Fuzzy logic has been studied extensively over the past 50 years and has shown promise in several engineering applications. In 1965, Zadeh [17] first developed the concept of fuzzy sets and membership functions. He observed that objects in the real world do not always fully belong, or not belong, to a specific classification. Human logic does not always clearly define what class or classes something belongs to and the lines can be imprecise or “fuzzy”. In 1975, Mamdani and Assililan [18] studied a linguistic synthesis experience on a controller for a steam plant. They observed the logic that a traditional control uses to make decisions and the logic a human uses are not the same. This study revealed that a fuzzy logic controller was able to use human experience to operate. The results showed the fuzzy logic controller had better quality of control compared to a traditional one. In 1996, Ralescu [19] wrote about a surge in fuzzy logic controllers in Japan. He stated that due to a lack of natural resources, Japan relied heavily on efficient energy management.

Fuzzy logic was used in steel technology artificial intelligence, among other applications. In 2005, Salsbury [20] surveyed control technologies in the building automation industry. System performance demands have increased due to environmental policies and rising energy costs. In commercial HVAC applications, automation has helped reduce costs by prioritizing energy savings over precision. Single input single output (SISO) systems are common with the room temperature as the input signal and the angle of the air dampener as the output signal. The main challenge is that the air systems in these buildings are time variant and nonlinear, which lead to sluggish or oscillatory control with a constant need for retuning. Suggestions have been made to implement new control systems such as fuzzy logic, neural networks, or updated plant models. In addition to HVAC systems, fuzzy logic has been applied to heat exchangers as well. In 2009, Ruiz-Mercado et al. [21] developed a Takagi-Sugeno fuzzy dynamic model for concentric-tube heat exchangers. The logic rules were derived from previously collected experimental flowrates and fluid temperatures. The model was able to accurately predict the nonlinear behavior of the system. Garpinger et al. [22] explored performance and robustness of PID controllers. PID controllers operate with simple tuning rules based on process models with few parameters. Controlled systems have certain requirements such as load disturbance reduction, robustness for uncertainty, noise control, and set point tracking. For PID controls, there is a tradeoff between performance and robustness that must be balanced. In 2015, Underwood [23] published a study on fuzzy logic used to control domestic heat pumps. In this work, a new dynamic model was developed and validated. This new controller showed good tracking of the system and furthermore reduced energy consumption by 20 percent. In 2016, Soufi et al. [24] implemented a fuzzy logic control strategy in a

photovoltaic system. It showed a faster tracking speed, zero oscillations, and the ability to operate in extreme weather conditions. This, combined with faster computing, allows this controller to increase performance and reduce costs. Fuzzy logic has been shown to be capable of controlling thermal systems in a variety of engineering applications. This work will extend the application to control the fluid flow stability in a toroidal natural convection loop.

#### **1.4 Objectives**

The objective of this thesis is to develop a robust control strategy, using fuzzy logic, to control the flow stability in a toroidal natural convection loop. To achieve this, a fuzzy logic controller is developed using the change in velocity (signal error), which is an excellent indicator of stability of the system. Several iterations of this fuzzy logic controller were developed; the first using only the signal error, the second adding the change in signal error, and the last adding the integration of the signal error. Each iteration added more information than the previous. Robustness was tested using different initial condition scenarios to ensure the controller could provide stability to the system as subjected to various perturbations that may occur. Testing included holding one variable steady while controlling the other to achieve and maintain stability, as well as varying both input variables simultaneously to determine what degree of stability, if any, could be achieved in an unstable region.

#### **1.5 Thesis Overview**

The contents of this document are organized in the following manner. Chapter 1 provides an introduction and brief summary of the subject matter as well as a literature review.

Chapter 2 provides a detailed description of the thermosyphon system as well as a mass, momentum, an energy balance that established the governing set of equations. Chapter 3 provides a steady state and dynamic analysis that describes the systems behavior. Chapter 4 provides an introduction to fuzzy logic and how it will be utilized on this system. Chapter 5 provides the stability results from implementing the fuzzy logic controller into this thermo-fluid system. In Chapter 6, the conclusions from this work are discussed as well as possible directions for future work.

Appendices are attached to this document to provide details not covered in the main text. Appendix A covers a detailed derivation of the dynamical system from the governing equations. Appendix B covers in detail the linear stability analysis using the Routh-Hurwitz Stability Criterion. Appendix C covers the MATLAB script used to solve the system of three ordinary differential equations.

## CHAPTER 2

### Problem Description and Mathematical Model

In Chapter 1, a summary of heat transfer, natural convection loops, system dynamics, and fuzzy logic was covered. Past research in these fields of study was covered in a literature review and the contributions this current work aims to provide. In this chapter, a detailed derivation will be covered in order to lead the reader to the final set of governing equations, provided as a dynamical system.

#### 2.1 Description

The mathematical model of a toroidal natural convection loop was derived and summarized in the work of Pacheco-Vega et al. [10]. To this end, the present work follows the study by Hummel [25]. Consider a loop filled with a single-phase fluid, as depicted in Fig. 2.1. The tube diameter is  $d$  and the length from the center of the loop to the midpoint of the tube is  $R$ , with  $R \gg d$ . The angle  $\theta$  describes the position along the circumference of the loop and the regions where heat enters and leaves the device. From  $0^\circ < \theta < 180^\circ$  heat leaves the system whereas from  $180^\circ < \theta < 360^\circ$  heat enters the system. This creates a temperature difference in the fluid, further creating a density difference, thus causing its motion. There are three possible heating conditions: known heat flux, known wall temperature and mixed conditions, all of which have been analyzed by Pacheco-Vega et al. [10]. These conditions determine if the heat flux or the wall temperature are known over the entire loop, or if these quantities are known for different parts of the loop.

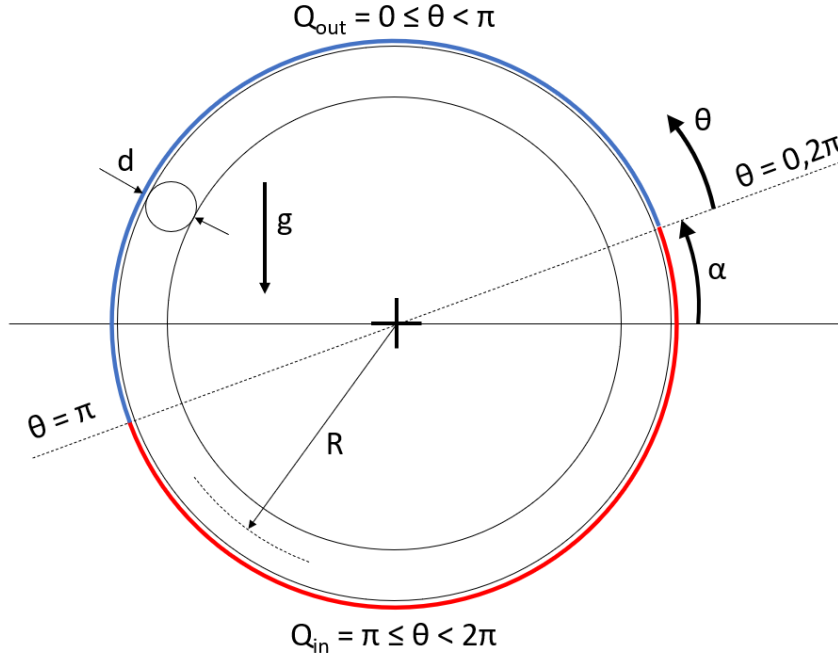


Figure 2.1: Toroidal thermosyphon.

## 2.2 Mathematical Model

The present study focuses on the “known heat flux” heating condition. Although a similar type of system has been modeled using two-dimensional versions of the conservation equations [6], one-dimensional versions have been very useful in studying the dynamics in these systems, and it is the type of model that will be used in this work. As it will be shown later in this section, mass conservation provides a velocity independent of the spatial coordinate; i.e.,  $u = u(t)$  and  $T = T(t, \theta)$ , which are the dependent variables, whereas time  $t$  and the angle  $\theta$ , as measured from the boundary separating heat input and output values, are the independent variables. Finally, the angle of inclination,  $\alpha$  (also known as tilt angle), is one of the input parameters with heat flux as the other.

As shown in Fig. 2.1, the length of the tube is  $L$ , where  $L = 2\pi R$  with a cross section

$A$ , where  $A = d^2\pi/4$ . Previously developed one-dimensional models have been compared against experimental data to predict the variation of flow rates. These results have been in agreement with experiments, as mentioned by Damerell and Schoenhals [4]. As a result, flow characteristics such as temperature and velocity profiles are assumed to be uniform at any given cross-sectional area. Next, the spacial variable  $s$ , where  $s = R\theta$ , is used to transfer the circular tube in cylindrical coordinates to a straight tube in cartesian coordinates.

To derive the mathematical equations that describe the thermal and fluid dynamics of this system, a balance of mass, momentum, and energy on a differential control volume of the torus is conducted. Thus, by following the work of Hummel [25], the three balance equations will follow the expression

$$E - S \pm G = A_{st}, \quad (2.1)$$

where  $E$  are in inlet terms,  $S$  are the outlet terms,  $G$  are the generation terms, and  $A_{st}$  are the accumulated terms. These balance methods will be covered in the next three sections.

### 2.2.1 Mass Balance

A differential element of the thermosyphon is shown below in Fig. 2.2(a). Consider an infinitesimal one-dimensional control volume, shown in Fig. 2.2(b) and described with

the following mathematical equation

$$\dot{m} - (\dot{m} + \frac{\partial \dot{m}}{\partial s} ds) = 0 \quad (2.2)$$

$$\frac{\partial \dot{m}}{\partial s} ds = 0. \quad (2.3)$$

The definition of  $\dot{m}$  is shown below,

$$\dot{m} = \int_A \rho(u \cdot \hat{n})dA, \quad (2.4)$$

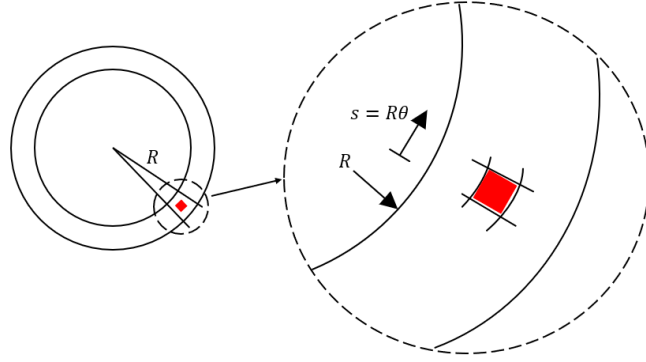
with fluid density  $\rho$ , cross-sectional area  $A$ , and fluid velocity  $u$  in the normal direction  $\hat{n}$ . With a given constant cross-sectional area, the above equations reduces as follows:

$$\dot{m} = \rho u A. \quad (2.5)$$

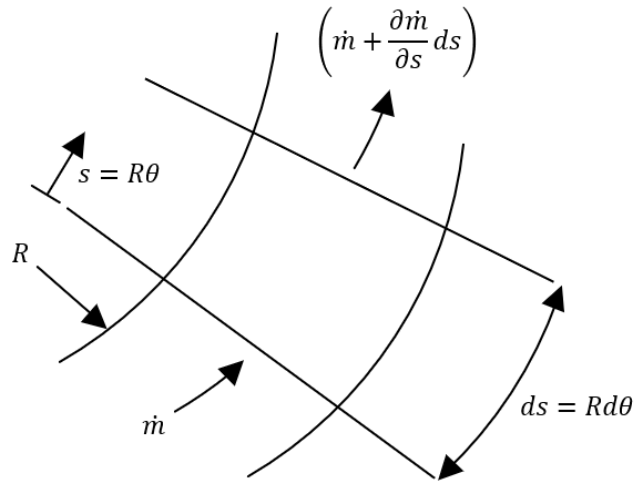
With no change in mass as defined in Eq. (2.3), it follows that there also must be no change in velocity. Further, since this is a one-dimensional analysis, velocity is taken as the average value of the cross-sectional area.

### 2.2.2 Momentum Balance

The momentum balance can be applied on the same differential element as shown below in Fig. 2.3. Two types of forces can act upon an element: body forces and surfaces forces. Body forces act on every particle of the material and include gravitational and magnetic forces. Surface forces act on the surface of the element and include tangential (shear) and normal (pressure and stress) forces. The forces that are applicable in this



(a) Differential element.



(b) Differential element, mass balance.

Figure 2.2: Differential element of the thermosyphon.

situation are from pressure, viscosity, and buoyancy. These are shown in Fig. 2.3. The pressure force,  $F_P$  is given by

$$F_p = PA - \left(P + \frac{\partial P}{\partial s} ds\right)A, \quad (2.6)$$

$$F_p = -A \frac{\partial P}{\partial s} ds, \quad (2.7)$$

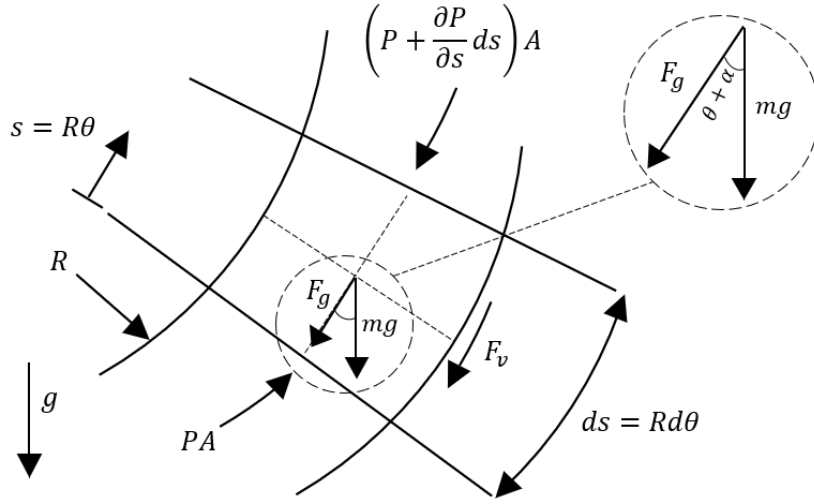


Figure 2.3: Differential element, momentum balance.

with the pressure exerted on the element given as  $P$ . The viscous force that acts on the fluid is given by

$$F_v = -\tau_w P_p ds, \quad (2.8)$$

with the shear stress given by  $\tau_w = K_f u$  and the perimeter given by  $P_p = \pi d$ .  $K_f$  is the assumed friction coefficient of Poiseuille flow in a circular duct and is defined as

$$K_f = \frac{8\mu}{d}, \quad (2.9)$$

where  $\mu$  is the fluid's dynamic viscosity. Note that the frictional wall shear has been taken to be proportional to the mean fluid velocity, of the fully-developed flow - which provides a parabolic velocity profile, and  $K_f$  is the proportional constant; i.e., the friction

coefficient. Gravity is the main component of the buoyancy force and is given by

$$F_g = -\rho A \tilde{g} ds, \quad (2.10)$$

where  $\rho$  is the density of the fluid and  $\tilde{g}$  is the local gravitational acceleration. Note in the momentum balance the density is a function of the fluid's temperature. Using trigonometric expressions from Figure 2.3,  $\tilde{g}$  can be expressed as

$$\tilde{g}(s) = g \cos(\theta + \alpha), \quad (2.11)$$

with  $\theta$  as the angular position around the torus and  $\alpha$  as the tilt angle. Next, consider integrating Eq. (2.11) around the torus as follows

$$\tilde{g}(s) = g \cos(\theta + \alpha), \quad (2.12)$$

$$\int_0^L \tilde{g}(s) ds = \int_0^L g \cos(\theta + \alpha) d\theta, \quad (2.13)$$

$$\int_0^L \tilde{g}(s) ds = g \left[ \cos \alpha \int_0^{2\pi} \cos \theta d\theta - \sin \alpha \int_0^{2\pi} \sin \alpha d\theta \right], \quad (2.14)$$

$$\int_0^L \tilde{g}(s) ds = 0. \quad (2.15)$$

Note that Eq. (2.15) shows the summation of the gravitational force around the torus equals 0 and will be important later in the derivation. The Boussinesq approximation, as validated by Damerell and Schoenhals [4], ignored variations in density except for temperature, thus, density in this problem is only a function of temperature. Its mathematical

expression is show below

$$\rho = \rho_0 [1 - \beta(T - T_0)], \quad (2.16)$$

with the fluid density  $\rho$  as a function of temperature,  $\rho_0$  the fluid density at the reference temperature,  $\beta$  the fluid's coefficient of thermal expansion,  $T = T(s, t)$  as the fluid temperature as a function of time and space ( $s$  if tangential and  $\theta$  if cylindrical coordinates), and  $T_0$  as the reference temperature. The reference temperature used is the initial condition before natural convection begins to drive the flow. To summarize, the three forces are shown below

$$F_p = -A \frac{\partial P}{\partial s} ds, \quad (2.17)$$

$$F_v = -\tau_w P_p ds, \quad (2.18)$$

$$F_g = -\rho A \tilde{g} ds. \quad (2.19)$$

Newton's second law,  $F = ma$ , is applied the differential element with the force  $F = F_p + F_v + F_g$  as the summation of individual forces listed in the above equations, the mass  $m = \rho_0 A ds$ , and the acceleration  $a = du/dt$ . Below is the momentum balance derivation.

$$ma = F, \quad (2.20)$$

Substitute the mass, acceleration, and summation of force equivalencies from Eqs. (2.17-2.19),

$$\rho_0 A ds \cdot \frac{du}{dt} = -A \frac{\partial P}{\partial s} ds - \tau_w P_p ds - \rho A \tilde{g} ds, \quad (2.21)$$

Recall that the shear stress and Bousinesq approximation are, respectively,  $\tau_w = K_f u$ ,  $\frac{\rho}{\rho_0} = [1 - \beta(T - T_0)]$ , and then integrate around the torus, thus we have

$$\frac{du}{dt} = -\frac{1}{\rho_0} \frac{\partial P}{\partial s} - \frac{K_f P_p}{\rho_0 A} u - [1 - \beta(T - T_0)] \tilde{g}, \quad (2.22)$$

$$\frac{du}{dt} \int_0^L ds = -\frac{1}{\rho_0} \int_0^L \frac{\partial P}{\partial s} ds - \frac{K_f P_p}{\rho_0 A} u \int_0^L ds - \int_0^L [1 - \beta(T - T_0)] \tilde{g} ds, \quad (2.23)$$

The buoyancy term can be simplified as follows:

$$\int_0^L [1 - \beta(T - T_0)] ds = \int_0^L \tilde{g}(s) ds - \beta \int_0^L T \tilde{g}(s) ds + \beta T_0 \int_0^L \tilde{g}(s) ds, \quad (2.24)$$

$$\text{recall } \int_0^L \tilde{g}(s) ds = 0,$$

$$\int_0^L [1 - \beta(T - T_0)] ds = -\beta \int_0^L T \tilde{g}(s) ds. \quad (2.25)$$

Considering the buoyancy term in Eq. (2.25) and the properties at  $s=0$  and  $s=L$  are the same since it is the same point along the torus, specifically  $P(0) = P(L)$ . Along with the substitutions for  $\tilde{g}(s) = g \cos(\theta + \alpha)$ ;  $A = \frac{d^2 \pi}{4}$ ;  $P_p = \pi d$ ;  $s = R\theta$ ;  $ds = R d\theta$ ;  $L = 2\pi R$ , we

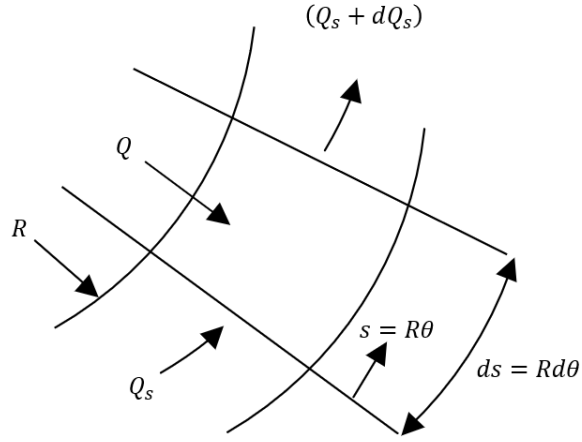


Figure 2.4: Differential element, energy balance.

have the following:

$$\frac{du}{dt} = -\frac{K_f P_p}{\rho_0 A} u + \frac{\beta}{L} \int_0^L T \tilde{g}(s) ds, \quad (2.26)$$

$$\frac{du}{dt} + \frac{4K_f}{\rho_0 d} u = \frac{\beta g}{2\pi} \int_0^{2\pi} T \cos(\theta + \alpha) d\theta. \quad (2.27)$$

The final momentum balance is shown above in Eq. (2.27).

### 2.2.3 Energy Balance

The energy balance is shown in Figure 2.4 on a differential element of the torus, and mathematically described below

$$Q_s + Q - (Q_s + dQ_s) = \rho_0 C_p A ds \frac{\partial T}{\partial t}, \quad (2.28)$$

$$Q - dQ_s = \rho_0 C_p A ds \frac{\partial T}{\partial t}, \quad (2.29)$$

where  $Q_s$  is the heat rate entering the element,  $Q$  is the known external heat rate input or output, and  $C_p$  is the specific heat. The two modes of heat transfer in this problem are conduction and convection as described below

$$dQ_s = \left[ \rho_0 c_p A u \frac{\partial T}{\partial s} - k A \frac{\partial^2 T}{\partial s^2} \right] ds, \quad (2.30)$$

where  $k$  is thermal conductivity. Due to the dynamic behavior of the fluid, heat transfer from convection is assumed to be much greater than conduction with the latter considered negligible. This assumption is reasonable for the following fluid flow conditions: parallel streamlines, uniform surface conditions, very long channels [26]. The mathematical impact is shown below

$$\rho_0 c_p A u \frac{\partial T}{\partial s} \gg k A \frac{\partial^2 T}{\partial s^2} ds. \quad (2.31)$$

An order of magnitude analysis of Eq. (2.31), shows that the left hand side of the equation, corresponding to the advection of heat, is much larger than the axial heat diffusion. Therefore,

$$dQ_s = \rho_0 c_p A u \frac{\partial T}{\partial s} ds. \quad (2.32)$$

In addition,

$$Q = qds, \quad (2.33)$$

with  $q$  as the input/output heat per unit length. Equation (2.29) can be combined with the equations above, including  $s = R\theta$ , to arrive at the following:

$$\frac{\partial T}{\partial t} + \frac{u}{R} \frac{\partial T}{\partial \theta} = \frac{4q}{\pi d^2 \rho_0 c_p}. \quad (2.34)$$

The final energy balance is shown above in Eq. (2.34).

### 2.3 System of Ordinary Differential Equations

After balancing the mass, momentum, and energy equations, two equations remain as shown below

$$\frac{du}{dt} + \frac{4K_f}{\rho_0 d} u = \frac{\beta g}{2\pi} \int_0^{2\pi} T \cos(\theta + \alpha) d\theta, \quad (2.35)$$

$$\frac{\partial T}{\partial t} + \frac{u}{R} \frac{\partial T}{\partial \theta} = \frac{4q}{\pi d^2 \rho_0 c_p}. \quad (2.36)$$

In order to analyze this problem independent of fluid properties and torus dimensions, the previous two equations will be put into non-dimensional terms. Following the derivation of Pacheco-Vega et al. [10], the substitutions and resulting equations are shown below

$$T^* = \frac{p_0^2 d^2 \beta g}{32 K_f^2 R} \cdot T, \quad (2.37)$$

$$u^* = \frac{p_0 d}{4 K_f R} \cdot u, \quad (2.38)$$

$$q^* = \frac{\rho_0^2 d \beta g}{32 \pi c_p K_f^3 R} \cdot q, \quad (2.39)$$

$$t^* = \frac{4 K_f}{\rho_0 d} \cdot t, \quad (2.40)$$

$$\frac{du^*}{dt^*} + u^* = \frac{1}{\pi} \int_0^{2\pi} T^* \cos(\theta + \alpha) d\theta, \quad (2.41)$$

$$\frac{\partial T^*}{\partial t^*} + u^* \frac{\partial T^*}{\partial \theta} = q^*, \quad (2.42)$$

with the non-dimensional parameters indicated with the superscript  $*$ . The two equations are coupled through temperature, which is a function of both time  $t$  and space  $s = R\theta$ . Numerical methods can be used to solve  $u^*(t^*)$  and  $T^*(t^*, \theta^*)$  and analyze the dynamic behavior of the system, however, it is expensive in both time and computation. One solution is to use a Fourier series expansion on  $T^*$ , as first proposed by Malkus in a seminal paper [27], as shown below

$$T^*(t^*, \theta) = T_0^{c*}(t^*) + \sum_{m=1}^{\infty} [T_m^{c*}(t) \cos m\theta + T_m^{s*}(t) \sin m\theta], \quad (2.43)$$

with  $T_m^{c*}(t)$  and  $T_m^{s*}(t)$  for  $m = 1, 2, \dots, \infty$  as the Fourier coefficients. This expansion is now substituted into the momentum balance equation as shown below

$$\frac{du^*}{dt^*} + u^* = \frac{1}{\pi} \int_0^{2\pi} T^* \cos(\theta + \alpha) d\theta, \quad (2.44)$$

$$T^*(t, \theta) = T_0^{c*}(t) + \sum_{m=1}^{\infty} [T_m^{c*}(t) \cos m\theta + T_m^{s*}(t) \sin m\theta], \quad (2.45)$$

$$\frac{du^*}{dt^*} + u^* = \frac{1}{\pi} \int_0^{2\pi} \left[ T_0^{c*}(t) + \sum_{m=1}^{\infty} [T_m^{c*}(t) \cos m\theta + T_m^{s*}(t) \sin m\theta] \right] \cos(\theta + \alpha) d\theta. \quad (2.46)$$

This systems of ODE's have been truncated to only consider the first term of an infinite set, where  $m = 1$ . A complete and detailed derivation can be found in Appendix A. The three governing equations that result are as follows:

$$\frac{du^*}{dt^*} = -u^* + T_1^{c*}(t) \cos \alpha - T_1^{s*}(t) \sin \alpha, \quad (2.47)$$

$$\frac{\partial T_1^{c*}(t)}{\partial t^*} = -u^* T_1^{s*}(t), \quad (2.48)$$

$$\frac{\partial T_1^{s*}(t)}{\partial t^*} = -Q + u^* T_1^{c*}(t). \quad (2.49)$$

For simplification let:  $x = u^*$ ,  $y = T_1^{c*}$ ;  $z = T_1^{s*}$ ,

$$\frac{dx}{dt} = -x + y \cos \alpha - z \sin \alpha, \quad (2.50)$$

$$\frac{dy}{dt} = -xz, \quad (2.51)$$

$$\frac{dz}{dt} = -Q + xy. \quad (2.52)$$

These set of equations contain two control parameter variables: the tilt angle  $\alpha$  and heat input  $Q$ . Now the complete velocity and temperature profiles can be solved for entire loop. In the next chapter, a stability and dynamic behavior analysis will be performed.

## CHAPTER 3

### Steady State and Dynamic Stability Analysis

In the previous chapter, the one-dimensional velocity and temperature profiles along the torus were derived by solving a set of three nonlinear differential equations with the known heat flux around the entire loop modeled as:  $Q = -\widehat{Q} \sin \theta$ . The known parameters that determine the behavior of the system are heat flux  $Q$  and tilt angle  $\alpha$ . This chapter describes how the fluid flow in system can show stable, limit cycle, or chaotic behavior.

#### 3.1 Integration Methods

The linear stability analysis and numerical solutions for this system, used to determine what type of behavior the fluid flow will exhibit, were first reported by Sen et. al [28]. In this research, the three nonlinear differential equations were solved by using a fourth order Runge-Kutta numerical integration method developed in MATLAB (detailed in Appendix C). The time step used was 0.01 with initial conditions for  $x_0$ ,  $y_0$ , and  $z_0$  set to 0. This simulation provides the entire velocity and temperature profiles, as well as stability behavior, for any given heat flux and tilt angle value. The stability can be determined by conducting a steady state analysis as covered in the next section.

#### 3.2 Steady State Analysis

A steady state analysis on this toroidal thermosyphon with known heat flux was performed by Pacheco-Vega et. al [10]. In their work, the steady state solutions provide two critical points that are key for further stability analysis. This is outlined below

Consider the velocity,  $x$ , of a fluid flow that after some amount of time,  $t$ , stabilizes to a constant value. The change in velocity over time,  $dx/dt$ , as well as the change in

temperature over time,  $dy/dt$  and  $dz/dt$ , would then be zero. These set of values,  $\bar{x}$ ,  $\bar{y}$ , and  $\bar{z}$ , are collectively called a critical point and correspond to the steady state values of velocity and temperature Fourier sin and cosine coefficients. In the present case, two critical points,  $P_1$  and  $P_2$ , can be found by setting the three governing equations to zero to solving for  $\bar{x}$ ,  $\bar{y}$ ,  $\bar{z}$ .

$$0 = -\bar{x} + \bar{y} \cos \alpha - \bar{z} \sin \alpha, \quad (3.1)$$

$$0 = -\bar{x}\bar{z}, \quad (3.2)$$

$$0 = -Q + \bar{x}\bar{y}. \quad (3.3)$$

Eq. (3.2) shows either  $\bar{x}$  or  $\bar{z}$  must be equal to 0. If  $\bar{x}$  equals zero, there is no fluid velocity and the entire system comes to rest. That does not provide a solution, so  $\bar{z}$  must equal 0. From here, a simple two variable system of equations can be solved.

$$0 = -\bar{x} + \bar{y} \cos \alpha, \quad (3.4)$$

$$0 = -Q + \bar{x}\bar{y}. \quad (3.5)$$

Rearranging Eq. (3.5) to isolate  $\bar{y}$  and substituting it into Eq. (3.4) results in the following:

$$0 = -\bar{x} + \left(\frac{Q}{\bar{x}}\right) \cos \alpha, \quad (3.6)$$

$$\bar{x} = \pm \sqrt{Q \cos \alpha}. \quad (3.7)$$

Substituting  $\bar{x}$  back into Eq. (3.4),

$$0 = -(\pm\sqrt{Q \cos \alpha}) + \bar{y} \cos \alpha \quad (3.8)$$

$$\bar{y} = \pm\sqrt{Q/\cos \alpha} \quad (3.9)$$

Solving for  $\bar{x}$  and  $\bar{y}$  provided both a positive and negative set of solutions. These make up the two critical points, or steady state solutions as noted below with  $P_1$  and  $P_2$ .

$$P_1 = (\bar{x}, \bar{y}, \bar{z}) = (\sqrt{Q \cos \alpha}, \sqrt{Q/\cos \alpha}, 0), \quad (3.10)$$

$$P_2 = (\bar{x}, \bar{y}, \bar{z}) = (-\sqrt{Q \cos \alpha}, -\sqrt{Q/\cos \alpha}, 0), \quad (3.11)$$

where both exist if  $-90^\circ < \alpha < 90^\circ$ .  $P_1$  corresponds to a steady state flow in the counterclockwise direction, whereas  $P_2$  refers to a flow in the clockwise direction. Next, the steady state solutions will be used in the linear stability analysis.

### 3.3 Linear Stability Analysis

A linear stability analysis on this toroidal thermosyphon with known heat flux was performed by Pacheco-Vega et. al [10]. In their work, a linear stability curve graph was developed that accurately predicted what type of behavior would result for any given heat input and tilt angle combination. This analysis is outlined below.

A linear stability analysis using the critical points can be performed, starting with

the following equations:

$$x(t) = \bar{x} + x'e^{\lambda t}, \quad (3.12)$$

$$y(t) = \bar{y} + y'e^{\lambda t}, \quad (3.13)$$

$$z(t) = \bar{z} + z'e^{\lambda t}, \quad (3.14)$$

with  $x(t), y(t), z(t)$  as the dimensionless variables,  $\bar{x}, \bar{y}, \bar{z}$  as the steady state solutions, and  $x'e^{\lambda t}, y'e^{\lambda t}, z'e^{\lambda t}$  as the perturbations in the system. As described in Sen et. al [28], these perturbations have an amplitude of  $x', y', z'$  and will either grow and decay depending on the value for  $\lambda$ , particularly if it is positive or negative. Further, the stability of the system will depend on if the lambda values are real, imaginary, or a combination of the two as is solved during this section. Taking the derivative of both sides provides the next set of equations,

$$\frac{dx}{dt} = \lambda x'e^{\lambda t}, \quad (3.15)$$

$$\frac{dy}{dt} = \lambda y'e^{\lambda t}, \quad (3.16)$$

$$\frac{dz}{dt} = \lambda z'e^{\lambda t}. \quad (3.17)$$

The above equations for  $x, y, z$  and  $dx/dt, dy/dt, dz/dt$  can be substituted in to the three governing Eq's, (3.34 - 3.36), shown below:

$$\lambda x' e^{\lambda t} = -[\bar{x} + x' e^{\lambda t}] + [\bar{y} + y' e^{\lambda t}] \cos \alpha - [\bar{z} + z' e^{\lambda t}] \sin \alpha, \quad (3.18)$$

$$\lambda y' e^{\lambda t} = -[\bar{x} + x' e^{\lambda t}][\bar{z} + z' e^{\lambda t}], \quad (3.19)$$

$$\lambda z' e^{\lambda t} = -Q + [\bar{x} + x' e^{\lambda t}][\bar{y} + y' e^{\lambda t}]. \quad (3.20)$$

Note this is a linear analysis and any nonlinear terms will be neglected. For example, the multiplication of  $x'y'$  will result in an infinitesimally small nonlinear terms so it will be neglected in this analysis. After mathematical reductions, these equations simplify to the following:

$$-(\lambda + 1)x' + (\cos \alpha)y' + (-\sin \alpha)z' = 0, \quad (3.21)$$

$$(\bar{z})x' + (-\lambda)y' + (-\bar{x})z' = 0, \quad (3.22)$$

$$(\bar{y})x' + (\bar{x})y' + (-\lambda)z' = 0. \quad (3.23)$$

These equation can now be put into matrices to combine the eigenvalues  $\lambda$ ,

$$\begin{bmatrix} -(\lambda + 1) & \cos \alpha & -\sin \alpha \\ \bar{z} & -\lambda & -\bar{x} \\ \bar{y} & \bar{x} & -\lambda \end{bmatrix} \begin{bmatrix} x' \\ y' \\ z' \end{bmatrix} = \begin{bmatrix} 0 \\ 0 \\ 0 \end{bmatrix},$$

where the determinant of the matrix must equal zero and results in the following

polynomial,

$$\lambda^3 + \lambda^2 + \lambda \left( Q \cos \alpha + \sqrt{\frac{Q}{\cos \alpha}} \sin \alpha \right) + 2Q \cos \alpha = 0. \quad (3.24)$$

This third order polynomial will produce three roots including the real part which can be positive, zero, or negative. A positive real root will produce an unstable oscillator and cause the system to be unstable. A zero root will produce an undamped oscillator, causing the system to remain in a repeating cycle. A negative root will produce a damped oscillator and will reach a stable condition. Consider using synthetic division on this polynomial to get a root of  $-1$ . To get an exact root, the last term in the division slot must equal 0, shown below,

$$2Q \cos \alpha - Q \cos \alpha - \sqrt{\frac{Q}{\cos \alpha}} = 0, \quad (3.25)$$

$$Q = \frac{\sin^2 \alpha}{\cos^3 \alpha}. \quad (3.26)$$

This means for the initial eigenvalue polynomial to have a root of  $-1$ , the above must be true. The remainder polynomial can be solved as follows:

$$\lambda^2 + Q \cos \alpha + \sqrt{\frac{Q}{\cos \alpha}} \sin \alpha = 0, \quad (3.27)$$

$$\lambda = \pm \sqrt{2Q \cos \alpha} i. \quad (3.28)$$

This provides three eigenvalues:  $(-1, +\sqrt{2Q \cos \alpha} i, -\sqrt{2Q \cos \alpha} i)$ . Next, the Routh-Hurwitz Stability Criterion (RHSC), as covered by K. Ogata [29], can be applied to check for unstable roots and evaluate stability in a control system. A detailed description can

Table 3.1: Routh-Hurwitz stabilization criterion table.

Eigenvalues	Column 1	Column 2	Column 3
$\lambda^3$	1	$Q \cos \alpha + \sqrt{\frac{Q}{\cos \alpha}} \sin \alpha$	0
$\lambda^2$	1	$2Q \cos \alpha$	0
$\lambda^1$	$\sqrt{\frac{Q}{\cos \alpha}} \sin \alpha - Q \cos \alpha$	0	0
$\lambda^0$	$2Q \cos \alpha$	0	0

be found in Appendix B, below is a summary applicable to the current study. First, the coefficients,  $a_1, a_2, a_3$ , are identified from the polynomial. Then, according to the RHSC, the rest of the coefficients are calculated. For this case those are  $b_1, b_2, c_1$ . These coefficients are then arranged into a table as shown below:

If the coefficients in column 1 of Table 3.1 are all positive, the system can be considered stable. This provides two conditions that must be considered. The first conditions is shown below:

$$\sqrt{\frac{Q}{\cos \alpha}} \sin \alpha - Q \cos \alpha \geq 0, \quad (3.29)$$

$$Q \leq \frac{\sin^2 \alpha}{\cos^3 \alpha}, \quad (3.30)$$

followed by the second condition:

$$2Q \cos \alpha \geq 0, \quad (3.31)$$

$$\cos \alpha \geq 0, \quad (3.32)$$

$$-90^\circ \geq \alpha \geq 90^\circ. \quad (3.33)$$

A final test is to determine if the system is dissipative, meaning, the right-hand side of

the governing equations diverge to  $-1$ . This is done by using the nabla operator on the governing equations as shown below:

$$\frac{dx}{dt} = -x + y \cos \alpha - z \sin \alpha, \quad (3.34)$$

$$\frac{dy}{dt} = -xz, \quad (3.35)$$

$$\frac{dz}{dt} = -Q + xy. \quad (3.36)$$

These equations are then put into the form of  $\dot{x} = Ax + b$ ,

$$\begin{bmatrix} \dot{x} \\ \dot{y} \\ \dot{z} \end{bmatrix} = \begin{bmatrix} -1 & \cos \alpha & -\sin \alpha \\ 0 & 0 & -x \\ 0 & x & 0 \end{bmatrix} \begin{bmatrix} x \\ y \\ z \end{bmatrix} + \begin{bmatrix} 0 \\ 0 \\ -Q \end{bmatrix} .$$

The nabla operator is then used on the system to determine if the system diverges,

$$\nabla \cdot (Ax + b) = \begin{bmatrix} \frac{\partial}{\partial x} & \frac{\partial}{\partial y} & \frac{\partial}{\partial z} \end{bmatrix} \begin{bmatrix} -x + y \cos \alpha - z \sin \alpha \\ -xz \\ -Q + xy \end{bmatrix} .$$

Expanding the equation results in the following:

$$\nabla \cdot (Ax + b) = \frac{\partial}{\partial x}(-x + y \cos \alpha - z \sin \alpha) + \frac{\partial}{\partial y}(-xz) + \frac{\partial}{\partial z}(-Q + xy) \quad (3.37)$$

$$\nabla \cdot (Ax + b) = -1 \quad (3.38)$$

In agreement with Sen et al. [28] who analyzed the same system, the negative value  $(-1)$

indicates the system is dissipative. This means any initial volume will shrink. If the right hand side contained a positive value, the system will increase exponentially and blow up. If the value is zero, there is neither an increase or decrease, the system remains the same as we see in mass conservation. The analysis conducted in this section produces a linear stability curve graph that can predict the stability of this system.

Consider the range  $0 < \alpha < 90^\circ$ ,  $P_1$  is stable while  $Q \leq \sin^2 \alpha / \cos^3 \alpha$  [10]. This linear stability curve is shown below in Figure 3.1 and shows the relationship between fluid flow stability, heat input, and tilt angle variables which provides the foundation for developing a control strategy. This behavior will be discussed in the next section.

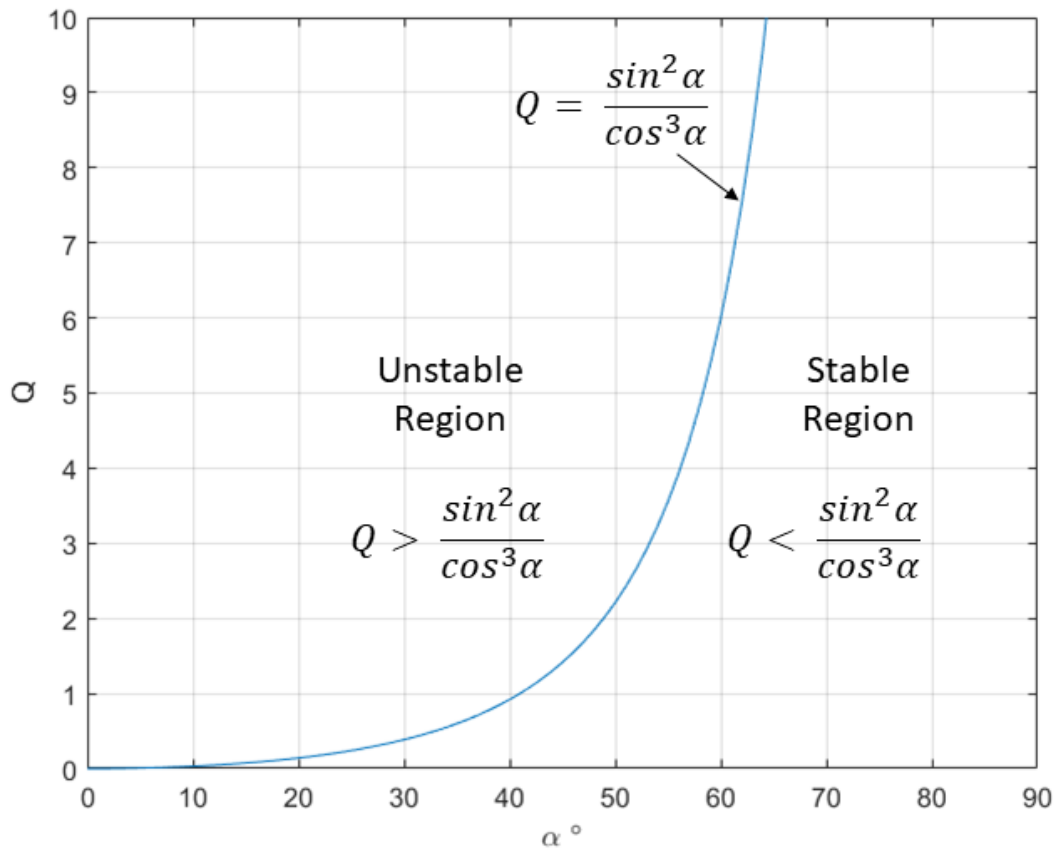


Figure 3.1: Linear stability curve.

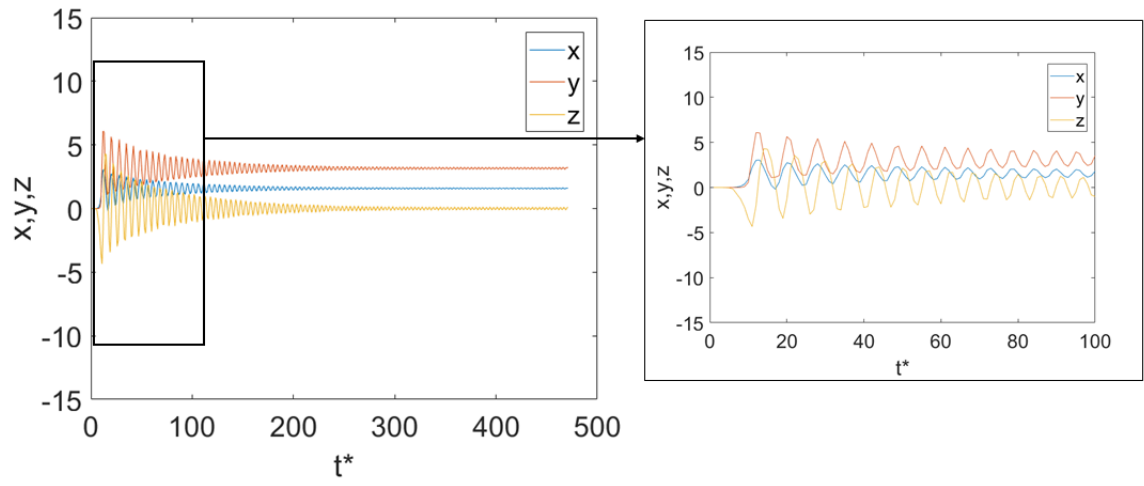
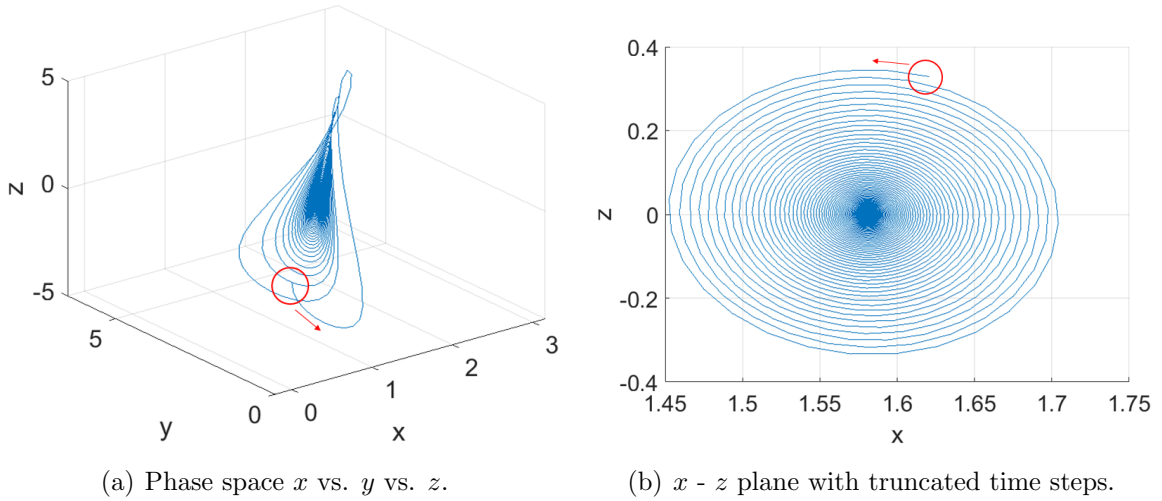
### 3.4 Stable, Oscillatory, and Chaos Dynamics

In the previous section, criteria for system stability were established along with a graph that connected system inputs,  $\alpha$  and  $Q$ , to stability behavior. Consider the range  $0 < \alpha < 90^\circ$  which contains the positive critical point  $P_1$  and the initial values of 0 for  $x, y, z$ . Three distinct behaviors can be observed: stable, oscillatory and chaotic.

For  $Q < \sin^2 \alpha / \cos^3 \alpha$ , the real eigenvalue root is negative and the critical point  $P_1$  is stable. Figure 3.2 shows the  $x, y, z$  values as they all stabilize with values of  $Q = 5$  and  $\alpha = 60^\circ$ . In Figure 3.2(a) the red arrow and circle indicate time step zero and the direction it initially moves in. In Figure 3.2(b), the time steps have been truncated to show the stable region, however, the  $x$  value continues to decrease so any range of time steps will produce the same view.

For  $Q = \sin^2 \alpha / \cos^3 \alpha$ , the real eigenvalue root is zero and the critical point  $P_1$  is neutrally stable. Figure 3.3 shows the  $x, y, z$  values as they begin to oscillate. They will not stabilize to a constant value, but will remain oscillatory within a fixed range at the neutral stability curve with values of  $Q = 5$  and  $\alpha = 58^\circ$ . In Figure 3.3(a) the red arrow and circle indicate time step zero and the direction it initially moves in. In Figure 3.2(b), the time steps have been truncated to only show region where the oscillations remain constant. The constant oscillations at a constant range are apparent as the shape repeats itself within 3 square units.

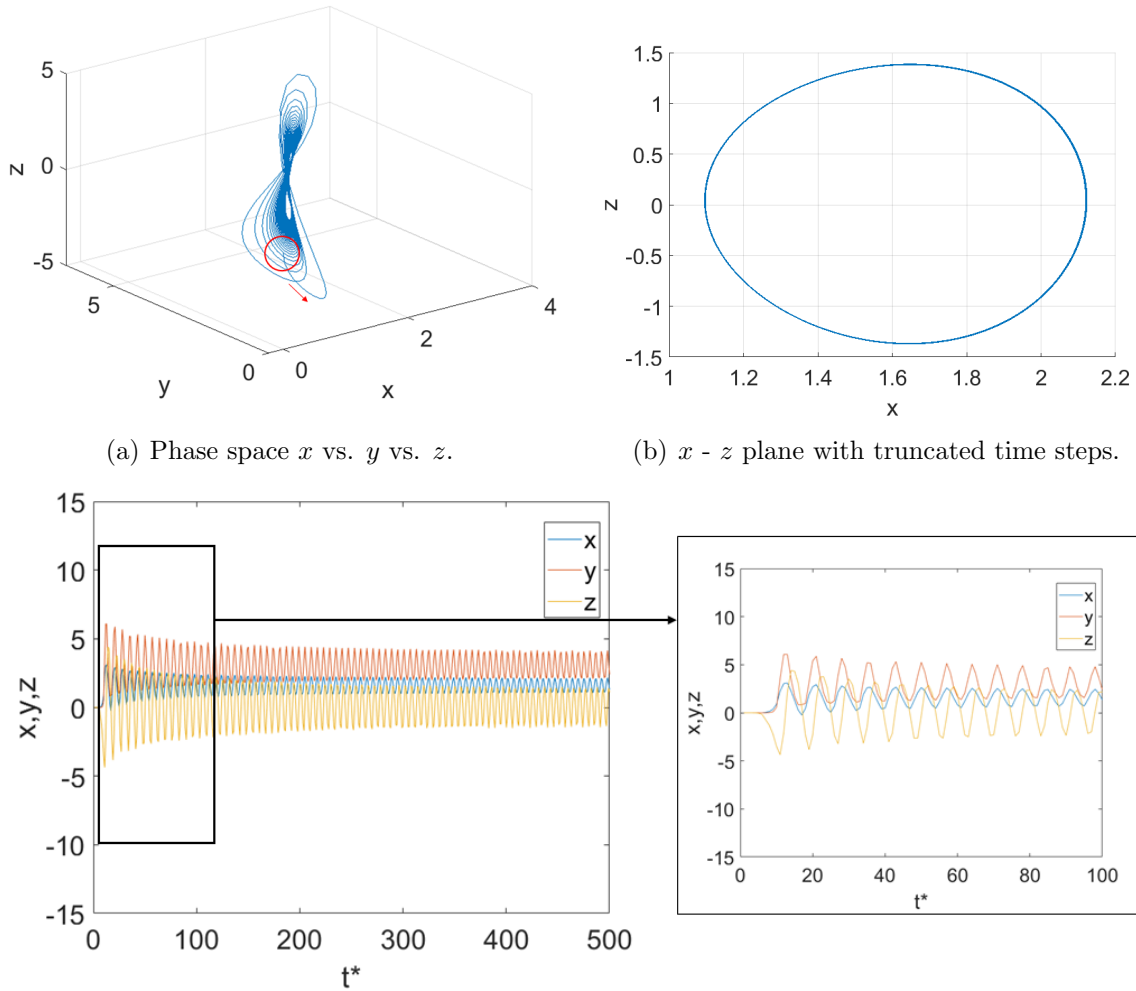
A combination of oscillatory and chaotic behavior can be observed when the value of  $\alpha$  is chosen close to the stability line,  $\alpha = 50^\circ$  for example. By definition it has a positive eigenvalue root so it should display chaotic behavior, however, it displays limit



(c) Time-dependent solution for  $x$ ,  $y$ , and  $z$  with detailed inset view.

Figure 3.2: Stable behavior for  $Q = 5, \alpha = 60^\circ$ .

cycle behavior. Figure 3.4 shows the  $x, y, z$  values as they cycle within a certain range. They will not stabilize to a constant value, but will remain in limit cycles indefinitely with values of  $Q = 5$  and  $\alpha = 50^\circ$ . Further, note the behavior does not decrease to the given cycle as observed in  $\alpha = 58$ , but rather increases. This was also observed in the research done by Sen et al. [28]. In Figure 3.4(a) the red arrow and circle indicate time step zero and the direction it initially moves in. In Figure 3.4(b), the time steps have been truncated to only show region where the oscillations remain constant. The



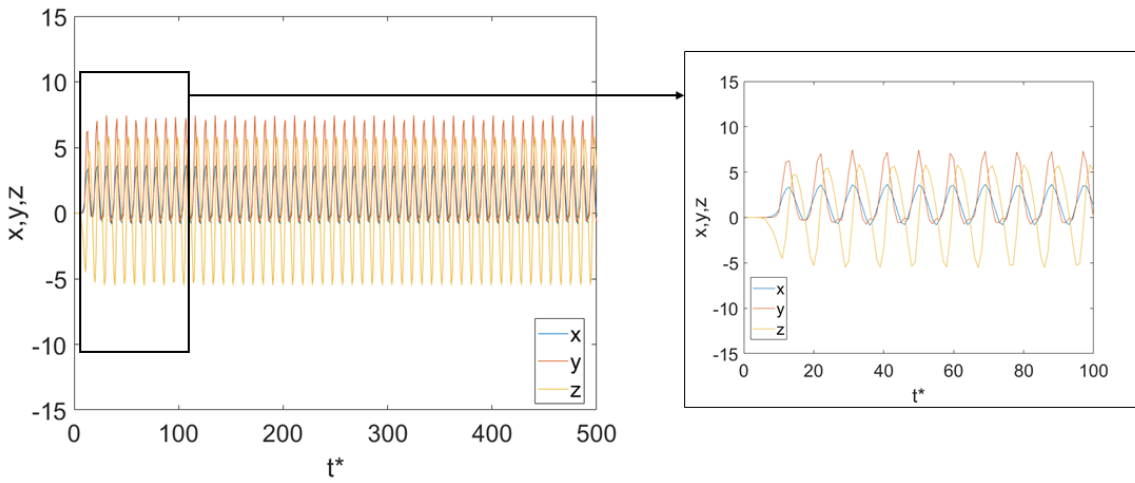
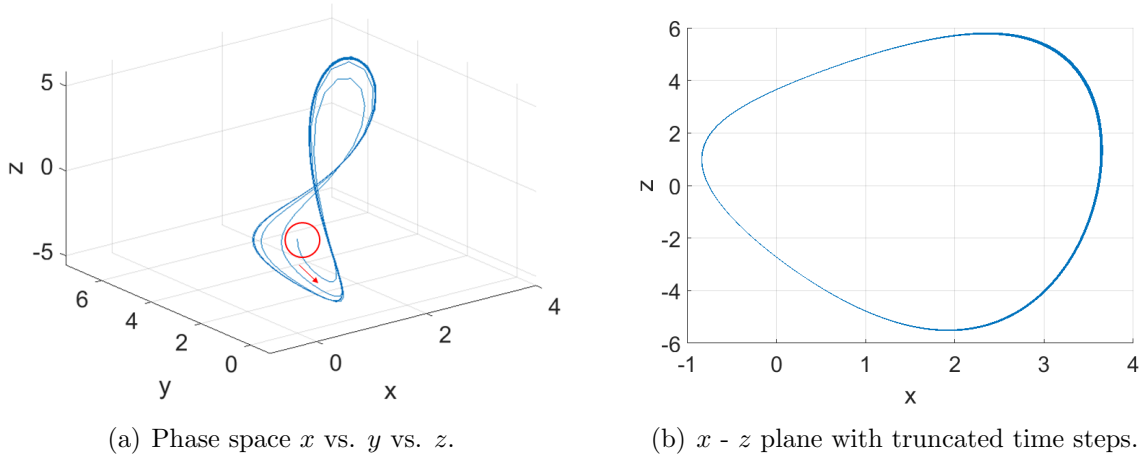
(c) Time-dependent solution for  $x$ ,  $y$ , and  $z$  with detailed inset view.

Figure 3.3: Oscillatory behavior at the neutral stability curve for  $Q = 5, \alpha = 58^\circ$ .

oscillations within a constant range are apparent as the shape repeats itself, however, different from the previous examples this shape has expanded into 72 square units.

For  $Q > \sin^2 \alpha / \cos^3 \alpha$ , the real eigenvalue root is positive and the critical point  $P_1$  is unstable. Figure 3.3 shows the  $x, y, z$  values as they do not stabilize to any value nor show any repetitive motion with values of  $Q = 5$  and  $\alpha = 30^\circ$ . In Figures 3.5(a) and 3.5(b), two distinct attractor points can be observed that the system orbits around.

In the next chapter, a review of fuzzy logic will be covered to explain how a controller



(c) Time-dependent solution for  $x$ ,  $y$ , and  $z$  with detailed inset view.

Figure 3.4: Limit cycle behavior with chaos parameters for  $Q = 5, \alpha = 50^\circ$ .

can maintain stability in this system.

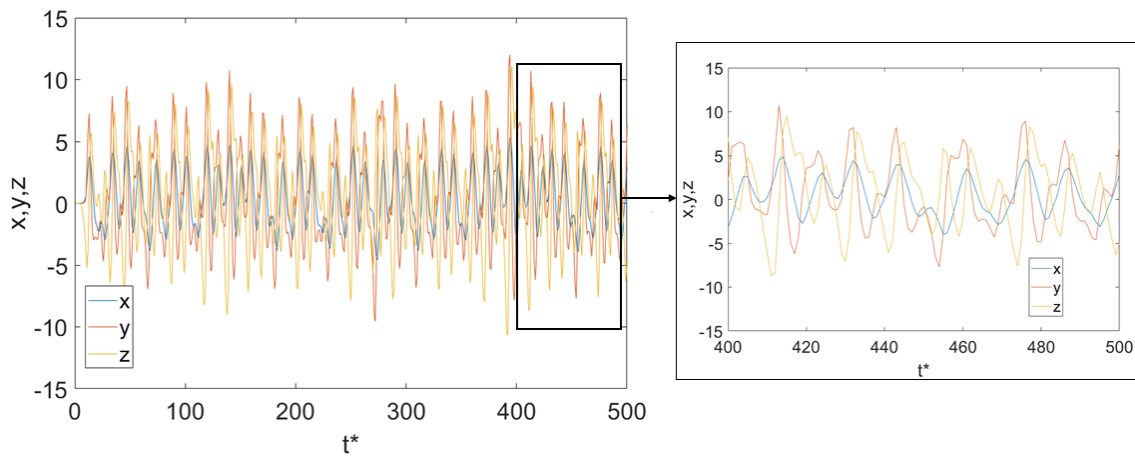
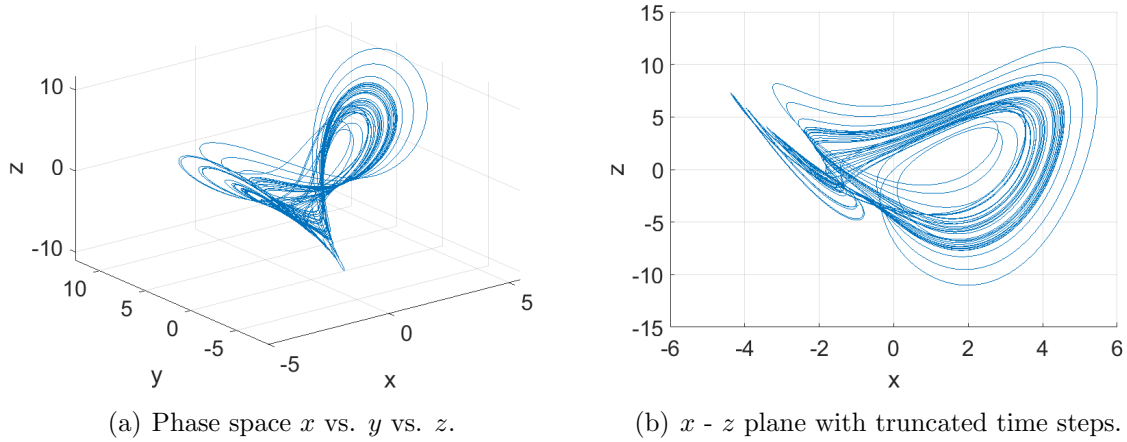


Figure 3.5: Chaos behavior for  $Q = 5, \alpha = 30^\circ$ .

## CHAPTER 4

### Introduction to Fuzzy Logic

The previous chapter described the dynamics of the heat convection loop as well as the key inputs and outputs that define its behavior. This chapter will focus on the background and concepts of fuzzy logic; the means by which the dynamic system will be controlled. Fuzzy logic (FL) is an if-then rule based method that uses non-rigid linguistic variables to describe an imprecise system [11]. Fuzzy logic has been used in many engineering applications including heat transfer and building temperature control systems [30]. This chapter will include an introduction of fuzzy logic, its application, membership functions and their relevance to fuzzy sets, fuzzy inference systems, fuzzy rules, and defuzzification. To conclude, a summary will be provided that ties all of the key concepts together to prepare the reader for controller development in the following chapter.

#### **4.1 Background on Fuzzy Logic**

In 1965 Lotfi Zadeh introduced the idea of fuzzy sets and challenged traditional binary logic [16, 17]. Traditional controllers are able to provide a high level of precision in complex problems, however, the higher the complexity and precision the higher the cost of time and/or resources. Furthermore, a problem may be too complex or not understood well enough that a precise controller may not be a viable option [16]. Fuzzy logic introduces a solution to control a problem that does not require a high level of precision or if the problem itself is not well understood [16]. It takes advantage of the use of linguistic variables, such as “young” and “old”, that can build logic based on human intuition. Fuzzy logic uses imprecise terms to describe a system. A good example is how we use

age to determine if someone is young or old? Let's take a general age range of 0 to 80, and say the 40 years old is where we draw the line between young and old. Binary logic would tell us someone is fully in the young category until moments before turning 40, then immediately fully belongs to the old category the next day. So, if a person is 39 years, 11 months, 29 days, they are still in the young category, then the next day they will belong to the old category. Not a very smooth transition and it doesn't seem like that's how it happens. Fuzzy logic can define that someone belongs to the fully young group from 0-20, and belongs to the fully old group from 60-80. In between those ages, a person can belong to both groups in varying degrees. Let's look at the age of 30; you belong more in the young category, but you also belong a little to the old category, or at least more than someone who is 20. This provides a transition from the young category to the old category instead of a complete switch from one day to another. This also feels more intuitive about how someone goes from being young to being old.

This highlights the concept of something not fully belonging to one group or another, but somewhere in between. Fuzzy logic can primarily be useful in two scenarios: where a cause-and-effect system can be observed but not completely understood, and where quickness takes priority over precision [16].

In a fuzzy logic control system, an input signal must be received and assigned to a set based on defined membership functions (fuzzification), put through a fuzzy inference system, then converted into an output signal (defuzzification) and delivered to the plant model. In this study, the Mamdani inference method will be used as it is the most common but there are others that have been developed such as the Sugeno and Tsukamoto methods [16].

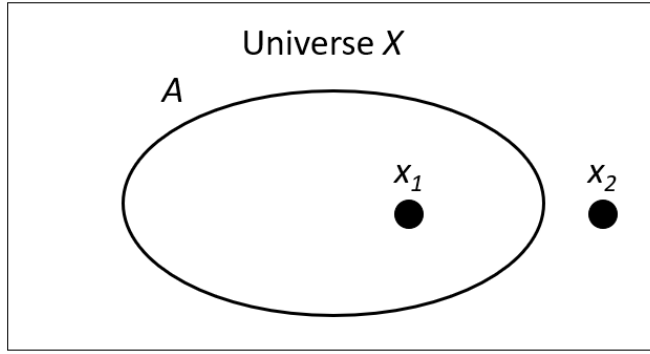


Figure 4.1: Universe  $X$ , set  $A$ , and elements  $x_1$  and  $x_2$ .

#### 4.1.1 Crisp Sets, Fuzzy Sets and Membership Functions

Fuzzy sets can be best described by first looking at crisp sets. Let us consider a given Universe  $X$ , which contains elements  $x_1$  and  $x_2$ . These elements can either belong or not belong to any given crisp set. In other words, a set is a clearly defined collection of elements. This is illustrated in Figure 4.1 with universe  $X$ , element  $x_1$  that belongs to set  $A$ , and element  $x_2$  that does not.

A crisp membership function,  $\mu(x)$ , determines if an element belongs to a set. Eq. (4.1) shows a crisp membership function  $\mu_A$  that maps an element  $x_i$  to set  $A$ . If  $x$  belongs to set  $A$ , then  $\mu(x) = 1$ . If not,  $\mu(x) = 0$ .

$$\mu_A(x) = \begin{cases} 0, & x \notin A \\ 1, & x \in A \end{cases} \quad (4.1)$$

In fuzzy sets, elements can belong to single or multiple sets and in varying degrees, depending on how the membership function is defined. A fuzzy membership function  $\mu_{\underline{A}}$

can have a value from 0 to 1, notated as

$$\mu_{\underline{A}}(x) \in [0, 1]. \quad (4.2)$$

Note fuzzy sets will be marked with a tilde underscore. Fuzzy sets that contain multiple elements in varying degree of memberships can be defined specifically as

$$\underline{A}(x) = \left\{ \sum_i \frac{\mu_{\underline{A}}(x_i)}{x_i} \right\}, \quad (4.3)$$

where the numerator is the membership function that maps its element to the correct set, and the denominator is the element.

Fuzzy memberships can have a variety of profiles; three commonly used ones are Trapezoid, Triangle, and Gaussian. The best function to use depends on the application, there is not one that is better or worse to use than the other. It is important to evaluate the different membership functions to determine which one works best for a given application. Their notation and graphs are located below:

*Triangular membership function*

$$f(x; a, b, m) = \begin{cases} 0, & x \leq a \\ \frac{x-a}{m-a}, & a < x \leq m \\ \frac{b-x}{b-m}, & m < x < b \\ 0, & x \geq b \end{cases} \quad (4.4)$$

*Trapezoidal membership function*

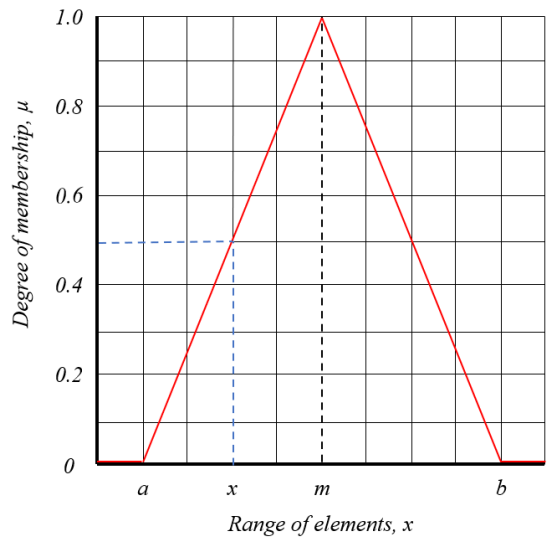
$$f(x; a, b, c, d) = \begin{cases} 0, & x \leq a \\ \frac{x-a}{b-a}, & a \leq x \leq b \\ 1, & b \leq x \leq c \\ \frac{d-x}{d-c}, & c \leq x \leq d \\ 0, & x \geq d \end{cases} \quad (4.5)$$

*Gaussian membership function*

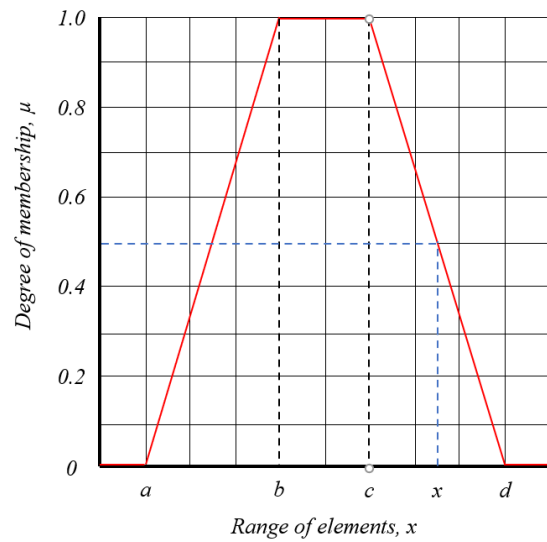
$$f(x; a, c, \sigma) = e^{-\frac{(x-c)^2}{2\sigma^2}} \quad (4.6)$$

The key parameters of the triangular function are its lower bounds,  $a$  and  $b$ , and its center  $m$ . The trapezoid has  $a$  and  $d$  as its lower bounds, and  $b$  and  $c$  as its upper bounds. The Gaussian has its center  $c$ , and standard deviation  $\sigma$ . These membership functions are what make a crisp value input signal into a fuzzy value: the definition of fuzzification. After fuzzification, the values will go through the inference engine which uses a rule base to output another fuzzy value. It will then go through defuzzification which will take that fuzzy value and convert it back into a crisp value output signal for the fuzzy logic controller. This process is illustrated in Fig. 4.3.

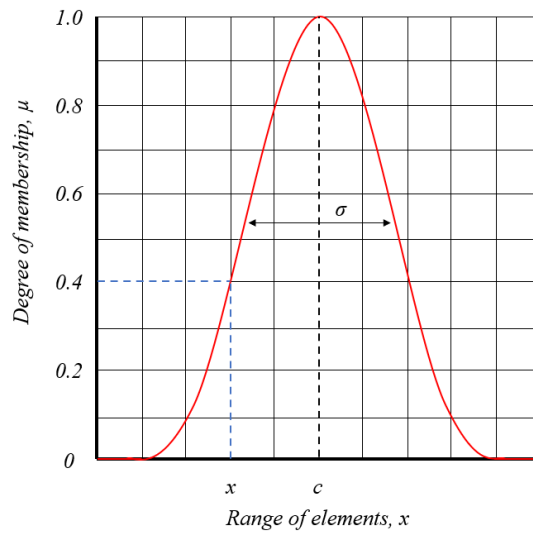
Fuzzy set operations are similar to those of crisp sets and use the standard union, intersection, and complement logic operators described in Figure 4.4 and Eqs. (4.7)-(4.9) for both crisp and fuzzy sets:



(a) Triangle membership function.



(b) Trapezoid membership function.



(c) Gaussian membership function.

Figure 4.2: Common types of membership functions.

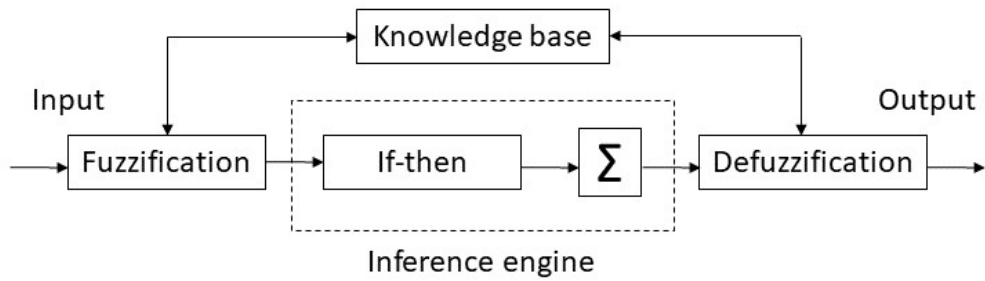


Figure 4.3: Fuzzy logic inference engine diagram.

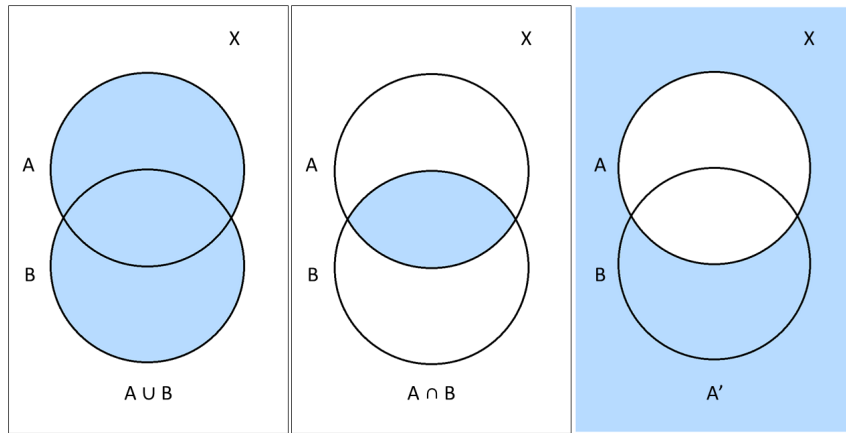


Figure 4.4: Logic operators; union, intersection, and complement.

$$\textit{Complement}; \quad \bar{A} = \{x|x \notin A, x \in X\} \quad (4.7)$$

$$\textit{Union}; \quad \underline{A} \cup \underline{B} = \{x|x \in \underline{A} \text{ or } x \in \underline{B}\} \quad (4.8)$$

$$\textit{Intersection}; \quad \underline{A} \cap \underline{B} = \{x|x \in \underline{A} \text{ and } x \in \underline{B}\} \quad (4.9)$$

The next section will cover the inference engine and knowledge base in more detail.

### 4.1.2 Inference Systems and Knowledge Base

There are several inference methods such as the Mamdani systems, Sugeno models, and Tsukamoto models [16]. This research will use the Mamdani method as it is the most common in practice [16]. This inference method defines antecedents (inference inputs), applies if-then rules based on logical operators built from a knowledge base, and produces consequents (inference outputs). In other words it takes a set or sets of fuzzy values from fuzzification, transforms them using linguistic variables based on established rules, then produces another fuzzy set to be defuzzified in the next step.

To explain this inference system, consider a two-valve shower that provides water temperature from 60°F to 120°F. From experience (the knowledge base in this example), one can conclude the water will come out cold, warm, or hot. With the cold water valve completely open, the temperature of the water can be controlled by opening or closing the hot water valve. These linguistic variables and their corresponding membership functions are mapped out in Figure 4.5. Consider two temperature values shown in the figure: 70°F (green line) and 80°F (purple line) and assume the desired temperature is 90°F. If the water comes out at 70°F, it will map to only one set, “cold”, with a  $\mu$  value of 1.0. At this temperature, one may want to open the hot water valve fully open to achieve the desired 90°F. However, if the water comes out at 80°F, this maps to two sets, cold and warm, with  $\mu$  values of 0.7 and 0.3 respectively. At this temperature, one may not want to open the hot water valve all the way, but likely more open than closed to still increase the water temperature. These two examples show the sliding scale of values and decisions that can be made by the Mamdani inference engine. These rules can be mapped out in a

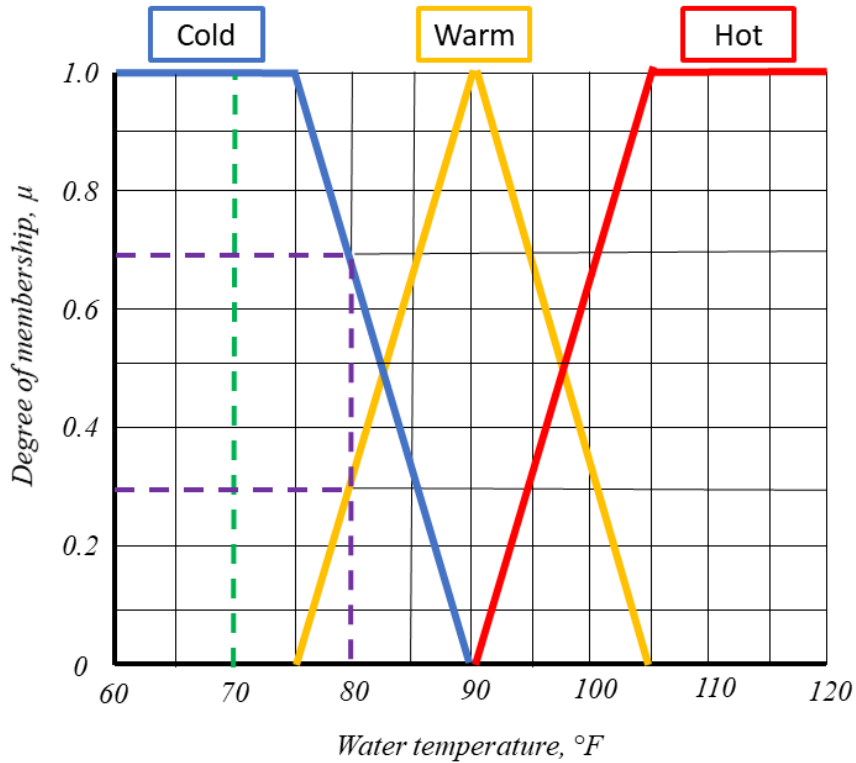


Figure 4.5: Example of membership functions for cold, warm, and hot water.

Table 4.1: General example of a truth table.

$z$	$x_1$	$x_2$
$y_1$	$z_1$	$z_2$
$y_2$	$z_3$	$z_4$

truth table for more complex systems, a general example is shown in Table 4.1 for inputs  $x$  and  $y$ , with output  $z$ . This table shows two input variables,  $x$  and  $y$ , which two each fuzzy sets  $x_1, x_2, y_1, y_2$ , that can be joined by the logic operators previously discussed: *and*, *or*. The inference engine determines the strength of each rule and applies it. For example an IF-THEN rule can be as follows: IF an input element (antecedant) belongs to set  $x_1$  AND  $y_2$  THEN the output element (consequent) belongs to set  $z_3$ .

After going through the inference engine, the fuzzy values must be converted back into crisp values through the defuzzification process described in more details in the next

section.

### 4.1.3 Defuzzification

Input values that have gone through membership functions, assigned to sets, and put through an inference system need one more step before becoming output values. Defuzzification is the last step in this process. Common methods include “max membership”, “centroid”, and “weighted”. [16]. The max membership method uses the single peak of the membership functions to determine the  $z$  output. The centroid method treats the membership functions as areas and calculates the centroid of the combined shape to determine the  $z$  output. The weighted average method takes the average of each membership function, then averages that to determine the  $z$  output. These methods are defined mathematically below:

*Max membership principle*

$$\mu_c(z^*) \geq \mu_c(z), \text{ for all } z \in Z \quad (4.10)$$

*Centroid method*

$$z^* = \frac{\int \mu_c(z) \cdot z dz}{\int \mu_c(z) dz} \quad (4.11)$$

*Weighted average*

$$z^* = \frac{\sum \mu_c(\bar{z}) \cdot \bar{z}}{\sum \mu_c(\bar{z})} \quad (4.12)$$

The centroid method is the most prevalent method which will be used in this research [16]. An example of the Mamdani inference method and a centroid defuzzification method is shown in Figure 4.6. Note the input signal is 80°F. The input membership functions

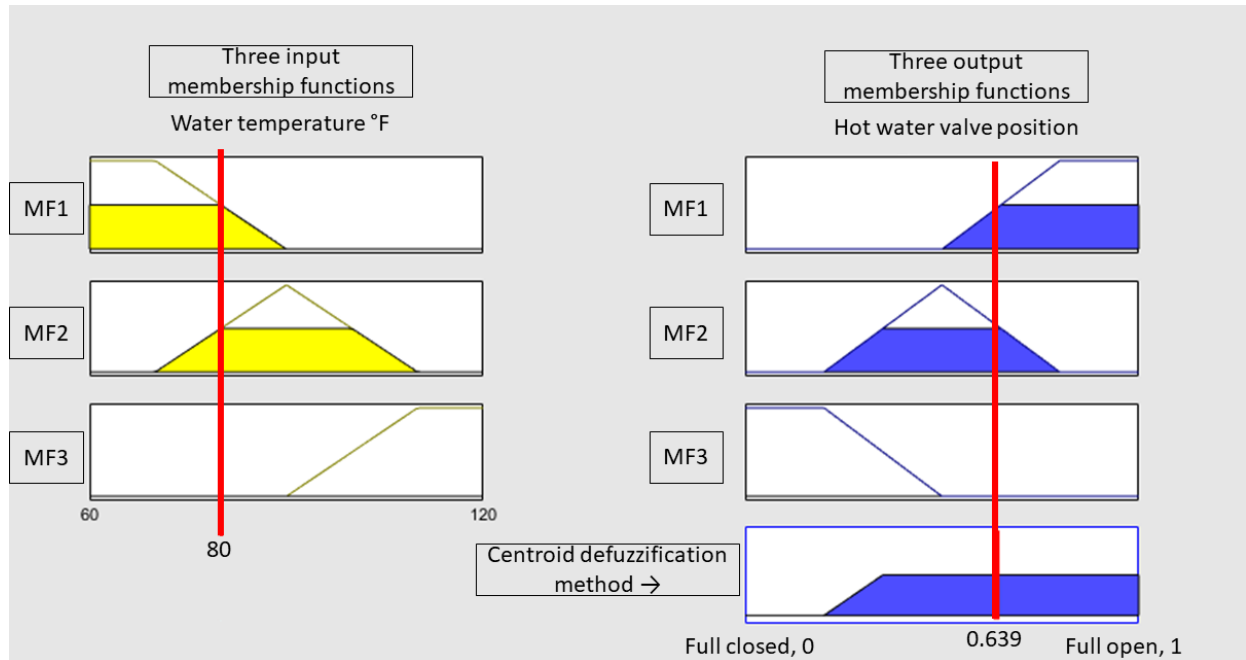


Figure 4.6: Mamdani inference method and centroid defuzzification method.

turn that crisp value into a set of fuzzy values. The inference engine then maps the three input and output membership functions, to produce a set of output fuzzy variables. The centroid method then turns that fuzzy set back into a crisp value to send along to the plant model. Now, a logical check can be discussed. This is taken from the earlier example: the desired temperature is 90°F so if the temperature is 80°F, one may open the valve not fully, but partially and more open than closed. The valve position of 0.639 reflects that as it is closer to 1.0, or fully open, and is expected to increase the water temperature.

To summarize, a fuzzy logic controller using the Mamdani inference engine performs

the following steps:

- Establish the fuzzy rules and input/output membership functions from a knowledge base
- Use the membership functions to convert the crisp values into fuzzy values
- Determine rule strength from fuzzy inputs (antecedants) to apply to output membership functions
- Sum up the output fuzzy values (consequents) to defuzzify into crisp output values

The next chapter will use the background and examples provided in this chapter to describe how the controllers were built and implemented for the current research.

## CHAPTER 5

### System and Stability Analysis

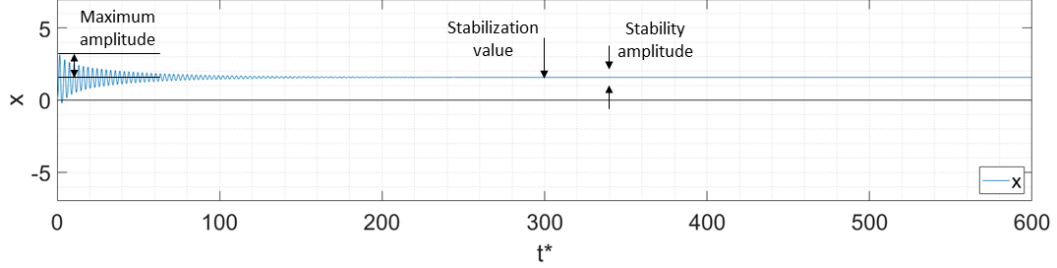
In the previous chapter, fuzzy logic background and controller design concepts were discussed. This chapter will discuss the development, design, and implementation of three fuzzy logic controllers, each one using more information than the one before it. First, a stable system without a controller will be analyzed to develop a baseline for comparison to a controlled system. Then, each controller design will be discussed. Lastly, the controller's ability to stabilize the system will be evaluated in three different applications: 1) evaluate controller functionality by holding heat input steady at  $Q = 5$  and controlling the tilt angle with an initial value of  $\alpha = 30^\circ$ , 2) evaluate disturbance rejection by changing values of  $Q$  in different increments while still using  $\alpha$  to control the system, and 3) evaluate disturbance rejection using the previous method but as  $Q$  changes, so does the setpoint for  $x$ .

#### 5.1 System Behavior without a Controller

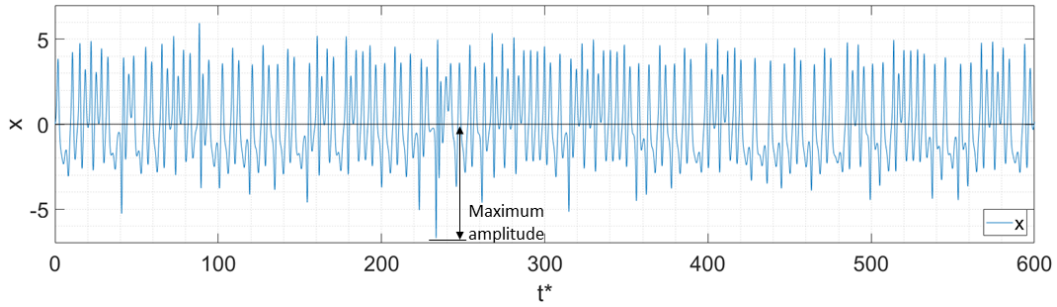
Numerical simulations were ran in MatLab using a custom 4th order Runge-Kutta code to solve the governing system of ODEs given in Eqs.(3.34)–(3.36) (provided in Appendix C). As covered in Chapter 3, the system can behave in a stable, oscillatory, or in a chaotic manner. The numerical simulation results provide the ability to predict what behavior will result from various combinations of inputs for the controller. Given a value of the heat input value  $Q = 5$  and values of  $\alpha = 60^\circ$ ,  $58^\circ$ , and  $30^\circ$ , Table 5.1 highlights the qualitative and quantitative flow characteristics. Maximum amplitude is the maximum value of  $x$  at any point during the simulation. Stabilization value is the  $x$  value after

Table 5.1: Quantitative measures of the dynamic behavior for the fluid velocity,  $x$ .

Input values	Dynamic behavior	Maximum amplitude	Stabilization value	Stability amplitude
$Q = 5, \alpha = 60$	Stable	1.68	1.58	0
$Q = 5, \alpha = 58$	Oscillatory	1.72	n/a	n/a
$Q = 5, \alpha = 30$	Chaotic	6.48	n/a	n/a



(a) Stable system for  $Q = 5$  and  $\alpha = 60^\circ$ .



(b) Chaotic system for  $Q = 5$  and  $\alpha = 30^\circ$ .

Figure 5.1: Baseline system behavior without a controller.

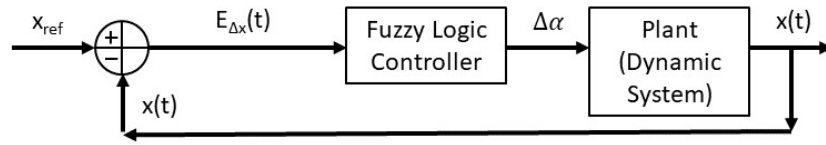
the system has stabilized, if applicable. Stability amplitude is the  $x$  value at which the system stabilizes to, if applicable. Figure 5.1 highlights these characteristics. From these simulations, it was observed that for  $Q = 5$  and  $\alpha = 60$  the  $x$  values will stabilize to 1.549 (which matches its steady state value  $P_1$ ) with a maximum amplitude of 0; complete stability. This is a critical parameter to evaluate stability discussed later in this section. The oscillatory and chaotic systems do not stabilize as observed earlier in Chapter 3.

It is to note that the three dependent variables, the nondimensional velocity, and the two Fourier coefficients of fluid temperature,  $x(t)$ ,  $y(t)$  and  $z(t)$ , are interconnected by the physics of the process of heat transfer by convection. Therefore, the three variables will not separate into different behaviors; if one is stable then the others will also be. From this fact, only  $x$  will be used to determine how much the tilt angle  $\alpha$ , would need to be changed. The error value  $\Delta x$ , will dictate the how much  $\Delta\alpha$  will change until the system stabilizes. The next section will cover controller development.

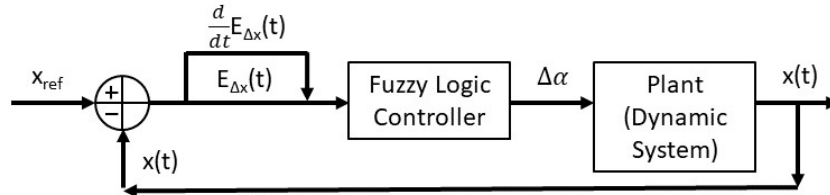
## 5.2 Fuzzy Logic Controller Development and Strategy

To develop a fuzzy logic controller, one must determine the range of input values, the type of membership functions (MF), the type of inference system, and expected output values. There are many different ways to implement these decisions into a controller and they can be derived from intuition, algorithms, or logical operations [16]. Intuition relies on previous experience from the user to determine what range of output should be expected from what range of input and is the method chosen for this study.

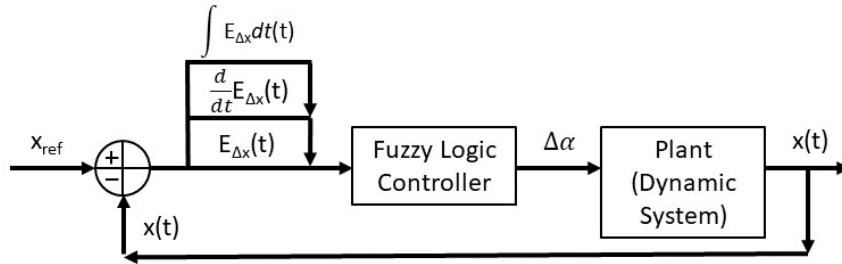
The objective of these controllers are to maintain the fluid flow setpoint inside the thermosyphon device while, at the same time, maintaining its stability. This is done by controlling the value of nondimensional velocity  $x$ , by adjusting the tilt angle  $\alpha$ , in a closed feedback loop. The initial setpoint was 1.549 as determined by the simulations performed in the previous section. As an example: if  $x$  was higher or lower than the setpoint, the system was not stable and the tilt angle  $\Delta\alpha$  needed to be increased. If  $x = 0$ , the system was stable and had the capacity for the flow to be increased slightly to match the possible change in the heat flux  $Q$ .



(a) Feedback loop using one input and one output.



(b) Feedback loop using two inputs and one output.



(c) Feedback loop using three inputs and one output.

Figure 5.2: Feedback loops with different number of inputs.

Three types of controllers have been developed: Fuzzy Logic Controller (FLC) 1, FLC 2, and FLC 3. The first uses the error ( $E_{\Delta x}$ ), which is the difference of  $x$  and the setpoint ( $x_{ref}$ ), as the single controller input, the second adds the derivative of the error ( $dE_{\Delta x}/dt$ ) as the second input, and the third adds the integral of the error ( $\int E_{\Delta x} dx$ ) as the third input. A schematic of each are shown in Figure 5.2.

The feedback loop starts with the setpoint, or reference, value which is the desired output value of the system. It then goes to the summation block which compares the incoming signal to the reference value, and in this case they are one in the same so the error signal is zero. Next, the controller takes that input value of zero and determines

an output value. In this case the input value is  $x$ , and the output value is the change in  $\alpha$ . The  $\alpha$  value is then fed into the plant, which contains the dynamic system. In experiemntal systems this is the test bed that produces signals from various instruments. This system is a simulated test bed so the governing system of equations produce the output signals. In the Simulink model, the three governing equations were solved using the built-in Runge-Kutta Fourth-order solver with a time step of 0.1. These simulations were ran using a 0.01 time step as well, but the results were the same. To reduce time, 0.1 was the chosen time step. Also, since this is a simulated system, an intial value can be assigned,  $\alpha = 30^\circ$  in this case. These output signals are whats recorded in the data loggers, and set back around to the summation block. The summation block compares the output signal  $x$  from the plant to the reference value. That difference is called the error ( $E_{\Delta x}$ ), which is again fed into the controller. This cycle repeats for the set amount of time steps. The fuzzy logic control paramters for each will be covered in the next sections.

### 5.2.1 Fuzzy Logic Controller 1

This fuzzy logic controller (FLC) uses a single-input single-output method for stability control, shown in Figure 5.3(a). The input is the difference value between  $x$  and  $x_{ref}$  as the error signal and the output is the change in  $\alpha$ . Figures 5.3(b)-5.3(c) show the membership functions of the input and output values,  $x$  and  $\Delta\alpha$ . Figure 5.3(d) shows the response line of the controller which provides a visual representation of how the error signal dictates the change in  $\alpha$ . For example if the error signal is approximately from -0.25 to 0.25, the controller will lower the value of alpha; if the error signal is outside of

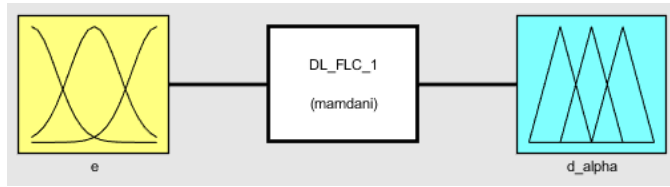
that range it will increase the value of alpha. Shown in Table 5.2 are the linguistic set of rules that have been developed.

Table 5.2: Decision table for tilt angle adjustment, FLC 1.

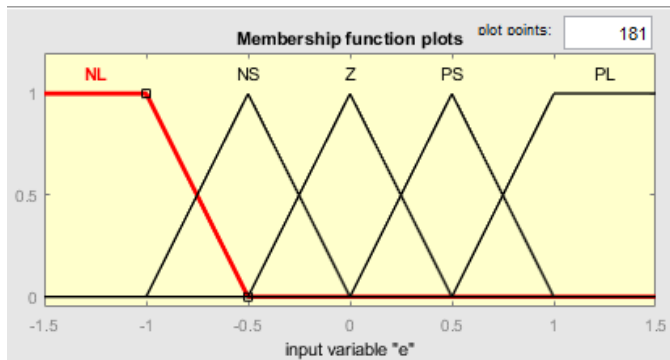
$E_{\Delta x}$	$\Delta\alpha^\circ$
Negative large (NL)	Increase large (IL)
Negative small (NS)	Increase small (IS)
Zero (Z)	Decrease small (DS)
Positive small (PS)	Increase small (IS)
Positive large (PL)	Increase large (IL)

To control the thermosyphon system, a feedback loop – shown in Figure 5.4 – was designed to test the ability of the fuzzy controller to manipulate the tilt angle to maintain stability of the system; i.e.,  $x$ ,  $y$  and  $z$ . The figure shows that the plant contains a Simulink block diagram that solves the system of non-linear ODEs [Eqs.(3.34)–(3.36)]. The initial reference for  $x$  is set to 1.549, which is perfect stability. A random value signal generator with an adjustable maximum amplitude can be used to induce perturbations in the  $x$ -value, simulating experimental data to test the controller. The cumulative block maintains the tilt angle value so a change in tilt angle can be added or subtracted after every time step. It can also set limits for maximum or minimum values of the tilt angle  $\alpha$ . To maintain an optimized value of  $x$ , the tilt angle was initially constrained to a maximum value of  $\alpha = 75^\circ$ . The cumulative block also allows for initial values of  $\alpha$  to be set. These conditions are used to determine if, when provided a value that should result in unstable behavior, the system can be stabilized.

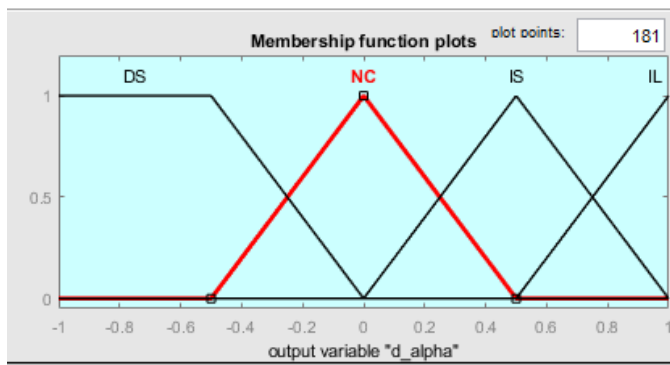
After several design iteration for this controller, a setpoint of 1.591 was assigned. This value will remain constant moving forward as well as the membership function ranges



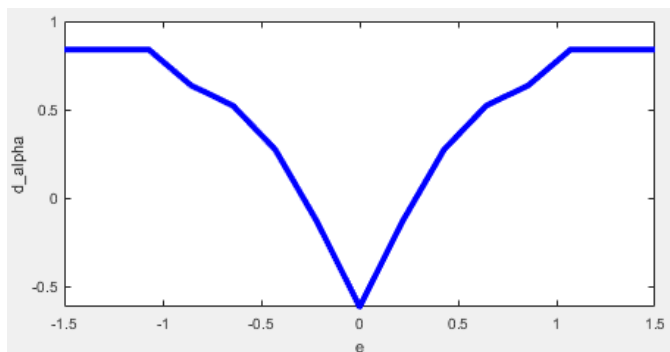
(a) FLC 1 using one input and one output.



(b) Membership functions for  $E_{\Delta x}$ .



(c) Membership functions for  $\Delta \alpha$  ( $^{\circ}$ ).



(d) Response line of FLC 1.

Figure 5.3: FLC 1 design parameters.

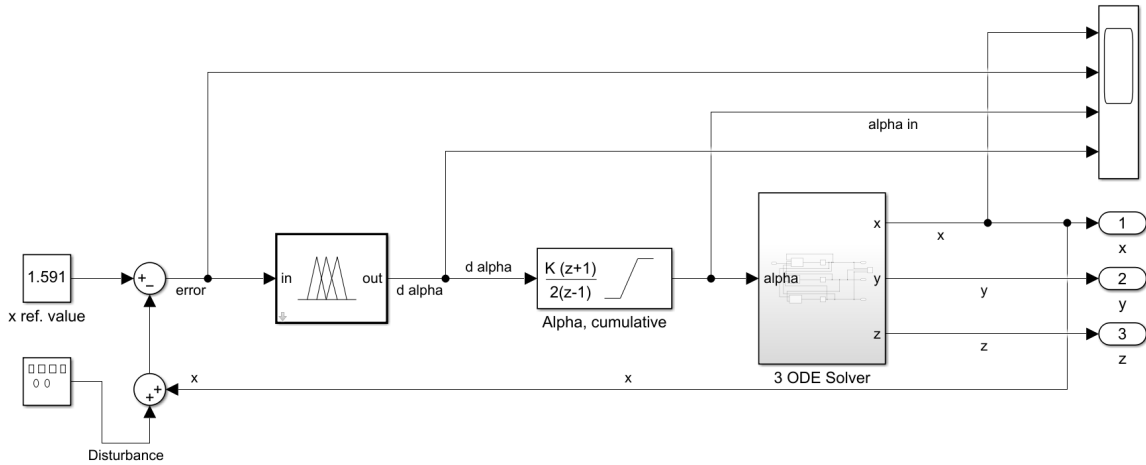
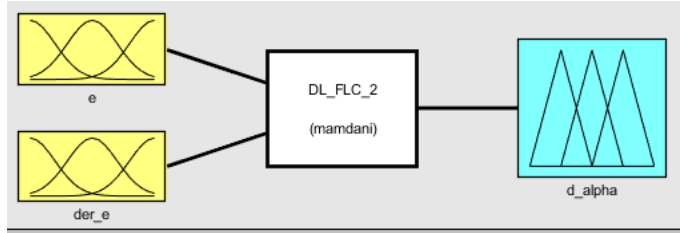


Figure 5.4: Feedback loop for the FLC 1.

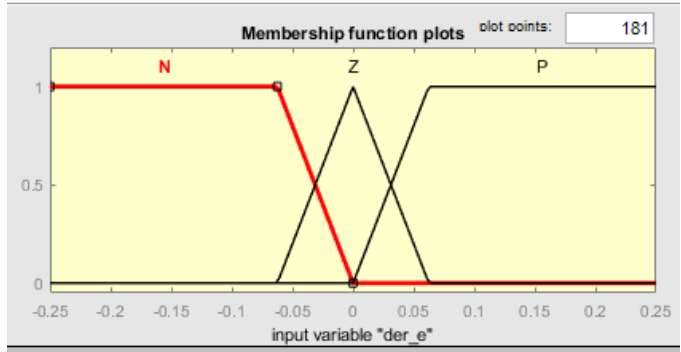
for  $E_{\Delta x}$  and  $\Delta\alpha$ . Additional iterations of this feedback loop and fuzzy logic controllers, were designed to include not only the signal error  $E_{\Delta x}$ , but the rate of change and the integration of it as well. The more information that is fed into the controller, the better it is expected to perform. These designs are covered in the next two sections.

### 5.2.2 Fuzzy Logic Controller 2

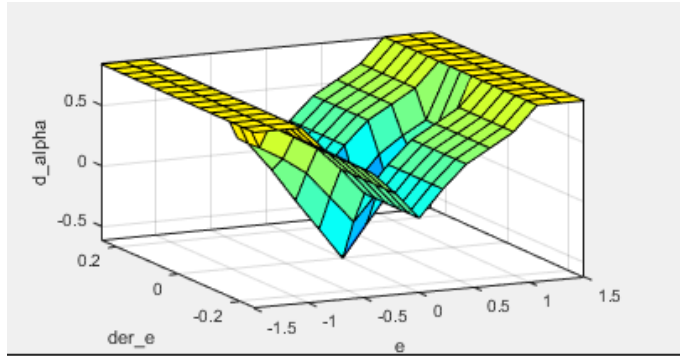
This controller uses a double-input single-output method for stability control, shown in Figure 5.5(a). The two inputs used are  $E_{\Delta x}$  and the change in  $E_{\Delta x}$ , and the output is the change in  $\alpha$ . Figures 5.5(b) show the membership function of the additional input; negative (N), zero (Z), and positive (P). Figure 5.5(c) shows the response plot of the controller which provides a visual representation of how the two input values dictates the change in  $\alpha$ . Shown in Table 5.3 are the linguistic set of rules that have been constructed. The rules can be read by taking an  $E_{\Delta x}$  MF value from any column, taking a  $dE_{\Delta x}/dt$  MF value from any row, and finding the  $\Delta\alpha$  value at their intersection. For example: if  $E_{\Delta x}$  is NS and  $dE_{\Delta x}/dt$  is N, then  $\Delta\alpha$  is IS. Values of NL and PL for  $E_{\Delta x}$  do not have



(a) FLC 2 using two inputs and one output.



(b) Additional membership functions for change of  $E_{\Delta x}$ .



(c) Response surface for FLC 2.

Figure 5.5: FLC 2 design parameters.

corresponding  $dE_{\Delta x}/dt$  values, either one will result in an increase large (IL) change in the angle  $\alpha$ .

A second feedback loop – shown in Figure 5.6 – was designed to include the second input value  $dE_{\Delta x}/dt$ . Aside from the additional input, the model remains the same.

The next iteration of this feedback loop and fuzzy logic controller is covered in the next section.

Table 5.3: Decision table for tilt angle andjustment, FLC 2.

$\Delta\alpha^\circ$		$E_{\Delta x}$		
		NS	Z	PS
$\frac{dE_{\Delta x}}{dt}$	N	IS	NC	IS
	Z	NC	DS	NC
	P	IS	NC	IS

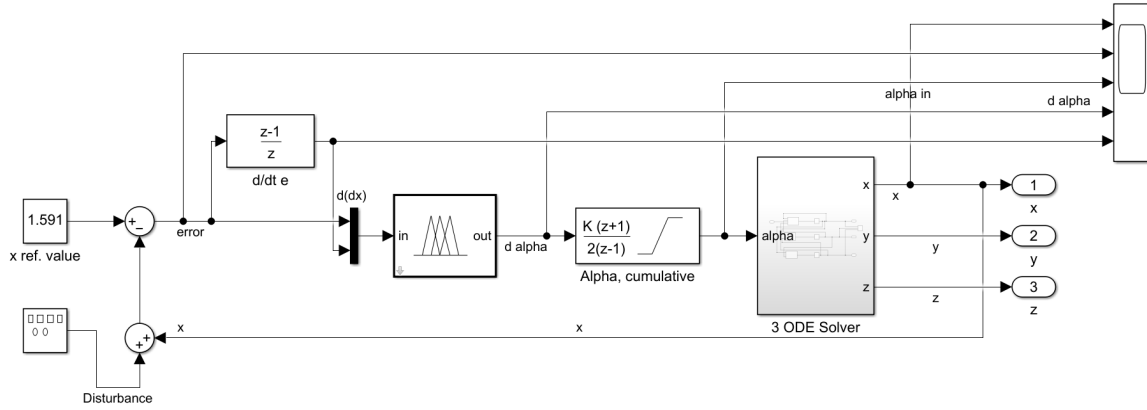


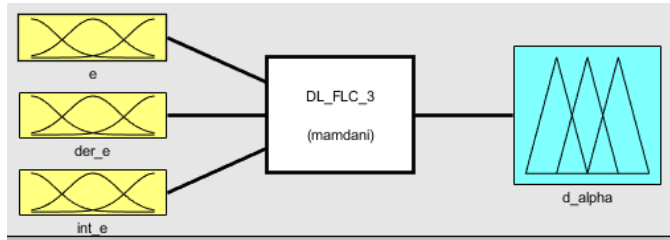
Figure 5.6: Feedback loop for the FLC 2.

### 5.2.3 Fuzzy Logic Controller 3

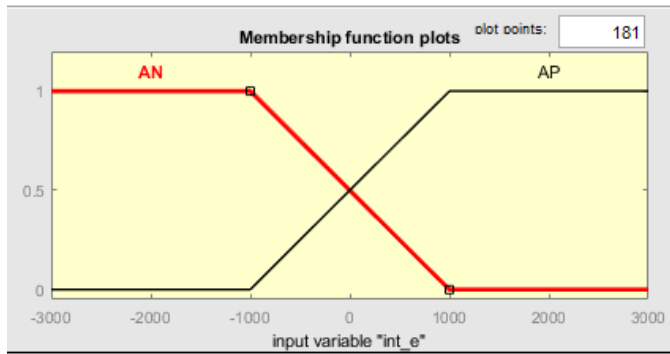
This controller uses a triple-input single-output method for stability control, shown in Figure 5.7(a). The three inputs used are  $E_{\Delta x}$ , the change  $E_{\Delta x}$ , and the integral of  $E_{\Delta x}$ , while the output is the change in  $\alpha$ . Figures 5.7(b) shows the membership functions of the additional input value; AN is any negative value and AP is any positive value. Figures 5.7(c)-5.7(d) shows the response plots of the controller which provides a visual representation of how the three input values dictates the change in  $\alpha$ . Shown in Table 5.3 are the linguistic set of rules that have been constructed.

A third feedback loop – shown in figure 5.8 – was designed to test and evaluate the ability of this controller with the additional input  $\int E_{\Delta x} dx$ .

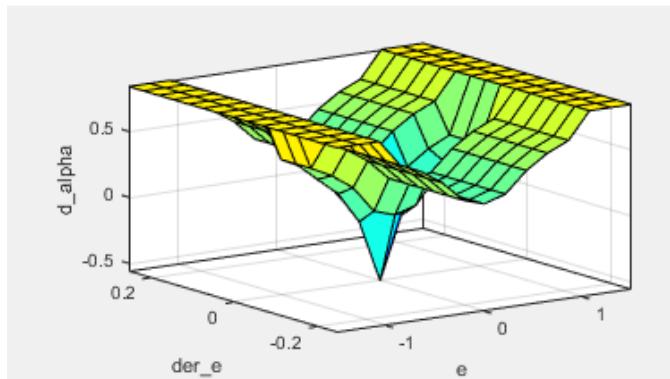
The next section will cover the results using all three FL controllers, evaluated against



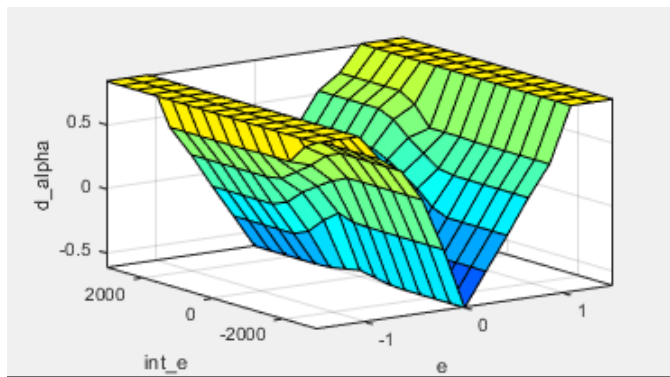
(a) FLC 3 using three inputs and one output.



(b) Additional membership function for the integral of  $E_{\Delta x}$ .



(c) First response surface for FLC 3.



(d) Second response surface for FLC 3.

Figure 5.7: FLC 3 design parameters.

Table 5.4: Decision table for tilt angle andjustment, FLC 3.

$E_{\Delta x} = NS$				$E_{\Delta x} = Z$				$E_{\Delta x} = PS$			
$\Delta\alpha^\circ$		$\int E_{\Delta x} dx$		$\Delta\alpha^\circ$		$\int E_{\Delta x} dx$		$\Delta\alpha^\circ$		$\int E_{\Delta x} dx$	
		AN	AP			AN	AP			AN	AP
$\frac{dE_{\Delta x}}{dt}$	N	IL	IS	$\frac{dE_{\Delta x}}{dt}$	N	IS	NC	$\frac{dE_{\Delta x}}{dt}$	N	IS	IL
	Z	IS	NC		Z	DS	DS		Z	NC	IS
	P	IL	IS		P	NC	IS		P	IS	IL

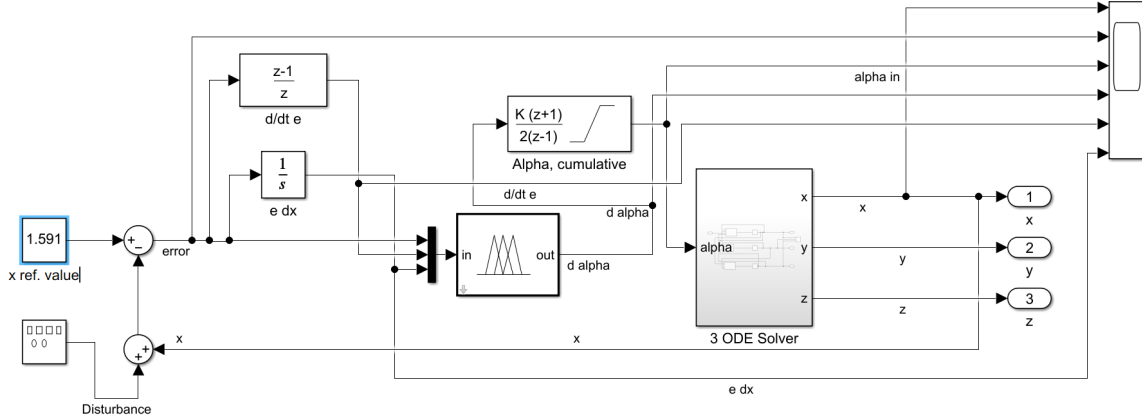


Figure 5.8: Feedback loop for the FLC 3.

the baseline performance.

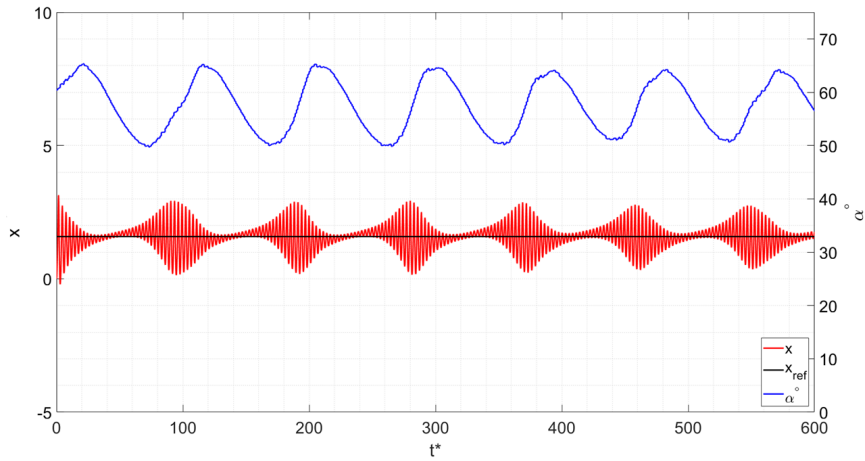
### 5.3 Stability Results

The dynamic model is a function of heat input,  $Q$ , and tilt angle,  $\alpha$ . These two parameters control the  $x$ ,  $y$ , and  $z$  output, which initially start at zero. The FL controllers aim to control the  $x$  output, which will increase or decrease  $E_{\Delta x}$  by adjusting  $\alpha$  and holding  $Q$  stable. Various initial values of  $\alpha$  and  $x$  setpoints were tested. As shown in Figure 3.1, a heat input value of  $Q = 5$  and tilt angles  $\alpha$  of  $60^\circ$ ,  $58^\circ$ , and  $30^\circ$  should produce – respectively – stable, oscillatory, and chaotic behavior. The next three sections will cover controller functionality, controller disturbance rejection, and additional controller behavior observations.

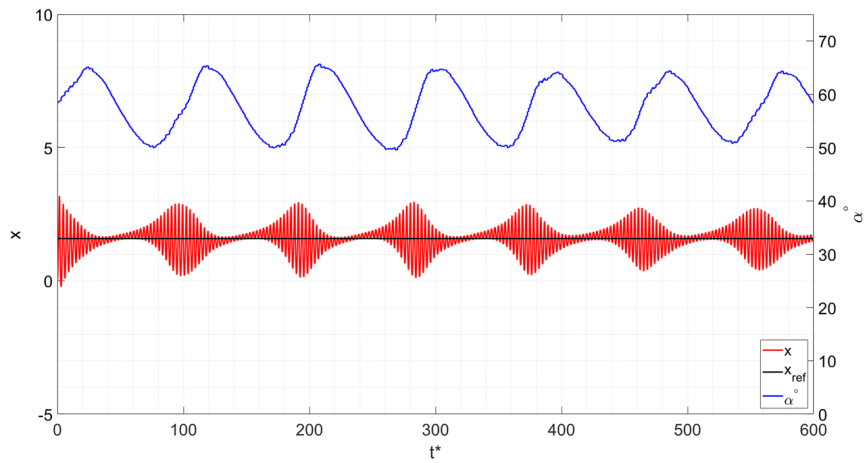
### 5.3.1 Controller Functionality

First, FLC 1 is used to stabilize the system under three initial  $\alpha$  values as shown in Figures 5.3. These values were chosen to initially induce stable, oscillatory, and chaotic behaviors to evaluate controller functionality. The first figure, Fig. 5.9(a), shows an initial stable condition, the second figure, Fig. 5.9(b), shows an initial oscillation condition, and Fig. 5.9(c), shows an initial chaotic condition. The initial chaotic condition highlights the performance of the controller. Initially, the  $x$  values is chaotic because it starts in the unstable region. As the controller increases  $\alpha$ , the system slowly begins to stabilize until it crosses over into the stable region and the error is minimal. The goal, however, is not to stay in the stable region; rather to maintain the set  $x_{ref}$  value. The controller then decreases  $\alpha$  to bring the system into the unstable region while maintaining a stable  $x$  values. Once the system begins to destabilize, the controller once again corrects itself to stabilize the system and the cycle continues. All three simulations show the robustness of the fuzzy controller to maintain stability for any initial value of  $\alpha$ . Note that after the initial stabilization the characteristics of all three simulations are the same, parameters will be marked up for reference on Figure 5.9(c). As mentioned previously, to control the fluid velocity  $x$  is to control the fluid temperature components  $y$  and  $z$  as shown in Figure 5.10.

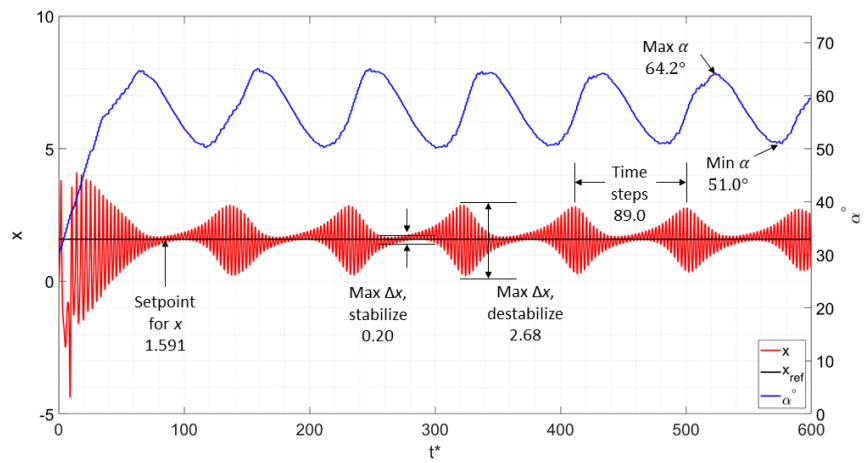
Additionally, results were collected and analyzed for FL controllers 2 and 3. Table 5.5 below summarizes these results, and a visual comparison is provided in Figure 5.11 for an initial  $\alpha$  value of  $30^\circ$ . The third column, time steps between stability cycles, refers to the time steps between the maximum values during adjacent period of instability.



(a) Initial condition:  $\alpha = 60^\circ$ .



(b) Initial condition:  $\alpha = 58^\circ$ .



(c) Initial condition:  $\alpha = 30^\circ$ .

Figure 5.9: Thermal stability results of FLC 1.

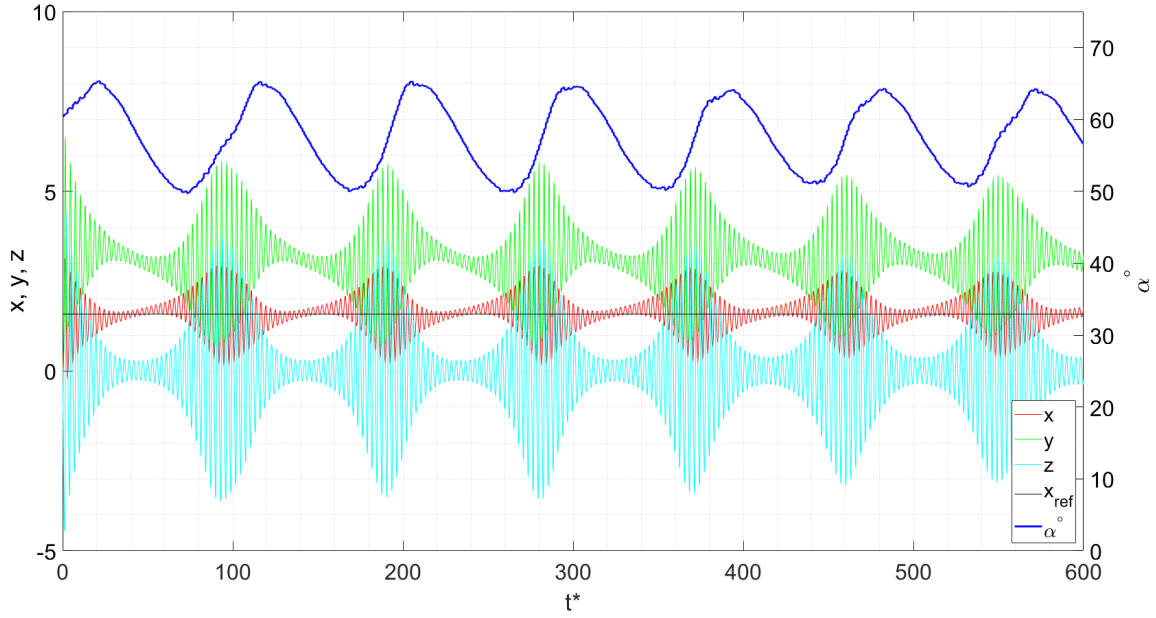


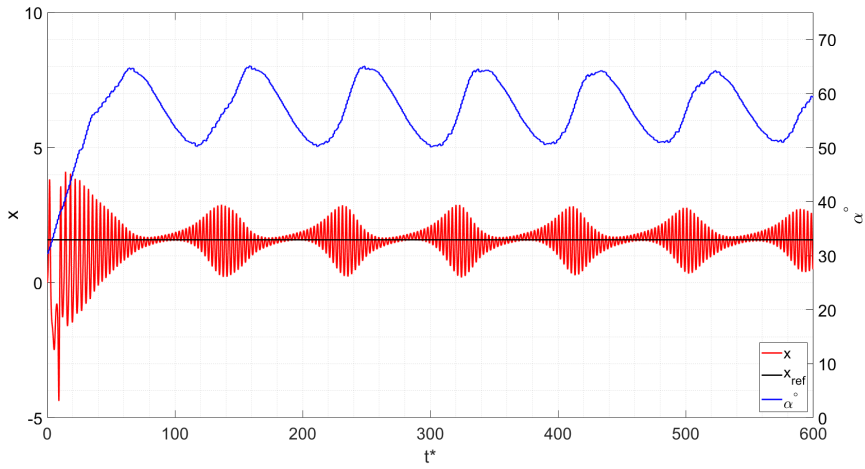
Figure 5.10: Stability correlation between  $x$ ,  $y$ , and  $z$ .

Table 5.5: Stability results for different FL controller configurations.

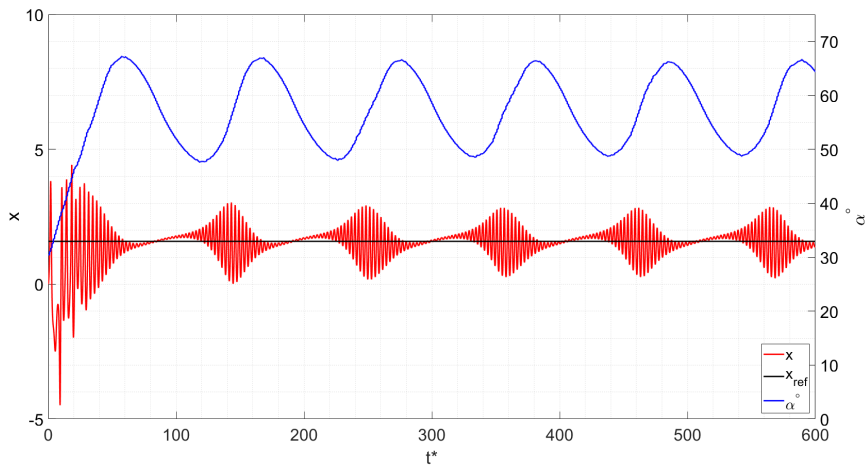
Controller type	Initial $\alpha^\circ$ value	Time steps	Max $\Delta x$ , destabilize	Min $\Delta x$ , stabilize	Max/min $\alpha^\circ$
FLC 1	30	89.0	2.68	0.20	64.2 / 51.0
FLC 2	30	105.2	2.54	0.08	66.4 / 48.7
FLC 3	30	148.6	2.49	0.03	67.4 / 48.4

Maximum  $\Delta x$  in the fourth column refers to the maximum difference between  $x$  values when the system began to destabilize. Minimum  $\Delta x$  in the fifth column refers to the minimum difference between  $x$  values during periods of stability. The last column shows the maximum and minimum  $\alpha$  values to reference the stable and unstable regions in the stability chart.

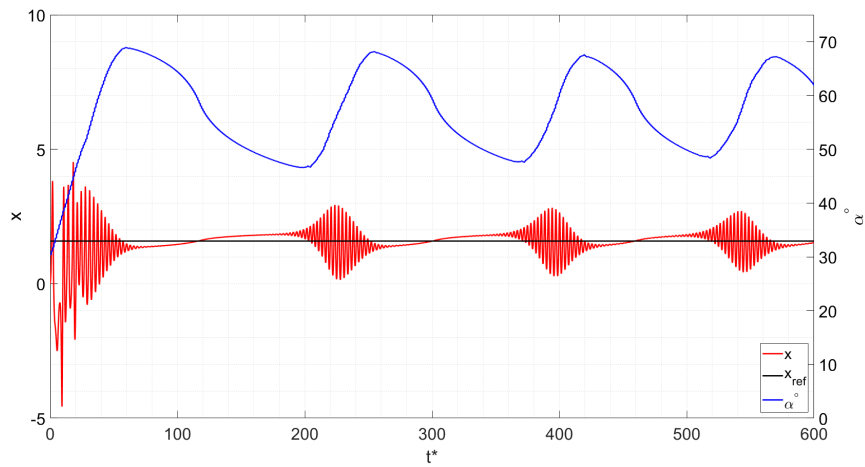
These results shown the ability of the FL controller to stabilize a system under otherwise unstable conditions. As expected, the more information that is fed into the controller, the better it performs. With each iteration of controller, the periods between



(a) FLC 1, initial condition:  $\alpha = 30^\circ$ .



(b) FLC 2, initial condition:  $\alpha = 30^\circ$ .



(c) FLC 3, initial condition:  $\alpha = 30^\circ$ .

Figure 5.11: Thermal stability comparison for FLC 1, FLC2, and FLC 3.

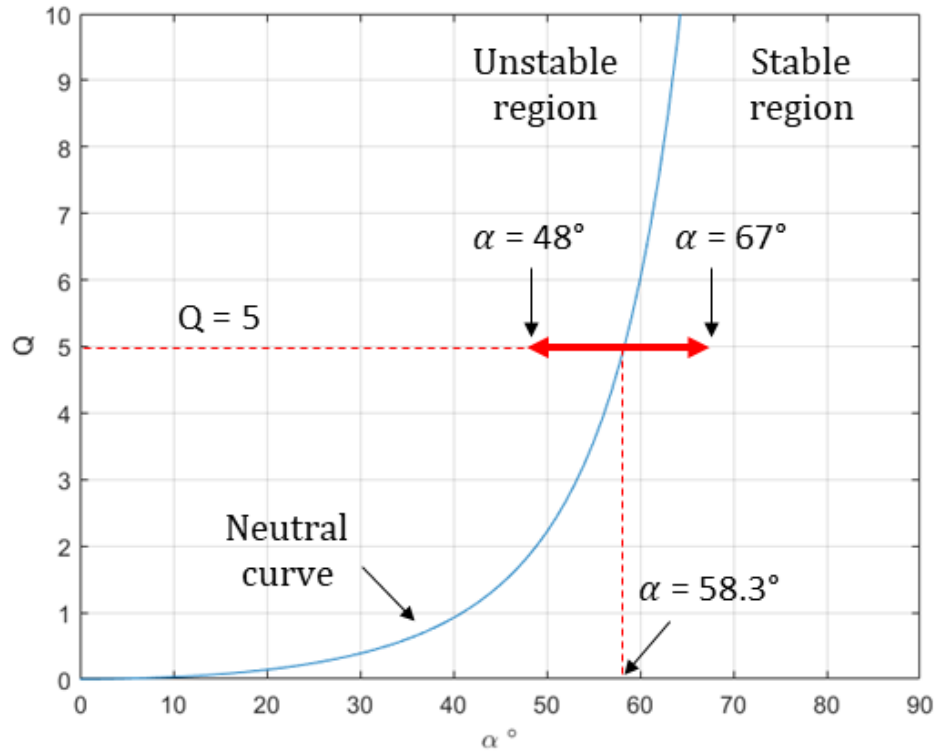


Figure 5.12: Controlled system behavior on the stability graph.

instability increased and the difference in  $x$  value during stability decreased.

It is helpful to relate system behavior to the stability graph and the  $x_{ref}$  value to its critical points (steady state values). For a value of  $Q = 5$  the stability point is  $58.3^\circ$ ; any angle below that will become unstable and any value above that will become stable. Figure 5.12 below shows the behavior of FLC 3 on the stability graph as it goes between stability regions. Next, recall that the critical point,  $P_1$ , for  $x$  is a function of  $Q$  and  $\alpha$ . At  $Q = 5$  and  $\alpha = 58.3^\circ$ ,  $P_1$  is 1.62. With  $x_{ref}$  set at 1.59, it is below the steady state value and will induce instability, forcing the controller to cycle in and out of the stability region. This will be explored more in the next section where disturbance rejection is evaluated in FLC 3 by changing the input  $Q$  at different intervals.

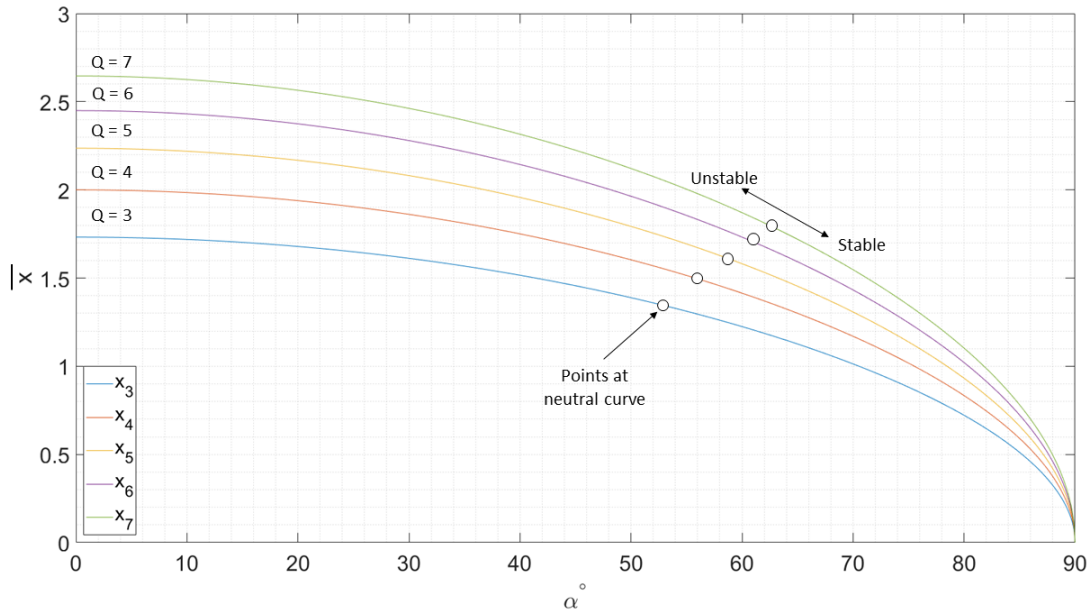


Figure 5.13: Critical points  $\bar{x}$  as a function of  $Q$  and  $\alpha$ .

### 5.3.2 Disturbance Rejection Method 1

The stability graph in Figure 5.12 provides valuable insight on relationship between  $Q$ ,  $\alpha$ , and stability, but does not provide information on critical points. Recall from Section 3.2 the steady state values,  $\bar{x}$ ,  $\bar{y}$ ,  $\bar{z}$ , are collectively called critical points ( $P_1$ ). Figure 5.13 shows the relationship between  $Q$ ,  $\alpha$  and  $\bar{x}$ .

For each value of  $Q$  and  $\alpha$  exists a steady state value  $\bar{x}$ . Certain steady state values exist at the neutral curve where if the system velocity  $x$  is above or below that value the system will stabilize and slow down or destabilize and speed up respectively. Note that as  $Q$  increases for any given  $\alpha$ , so does the steady state value as summarized in Table 5.6. This is key because if the controller has a fixed  $x_{ref}$  and the  $Q$  input changes, so does the stability dynamics. This is important to evaluate disturbance rejection as discussed next.

Table 5.6: Corresponding values of  $Q$ ,  $\alpha$ , and  $\bar{x}$ .

	Values at neutral curve	
Q values	$\alpha^\circ$	$\bar{x}$
$Q = 3$	53.3	1.34
$Q = 4$	56.2	1.49
$Q = 5$	58.3	1.62
$Q = 6$	60.0	1.73
$Q = 7$	61.4	1.83

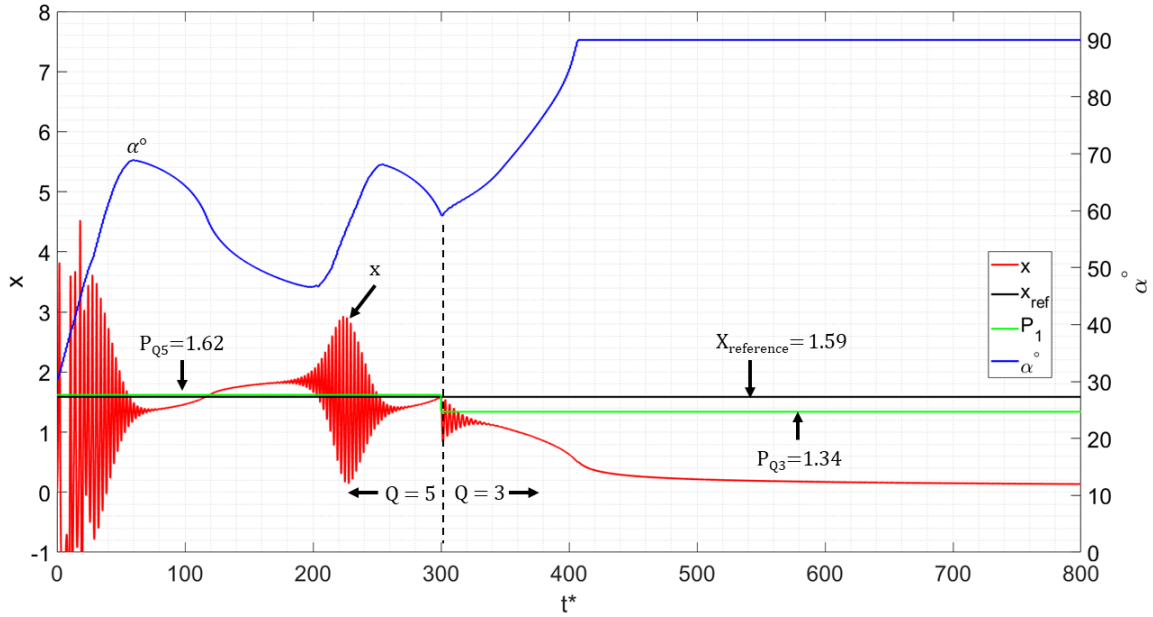


Figure 5.14: Disturbance rejection results with a change of  $Q$  from 5 to 3.

The next series of tests will evaluate the controllers functionality for various changes of  $Q$ . Figure 5.14 shows a change in  $Q$  from 5 to 3 at 300 time steps into the simulation. With an initial tilt angle of  $\alpha = 30^\circ$  and  $Q = 5$ , the controller increases  $\alpha$  to stabilize the system and produce a stable  $x$  value. However, the setpoint ( $x_{ref} = 1.59$ ) is below the critical point ( $P_1 = 1.62$ ), in the unstable region, so eventually the system begins to destabilize and speed up. The controller then raises  $\alpha$  to slow down and stabilize the system as it begins to repeat. At 300 time steps  $Q$  changes from 5 to 3 and the critical

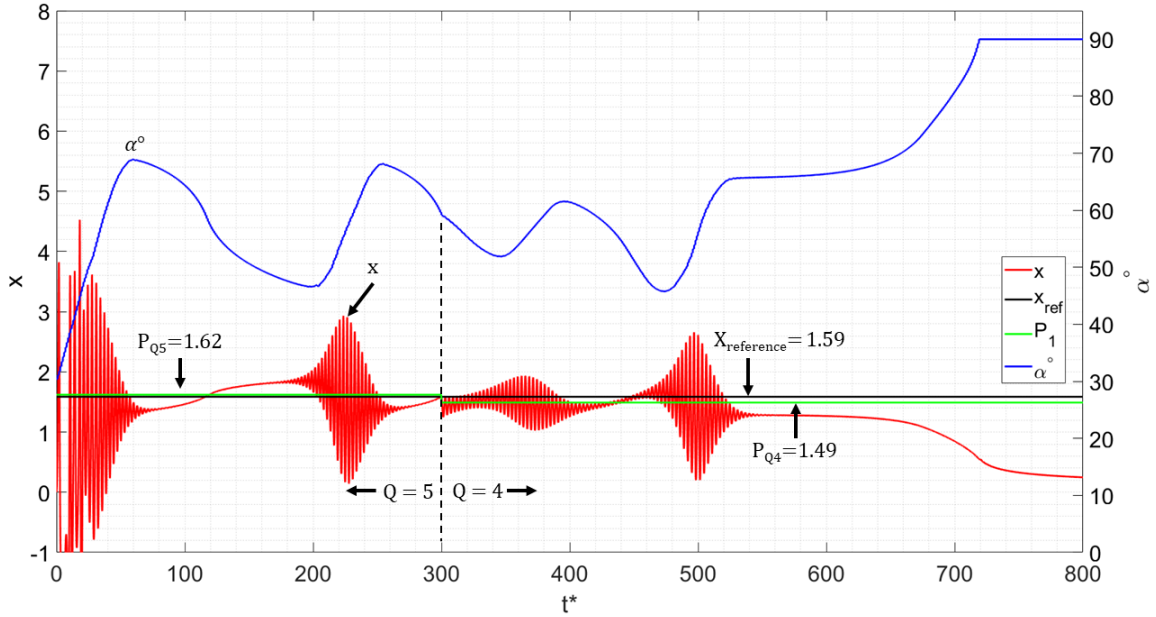


Figure 5.15: Disturbance rejection results with a change of  $Q$  from 5 to 4.

point  $P_1$  changes from 1.62 to 1.34. The setpoint is now above the critical point, in the stable region. As the controller brings the system to the setpoint, the system no longer become unstable; rather it begins to slow down. That combination ultimately casues the system to freeze as  $x$  approaches 0 near the end of the siulation.

Next, the system will change  $Q$  from 5 to 4 as shown in Figure 5.15. The graph shows normal operation as previously discussed up to 300 time steps.  $Q$  then changes from 5 to 4 and the critical point  $P_1$  changes from 1.62 to 1.49. The setpoint is again above the critical point, in the stable reigon. As the controller brings the system to the setpoint, the system no longer become unstable; rather it begins to slow down. Since the new critical point is closer to the setpoint than the last example it takes longer and even enters another cycle, but ultimately that combination again casues the system to slow down as  $x$  approaches 0 near the end of the simulation.

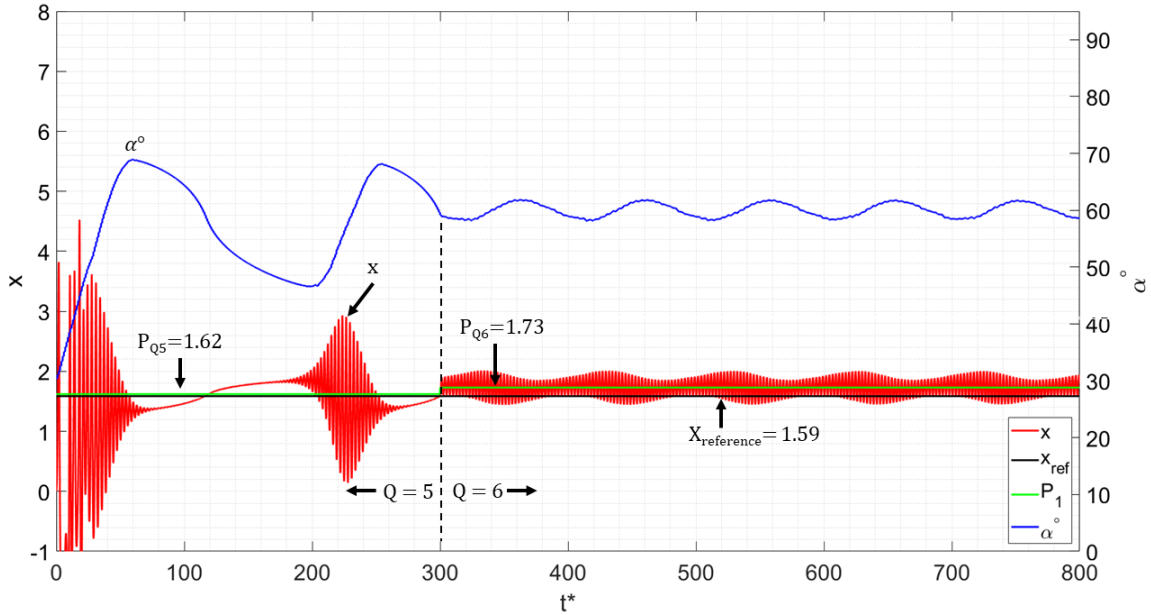


Figure 5.16: Disturbance rejection results with a change of  $Q$  from 5 to 6.

Next, the value of  $Q$  will be increased from 5 to 6 as shown in Figure 5.16. The graph shows normal operation as previously discussed up to 300 time steps.  $Q$  then changes from 5 to 6 and the critical point  $P_1$  changes from 1.62 to 1.73. The setpoint is below the critical point, in the unstable region. As the controller brings the system to the setpoint, the system becomes unstable, just as when  $Q = 5$ . This setpoint, however, is further into the unstable region so the system stays there longer, which results in increased oscillations during the periods of expected stability.

Next, the value of  $Q$  will be increased from 5 to 7 as shown in Figure 5.17. The graph shows normal operation as previously discussed up to 300 time steps.  $Q$  then changes from 5 to 7 and the critical point  $P_1$  changes from 1.62 to 1.83. The setpoint is again below the critical point, even further into the unstable region. As the controller brings the system to the setpoint, the system becomes unstable, just as when  $Q = 5$ . This setpoint

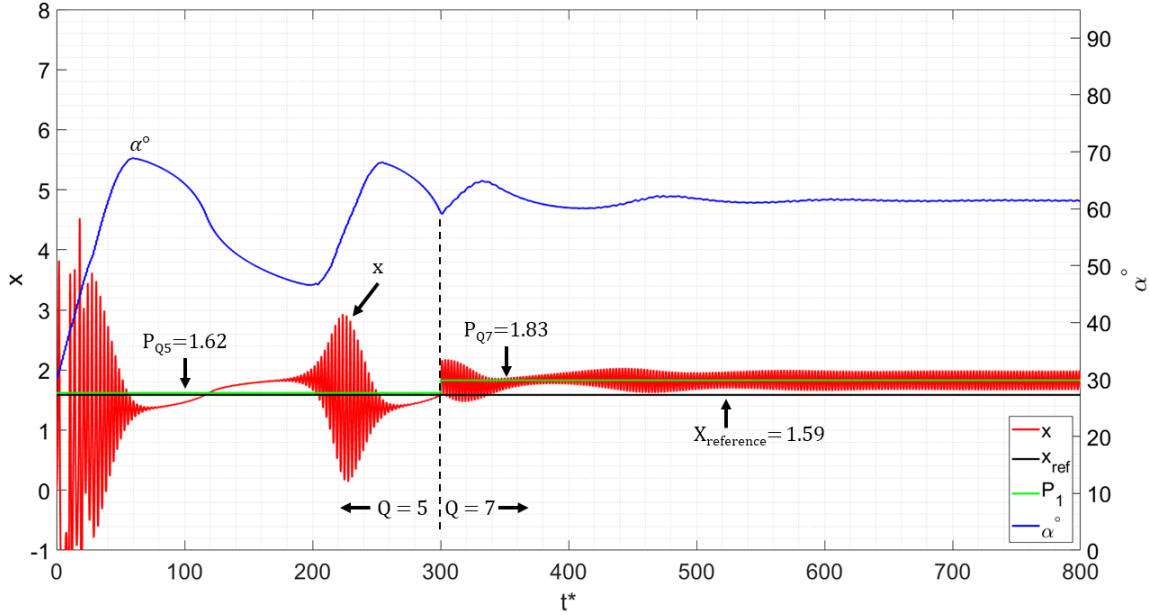


Figure 5.17: Disturbance rejection results with a change of  $Q$  from 5 to 7.

causes the system to remain in the unstable region almost entirely which produces an almost completely oscillatory changes in  $x$  without a distinct period of stability.

The controllers were design for  $Q = 5$  and had a setpoint that kept the system balanced between the stable and unstable region. As the values of  $Q$  changed, so did the neutral curve and the respective steady state values. This change in system dynamics were outside the designed range of the FLC and therefore did not replicate the results as when the value of  $Q$  remained stable. Next, simulations will be performed where both  $Q$  and  $x_{ref}$  will change.

### 5.3.3 Disturbance Rejection Method 2

This method will provide more insight on disturbance rejection by also changing the  $x$  setpoint with  $Q$  at 300 time steps. Shown in Figure 5.18 is a system that changes  $Q$  from 5 to 3 and the setpoint for  $x$  from 1.59 to 1.31. The system behaves as previously

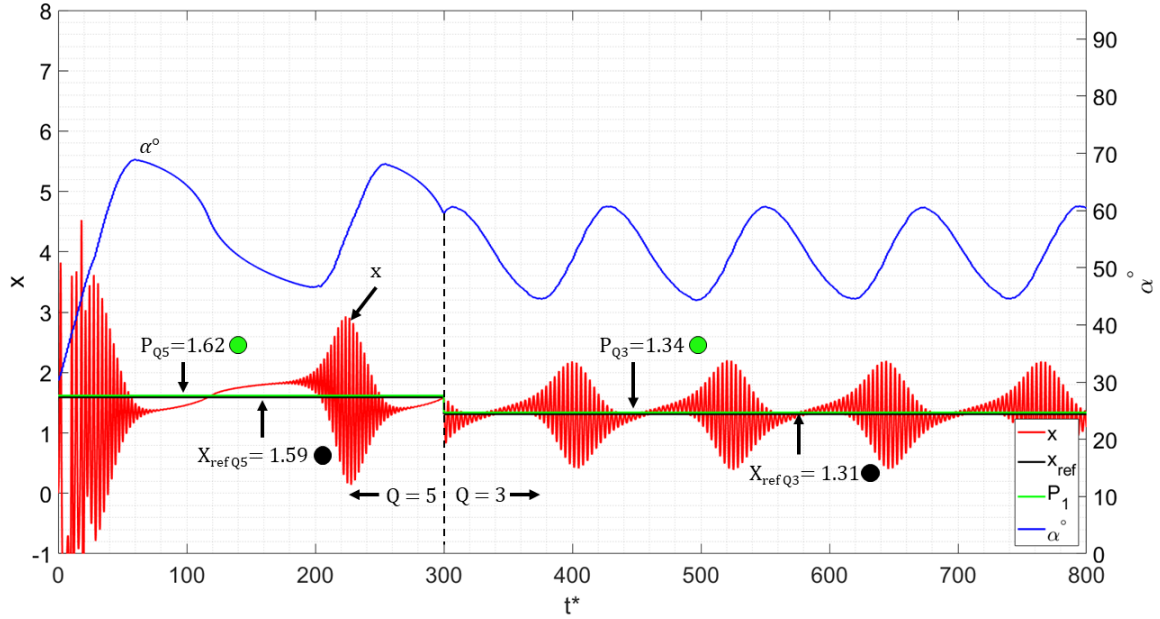


Figure 5.18: Disturbance rejection results with a change of  $Q$  (5 to 3) and  $x_{ref}$  (1.59 to 1.31).

discussed up to 300 time steps, however, after the switch the systems behaves significantly different than the previous section. In this case, since the  $x$  setpoint changes with  $Q$ , it stays within 0.3 of the steady state value at the neutral curve. What this means is that as the controller begins to respond, it is able to maintain a balance between the stable and unstable region to maintain stability in the system. These are all in contrast to the previous section where this performance was not achieved. No changes were made to FLC 3, only to  $Q$  and the setpoint  $x_{ref}$ . With this change to  $x_{ref}$ , the controller is able to pass a functionality check for a change in  $Q$ . Figures 5.19 - 5.21 shows the controller's successful disturbance rejection for changes in  $Q$ .

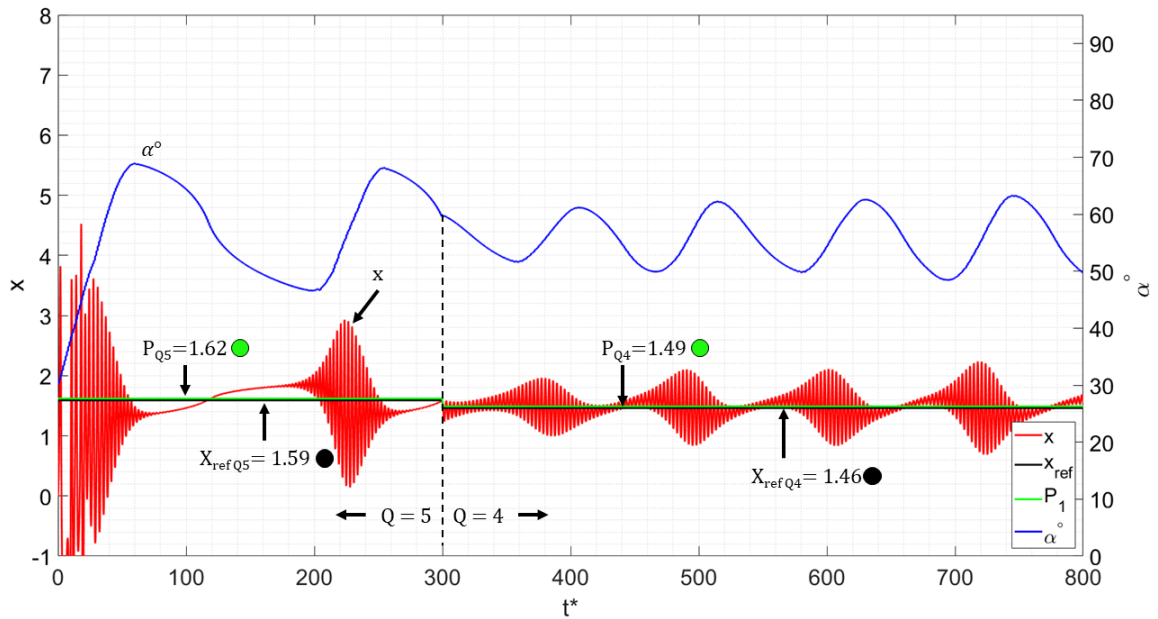


Figure 5.19: Disturbance rejection results with a change of  $Q$  (5 to 4) and  $x_{ref}$  (1.59 to 1.46).

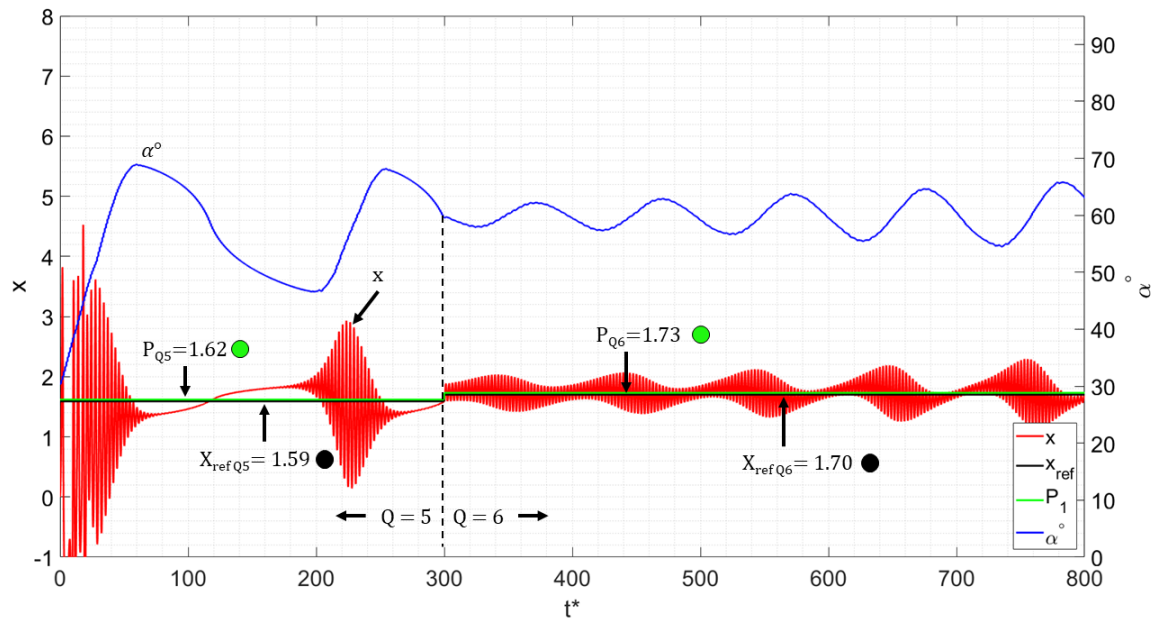


Figure 5.20: Disturbance rejection results with a change of  $Q$  (5 to 6) and  $x_{ref}$  (1.59 to 1.70).

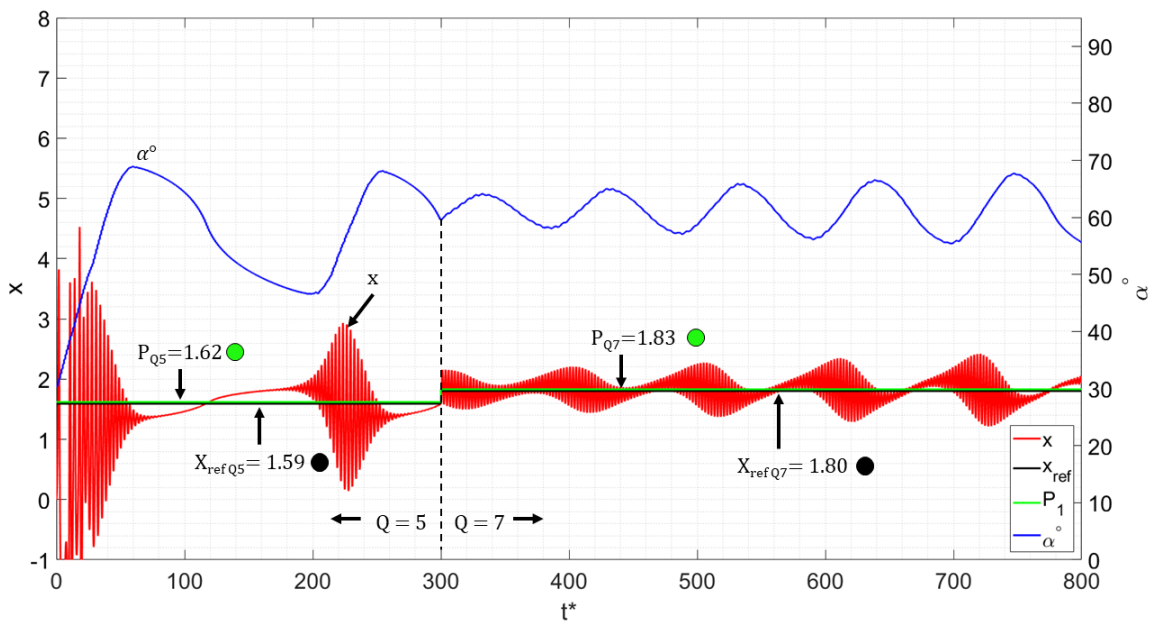


Figure 5.21: Disturbance rejection results with a change of  $Q$  (5 to 7) and  $x_{ref}$  (1.59 to 1.80).

## CHAPTER 6

### Conclusion and Future Work

#### 6.1 Conclusions

Robust and efficient controllers are important to both ensure thermal stability of complex systems, like natural convection loops. Although PID controllers are well established in industry, they lack robustness and often require constant retuning. In this work we have developed three fuzzy-based controller that use information on the velocity error, the difference of that error, and the integral of that error to provide inputs on the tilt angle in order to stabilize the velocity and corresponding temperature. As expected, the more information provided to the controllers, the better they perform. The simulations show that the fuzzy controller successfully performs the control actions and it is able to stabilize the system under different operating conditions. The controller has been tested against different initial conditions as well as changes in heat input to simulate possible situations in experimental situations. This work has provided a functionality check that a fuzzy logic controller can be used for this application.

#### 6.2 Future Work

A succesful implementation of fuzzy logic control in a natural convection loop opens the door to several different paths to continue this work. Several optimization and applications can explored as listed below:

- Controller optimization: There are several membership function parameters in FL controller design such as type, number, range, and weight for both the input and the output. In addition, with each additional input and output added the amount

of rules increase as well as the amount of possible combinations. The magnitude of combinations available leave plenty of room for design optimization, most likely using an optimization tool to run iterations instead of manually,

- Energy efficiency: optimizing the controller to find a balance between performance and energy consumption,
- Implementation of a PID controller into the natural convection loop simulation to compare against an optimized fuzzy logic controller
- Disturbance rejection: implement a design to automatically adjust the setpoint on the feedback loop to compensate for any adjustments to heat input
- Disturbance rejection: test smaller changes in  $Q$  (such as 5 to 5.1) to determine the functional range of the controller
- Disturbance rejection: determine if there exists a more complex controller design that does not need to adjust the setpoint to controller different heat input values
- Scaling: if possible, determine the scale of a possible physical testbed by using physical dimensions in a simulation instead of dimensionless values
- Experimental: build a testbed to test the controllers in a physical environment

## REFERENCES

- [1] T.L. Bergman, A.S. Lavine, F.P. Incropera, and D.P. Dewitt. *Introduction to Heat Transfer*. John Wiley & Sons, Inc., Hoboken, NJ, 2011.
- [2] D. Japiske. Advances in thermosyphon technology. *Advances in Heat Transfer*, 9:1–111, 1973.
- [3] H.F. Creveling, J.F. De Paz, J.Y. Balidi, and R.J. Schoenhals. Stability characteristics of a single-phase free convection loop. *Journal of Fluid Mechanics*, 67:65–84, 1975.
- [4] P.S. Damerell and R.J. Schoenhals. Flow in a toroidal thermosyphon with angular displacement of heat and cooled sections. *ASME Journal of Heat Transfer*, 101:672–676, 1979.
- [5] R. Greif, Y. Zvirin, and A. Mertol. The transient and stability behavior of a natural convection loop. *ASME Journal of Heat Transfer*, 101:684–688, 1979.
- [6] A. Mertol, R. Greif, and Y. Zvirin. Two-dimensional study of heat transfer and fluid flow in a natural convection loop. *ASME Journal of Heat Transfer*, 104:508–514, 1982.
- [7] A.S. Lavine, R. Greif, and J.A.C. Humphrey. A three-dimensional analysis of natural convection in a toroidal loop - the effect of tilt angle. *Int. J. Heat Mass Transfer*, 108:796–805, 1986.

- [8] A.S. Lavine, R. Greif, and J.A.C. Humphrey. A three-dimensional analysis of natural convection in a toroidal loop - the effect of grashof number. *Int. J. Heat Mass Transfer*, 30(2):251–262, 1987.
- [9] M. Bernier and B.R. Baliga. A 1-d/2-d model and experimental results for a closed-loop thermosyphon with vertical heat transfer sections. *Int. J. Heat Mass Transfer*, 35:2969–2982, 1992.
- [10] A. Pacheco-Vega, W. Franco, H.C. Chang, and M. Sen. Nonlinear analysis of tilted toroidal thermosyphon models. *Int. J. Heat Mass Transfer*, 45:1379–1391, 2002.
- [11] J. Baltazar, A. Yarian, and A. Pacheco-Vega. Development of P- PD- and PID-fuzzy SISO controllers of a sub-scaled multi-room building test-bed. In *Proceedings of the 3rd Thermal and Fluids Engineering Conference (TFEC)*, Tampa, FL, 2018. TFEC-2018-21805.
- [12] D.N. Basu, S. Bhattacharyya, and P.K. Das. A review of modern advances in analyses and applications of single-phase natural circulation loop in nuclear thermal hydraulics. *Nuclear Energy and Design*, 280:326–348, 2014.
- [13] S.V. Joshi, R.S. Bokil, and J.K. Nayak. Test standards for thermosyphon-type solar domestic hot water system: review and experimental evaluation. *Solar Energy*, 78(6):781–798, 2005.
- [14] W. He, T.T. Chow, and J. Ji. Hybrid photovoltaic and thermal solar-collector designed for natural circulation of water. *Applied Energy*, 83(3):199–210, 2006.

- [15] M. Bernier and B.R. Baliga. Comparison of one-dimensional models and 1-d/2-d model for closed-loop thermosyphon with vertical heat transfer sections. *Warme-und Stoffubertragung*, 29:309–317, 1994.
- [16] T.J. Ross. *Fuzzy Logic with Engineering Applications*. McGraw-Hill, New York, NY, 1995.
- [17] L.A. Zadeh. Fuzzy sets. *Information & Control*, 8:338–353, 1965.
- [18] E.H. Mamdani and S. Assilian. An experiment in linguistic synthesis with a fuzzy logic controller. *International Journal of Man-Machine Studies*, 7:1–13, 1975.
- [19] A.L. Ralescu. Fuzzy engineering and its social impact. In *Proceedings of the 13th Triennial World Congress*, San francisco, CA, 1996.
- [20] T. I. Salsbury. A survey of control technologies in the building automation industry. In *Proceedings of the 16th Triennial World Congress*, Prague, Czech Republic, 2005.
- [21] C. Ruiz-Mercado, A. Pacheco-Vega, and G. Torres-Chavez. A takagi-sugeno fuzzy dynamic model of a concentric-tubes heat exchanger. *Chemical Product and Process Modeling*, 4(2):1–22, 2009.
- [22] O. Garpinger, T. Hagglund, and K.J. Astrom. Performance and robustness trade-offs in pid control. *Journal of Process Control*, 24:568–577, 2014.
- [23] C.P Underwood. Fuzzy multivariable control of domestic heat pumps. *Applied Thermal Engineering*, 90:957–969, 2015.

- [24] Y. Soufi, M. Bechouat, and S. Kahla. Fuzzy-PSO controller design for maximum power point tracking in photovoltaic system. *International Journal of Hydrogen energy*, 42:8680–8688, 2017.
- [25] T. Hummel. Developmenmt of low-dimensional models of a natural convection loop with karhunen-loeve expansions for known heat flux. MS Thesis, California State University Los Angeles, Los Angeles, CA, 2011.
- [26] L. M. Jiji. *Heat Convection*. Springer Berlin, Heidelberg, Netherlands, 2006.
- [27] Malkus W.V.R. Non-periodic convection at high and low prandtl number. *Memoires Societe Royale des Science de Liege 4*, pages 125–128, 1972.
- [28] M. Sen, E. Ramos, and C. Trevino. The toroidal thermosyphon with known heat flux. *Int. J. Heat Mass Transfer*, 28(1):219–233, 1985.
- [29] K. Ogata. *Modern Control Engineering*. Prentice-Hall, Upper Saddle River, NJ, 1997.
- [30] A Pacheco-Vega, C Ruiz-Mercado, K Peters, and L Vilchiz-Bravo. On-line fuzzy-logic-based temperature control of a concentric-tube heat exchanger facility. *Heat Transfer Eng*, 30(14):1208–1215, 2009.

## APPENDIX A

### Development of Dynamical System

The following information provides detailed derivations of Eqs. (2.44) - (2.49). To this end, we start with the governing equations as integro-differential equations. (2.44)-(2.46) and a subsequent expansion in Fourier series for the temperature. Thus,

$$\frac{du^*}{dt^*} + u^* = \frac{1}{\pi} \left[ \int_0^{2\pi} T_0^c(t) \cos(\theta + \alpha) d\theta + \int_0^{2\pi} \cos(\theta + \alpha) \sum_{m=1}^{\infty} [T_m^c(t) \cos m\theta + T_m^s(t) \sin m\theta] \cos(\theta + \alpha) d\theta \right]. \quad (\text{A.1})$$

Equation (A.1) will be broken down and each term simplified as shown next.

To simplify

$$\int_0^{2\pi} T_0^c(t) \cos(\theta + \alpha) d\theta \quad (\text{A.2})$$

$$\int_0^{2\pi} T_0^c(t) \cos(\theta + \alpha) d\theta = T_0^c(t) \int_0^{2\pi} \cos(\theta + \alpha) d\theta \quad (\text{A.3})$$

Recall:

$$\cos(\theta + \alpha)d\theta = (\cos \theta \cos \alpha - \sin \theta \sin \alpha)d\theta \quad (\text{A.4})$$

$$\int_0^{2\pi} T_0^c(t) \cos(\theta + \alpha)d\theta = T_0^c(t) \int_0^{2\pi} (\cos \theta \cos \alpha - \sin \theta \sin \alpha)d\theta \quad (\text{A.5})$$

$$\int_0^{2\pi} T_0^c(t) \cos(\theta + \alpha)d\theta = T_0^c(t) \left[ \int_0^{2\pi} \cos \theta \cos \alpha d\theta - \int_0^{2\pi} \sin \theta \sin \alpha d\theta \right] \quad (\text{A.6})$$

$$\int_0^{2\pi} T_0^c(t) \cos(\theta + \alpha)d\theta = T_0^c(t) \left[ \cos \alpha \int_0^{2\pi} \cos \theta d\theta - \sin \alpha \int_0^{2\pi} \sin \theta d\theta \right] \quad (\text{A.7})$$

To simplify,

$$\int_0^{2\pi} \cos \theta = \sin \theta \Big|_0^{2\pi} = \sin 2\pi - \sin 0 = 0 - 0 = 0 \quad (\text{A.8})$$

$$\int_0^{2\pi} \sin \theta = -\cos \theta \Big|_0^{2\pi} = -(\cos 2\pi - \cos 0) = 1 - 1 = 0 \quad (\text{A.9})$$

$$\int_0^{2\pi} T_0^c(t) \cos(\theta + \alpha)d\theta = T_0^c(t) [(\cos \alpha)(0) - (\sin \alpha)(0)] = 0 \quad (\text{A.10})$$

The above term will be substituted back into Equation A.1.

$$\frac{du^*}{dt^*} + u^* = \frac{1}{\pi} \left[ (0) + \int_0^{2\pi} \cos(\theta + \alpha) \sum_{m=1}^{\infty} [T_m^c(t) \cos m\theta + T_m^s(t) \sin m\theta] \cos(\theta + \alpha)d\theta \right] \quad (\text{A.11})$$

Next, the term in the brackets will be expanded then simplified.

$$\frac{du^*}{dt^*} + u^* = \frac{1}{\pi} \left[ \int_0^{2\pi} \cos(\theta + \alpha) \sum_{m=1}^{\infty} [T_m^c(t) \cos m\theta + T_m^s(t) \sin m\theta] \cos(\theta + \alpha) d\theta \right] \quad (\text{A.12})$$

$$\left[ \int_0^{2\pi} \cos(\theta + \alpha) \sum_{m=1}^{\infty} [T_m^c(t) \cos m\theta + T_m^s(t) \sin m\theta] \cos(\theta + \alpha) d\theta \right] = \quad (\text{A.13})$$

$$\sum_{m=1}^{\infty} \left[ \int_0^{2\pi} \cos(\theta + \alpha) T_m^c(t) \cos m\theta d\theta + \int_0^{2\pi} \cos(\theta + \alpha) T_m^s(t) \sin m\theta d\theta \right] \quad (\text{A.14})$$

The “first term” term with the variable  $T_m^c(t)$  will be simplified.

$$\sum_{m=1}^{\infty} \int_0^{2\pi} \cos(\theta + \alpha) T_m^c(t) \cos m\theta d\theta = \quad (\text{A.15})$$

$$= \sum_{m=1}^{\infty} T_m^c(t) \int_0^{2\pi} (\cos \theta \cos \alpha - \sin \theta \sin \alpha) \cos m\theta d\theta \quad (\text{A.16})$$

$$= \sum_{m=1}^{\infty} T_m^c(t) \left[ \int_0^{2\pi} \cos \theta \cos \alpha \cos m\theta d\theta - \int_0^{2\pi} \sin \theta \sin \alpha \cos m\theta d\theta \right] \quad (\text{A.17})$$

$$= \sum_{m=1}^{\infty} T_m^c(t) \left[ \cos \alpha \int_0^{2\pi} \cos \theta \cos m\theta d\theta - \sin \alpha \int_0^{2\pi} \sin \theta \cos m\theta d\theta \right] \quad (\text{A.18})$$

By recalling the orthogonality conditions, namely,

$$\int_{\tau} \sin nx \cos kx dx = 0 \quad (\text{A.19})$$

$$\int_{\tau} \cos nx \cos kx dx = 0; n \neq k \quad (\text{A.20})$$

$$\int_{\tau} \sin nx \sin kx dx = 0, n \neq k, \quad (\text{A.21})$$

we can simplify the above expressions. Note: for  $m$  values  $> 1$ , the entire term will go to zero as shown below and will not allow the variable  $T_m^c(t)$  to be solved. Therefore, we

will consider  $m = 1$  moving ahead with the derivation.

$$= \sum_{m=2}^{\infty} T_m^c(t) \left[ (\cos \alpha)(0) - (\sin \alpha)(0) \right] = 0 \quad (\text{A.22})$$

For  $m=1$ :

$$= \sum_{m=1}^1 T_m^c(t) \left[ \cos \alpha \int_0^{2\pi} \cos \theta \cos m\theta d\theta - (\sin \alpha)(0) \right] \quad (\text{A.23})$$

$$= \sum_{m=1}^1 T_1^c(t) \cos \alpha \int_0^{2\pi} \cos \theta \cos \theta d\theta = T_1^c(t) \cos \alpha \int_0^{2\pi} \cos^2 \theta d\theta \quad (\text{A.24})$$

$$= T_1^c(t) \cos \alpha \int_0^{2\pi} \left[ \frac{1}{2}(1 + \cos 2\theta) \right] d\theta = T_1^c(t) \cos \alpha \left( \frac{1}{2} \right) \int_0^{2\pi} (1 + \cos 2\theta) d\theta \quad (\text{A.25})$$

$$= T_1^c(t) \cos \alpha \left( \frac{1}{2} \right) \left[ \int_0^{2\pi} d\theta + \int_0^{2\pi} \cos 2\theta d\theta \right] \quad (\text{A.26})$$

$$= T_1^c(t) \cos \alpha \left( \frac{1}{2} \right) \left[ \theta \Big|_0^{2\pi} + \frac{1}{2} \sin 2\theta \Big|_0^{2\pi} \right] \quad (\text{A.27})$$

$$= T_1^c(t) \cos \alpha \left( \frac{1}{2} \right) \left[ (2\pi - 0) + \frac{1}{2} (\sin 4\pi - \sin 0) \right] \quad (\text{A.28})$$

$$= T_1^c(t) \cos \alpha \left( \frac{1}{2} \right) \left[ (2\pi) + \frac{1}{2} (0 - 0) \right] \quad (\text{A.29})$$

$$= \pi T_1^c(t) \cos \alpha \quad (\text{A.30})$$

$$\sum_{m=1}^1 T_1^c(t) \cos \alpha \int_0^{2\pi} \cos \theta \cos m\theta d\theta = \pi T_1^c(t) \cos \alpha \quad (\text{A.31})$$

$$\int_0^{2\pi} \cos \theta \cos m\theta d\theta = \pi \quad (\text{A.32})$$

$$= \sum_{m=1}^{\infty} T_m^c(t) \left[ \cos \alpha \int_0^{2\pi} \cos \theta \cos m\theta d\theta - \sin \alpha \int_0^{2\pi} \sin \theta \cos m\theta d\theta \right] \quad (\text{A.33})$$

$$= T_1^c(t) \left[ (\cos \alpha)(\pi) - (\sin \alpha)(0) \right] \quad (\text{A.34})$$

$$\sum_{m=1}^{\infty} \int_0^{2\pi} \cos(\theta + \alpha) T_m^c(t) \cos m\theta d\theta = T_1^c(t) (\cos \alpha)(\pi) \quad (\text{A.35})$$

The “first term” has been simplified as shown above. Next, the “second term” with the variable  $T_m^s(t)$  will be simplified.

$$\sum_{m=1}^{\infty} \left[ \int_0^{2\pi} \cos(\theta + \alpha) T_m^c(t) \cos m\theta d\theta + \int_0^{2\pi} \cos(\theta + \alpha) T_m^s(t) \sin m\theta d\theta \right] \quad (\text{A.36})$$

$$\sum_{m=1}^{\infty} \int_0^{2\pi} \cos(\theta + \alpha) T_m^s(t) \sin m\theta d\theta = \quad (\text{A.37})$$

$$= \sum_{m=1}^{\infty} T_m^s(t) \int_0^{2\pi} \sin m\theta (\cos \theta \cos \alpha - \sin \theta \sin \alpha) d\theta \quad (\text{A.38})$$

$$= \sum_{m=1}^{\infty} T_m^s(t) \left[ \int_0^{2\pi} \sin m\theta \cos \theta \cos \alpha - \int_0^{2\pi} \sin m\theta \sin \theta \sin \alpha d\theta \right] \quad (\text{A.39})$$

$$= \sum_{m=1}^{\infty} T_m^s(t) \left[ \cos \alpha \int_0^{2\pi} \sin m\theta \cos \theta d\theta - \sin \alpha \int_0^{2\pi} \sin m\theta \sin \theta d\theta \right] \quad (\text{A.40})$$

$$= \sum_{m=1}^{\infty} T_m^s(t) \left[ (\cos \alpha)(0) - \sin \alpha \int_0^{2\pi} \sin m\theta \sin \theta d\theta \right] \quad (\text{A.41})$$

Recall orthogonality conditions:

$$= \sum_{m=2}^{\infty} T_m^s(t) \left[ (\cos \alpha)(0) - \sin \alpha(0) \right] = 0 \quad (\text{A.42})$$

$$= \sum_{m=1}^1 T_1^s(t) \left[ -\sin \alpha \int_0^{2\pi} \sin^2 \theta d\theta \right] \quad (\text{A.43})$$

Note above in equation x, for values of  $m > 1$  the term will go to zero and the term  $T_1^s(t)$  will go to zero. Therefore, the derivation will proceed with  $m = 1$ .

$$= -T_1^s(t) \sin \alpha \int_0^{2\pi} \sin^2 \theta d\theta \quad (\text{A.44})$$

$$= -T_1^s(t) \sin \alpha \int_0^{2\pi} \left( \frac{1}{2} - \frac{1}{2} \cos 2\theta d\theta \right) \quad (\text{A.45})$$

$$= -T_1^s(t) \sin \alpha \frac{1}{2} \int_0^{2\pi} (1 - \cos 2\theta d\theta) \quad (\text{A.46})$$

$$= -T_1^s(t) \sin \alpha \frac{1}{2} \left[ \int_0^{2\pi} d\theta - \int_0^{2\pi} \cos 2\theta d\theta \right] \quad (\text{A.47})$$

$$= -T_1^s(t) \sin \alpha \frac{1}{2} \left[ \theta \Big|_0^{2\pi} - (-\sin 2\theta) \Big|_0^{2\pi} \right] \quad (\text{A.48})$$

$$= -T_1^s(t) \sin \alpha \frac{1}{2} \left[ (2\pi - 0) + (\sin 4\pi - \sin 0) \right] \quad (\text{A.49})$$

$$= -T_1^s(t) \sin \alpha \frac{1}{2} \left[ 2\pi + (0 - 0) \right] \quad (\text{A.50})$$

$$\sum_{m=1}^{\infty} \int_0^{2\pi} \cos(\theta + \alpha) T_m^s(t) \sin m\theta d\theta = -T_1^s(t) (\sin \alpha) (\pi) \quad (\text{A.51})$$

Below is the term in brackets, followed by the substitutions of the first and second terms

that were just simplified.

$$\frac{du^*}{dt^*} + u^* = \frac{1}{\pi} \left[ (0) + \int_0^{2\pi} \cos(\theta + \alpha) \sum_{m=1}^{\infty} [T_m^c(t) \cos m\theta + T_m^s(t) \sin m\theta] \cos(\theta + \alpha) d\theta \right] \quad (\text{A.52})$$

$$\frac{du^*}{dt^*} + u^* = \frac{1}{\pi} \left[ [T_1^c(t)(\cos \alpha)(\pi)] + [-T_1^s(t)(\sin \alpha)(\pi)] \right] \quad (\text{A.53})$$

$$\frac{du^*}{dt^*} + u^* = T_1^c(t) \cos \alpha - T_1^s(t) \sin \alpha \quad (\text{A.54})$$

$$\frac{du^*}{dt^*} = -u^* + T_1^c(t) \cos \alpha - T_1^s(t) \sin \alpha \quad (\text{A.55})$$

$$(\text{A.56})$$

The equation above is the simplified momentum equation. Next, the energy equation will be simplified. Recall the heated condition is known heat flux around the thermosyphon loop. The following equations apply to this condition.

$$\frac{\partial T^*}{\partial t^*} + u^* \frac{\partial T^*}{\partial \theta} = q^* \quad (\text{A.57})$$

$$q^* = -Q \sin \theta \quad (\text{A.58})$$

$$\frac{\partial T^*}{\partial t^*} = \frac{\partial}{\partial t^*} T^* \quad (\text{A.59})$$

The temperature term can be expanded using the Fourier series as shown below, and will

substituted into the energy equation.

$$T(t, \theta) = T_0^c(t) + \sum_{m=1}^{\infty} [T_m^c(t) \cos m\theta + T_m^s(t) \sin m\theta] \quad (\text{A.60})$$

Expand and simplify:

$$\frac{\partial T^*}{\partial t^*} \quad (\text{A.61})$$

$$\frac{\partial T^*}{\partial t^*} = \frac{\partial}{\partial t^*} T^* \quad (\text{A.62})$$

$$\frac{\partial}{\partial t^*} T^* = \frac{\partial}{\partial t^*} \left[ T_0^c(t) + \sum_{m=1}^{\infty} [T_m^c(t) \cos m\theta + T_m^s(t) \sin m\theta] \right] \quad (\text{A.63})$$

$$= \frac{\partial}{\partial t^*} T_0^c(t) + \frac{\partial}{\partial t^*} \sum_{m=1}^{\infty} [T_m^c(t) \cos m\theta + T_m^s(t) \sin m\theta] \quad (\text{A.64})$$

$$= \frac{\partial}{\partial t^*} T_0^c(t) + \sum_{m=1}^{\infty} \left[ \frac{\partial}{\partial t^*} T_m^c(t) \cos m\theta + \frac{\partial}{\partial t^*} T_m^s(t) \sin m\theta \right] \quad (\text{A.65})$$

$$\frac{\partial}{\partial t^*} T^* = \frac{\partial}{\partial t^*} T_0^c(t) + \sum_{m=1}^{\infty} \left[ \frac{\partial T_m^c(t)}{\partial t^*} \cos m\theta + \frac{\partial T_m^s(t)}{\partial t^*} \sin m\theta \right] \quad (\text{A.66})$$

Expand and simplify:

$$\frac{\partial T^*}{\partial \theta} \quad (\text{A.67})$$

$$\frac{\partial T^*}{\partial \theta} = \frac{\partial}{\partial \theta} T^* = \frac{\partial}{\partial \theta} \left[ T_0^c(t) + \sum_{m=1}^{\infty} [T_m^c(t) \cos m\theta + T_m^s(t) \sin m\theta] \right] \quad (\text{A.68})$$

$$\frac{\partial}{\partial \theta} T^* = \frac{\partial}{\partial \theta} T_0^c(t) + \sum_{m=1}^{\infty} \left[ \frac{\partial}{\partial \theta} T_m^c(t) \cos m\theta + \frac{\partial}{\partial \theta} T_m^s(t) \sin m\theta \right] \quad (\text{A.69})$$

$$\frac{\partial}{\partial \theta} T^* = (0) + \sum_{m=1}^{\infty} \left[ -mT_m^c(t) \sin m\theta + mT_m^s(t) \cos m\theta \right] \quad (\text{A.70})$$

The two terms that were expanded and simplified will be substituted back into the energy equation.

$$\frac{\partial T^*}{\partial t^*} + u^* \frac{\partial T^*}{\partial \theta} = q^* \quad (\text{A.71})$$

Recall:

$$q^* = -Q \sin \theta \quad (\text{A.72})$$

$$\frac{\partial}{\partial t^*} T_0^c(t) + \sum_{m=1}^{\infty} \left[ \frac{\partial T_m^c(t)}{\partial t^*} \cos m\theta + \frac{\partial T_m^s(t)}{\partial t^*} \sin m\theta \right] + \quad (\text{A.73})$$

$$u^* \sum_{m=1}^{\infty} \left[ -mT_m^c(t) \sin m\theta + mT_m^s(t) \cos m\theta \right] = -Q \sin \theta \quad (\text{A.74})$$

Multiply the entire equation by:

$$\int_0^{2\pi} \cos n\theta d\theta; \quad (\text{A.75})$$

$$\frac{\partial}{\partial t^*} T_0^c(t) \left[ \int_0^{2\pi} \cos n\theta d\theta \right] + \quad (\text{A.76})$$

$$\sum_{m=1}^{\infty} \left[ \frac{\partial T_m^c(t)}{\partial t^*} \cos m\theta + \frac{\partial T_m^s(t)}{\partial t^*} \sin m\theta \right] \left[ \int_0^{2\pi} \cos n\theta d\theta \right] + \quad (\text{A.77})$$

$$u^* \sum_{m=1}^{\infty} \left[ -mT_m^c(t) \sin m\theta + mT_m^s(t) \cos m\theta \right] \left[ \int_0^{2\pi} \cos n\theta d\theta \right] = \quad (\text{A.78})$$

$$-Q \sin \theta \left[ \int_0^{2\pi} \cos n\theta d\theta \right] \quad (\text{A.79})$$

$$\frac{\partial}{\partial t^*} T_0^c(t) \left[ \int_0^{2\pi} \cos n\theta d\theta \right] + \quad (\text{A.80})$$

$$\sum_{m=1}^{\infty} \left[ \frac{\partial T_m^c(t)}{\partial t^*} \int_0^{2\pi} \cos n\theta \cos m\theta d\theta + \frac{\partial T_m^s(t)}{\partial t^*} \int_0^{2\pi} \cos n\theta \sin m\theta d\theta \right] + \quad (\text{A.81})$$

$$u^* \sum_{m=1}^{\infty} \left[ -mT_m^c(t) \int_0^{2\pi} \cos n\theta \sin m\theta d\theta + mT_m^s(t) \int_0^{2\pi} \cos n\theta \cos m\theta d\theta \right] = \quad (\text{A.82})$$

$$-Q \left[ \int_0^{2\pi} \cos n\theta \sin \theta d\theta \right] \quad (\text{A.83})$$

$$\frac{\partial}{\partial t^*} T_0^c(t) \left[ \frac{1}{n} \sin n\theta \Big|_0^{2\pi} \right] + \quad (\text{A.84})$$

$$\sum_{m=1}^{\infty} \left[ \frac{\partial T_m^c(t)}{\partial t^*} \int_0^{2\pi} \cos n\theta \cos m\theta d\theta + \frac{\partial T_m^s(t)}{\partial t^*} (0) \right] + \quad (\text{A.85})$$

$$u^* \sum_{m=1}^{\infty} \left[ -mT_m^c(t)(0) + mT_m^s(t) \int_0^{2\pi} \cos n\theta \cos m\theta d\theta \right] = \quad (\text{A.86})$$

$$-Q \left[ (0) \right] \quad (\text{A.87})$$

$$\frac{\partial}{\partial t^*} T_0^c(t) \left[ (0) \right] + \quad (\text{A.88})$$

$$\sum_{m=1}^{\infty} \left[ \frac{\partial T_m^c(t)}{\partial t^*} \int_0^{2\pi} \cos n\theta \cos m\theta d\theta + (0) \right] + \quad (\text{A.89})$$

$$u^* \sum_{m=1}^{\infty} \left[ (0) + m T_m^s(t) \int_0^{2\pi} \cos n\theta \cos m\theta d\theta \right] = 0 \quad (\text{A.90})$$

$$\sum_{m=1}^{\infty} \left[ \frac{\partial T_m^c(t)}{\partial t^*} \int_0^{2\pi} \cos n\theta \cos m\theta d\theta \right] + \quad (\text{A.91})$$

$$u^* \sum_{m=1}^{\infty} \left[ + m T_m^s(t) \int_0^{2\pi} \cos n\theta \cos m\theta d\theta \right] = 0 \quad (\text{A.92})$$

$$\sum_{m=2}^{\infty} \left[ \frac{\partial T_m^c(t)}{\partial t^*} (0) \right] + \quad (\text{A.93})$$

$$u^* \sum_{m=2}^{\infty} \left[ + m T_m^s(t) (0) \right] = 0 \quad (\text{A.94})$$

$$0 = 0 \quad (\text{A.95})$$

Note the above equation shows that for  $m \neq n$  the term  $T_m^s(t)$  will dissapear, the derivation will continue with  $m = n$ .

$$\sum_{m=1}^1 \left[ \frac{\partial T_1^c(t)}{\partial t^*} \int_0^{2\pi} \cos^2 \theta d\theta \right] + \quad (\text{A.96})$$

$$u^* \sum_{m=1}^1 \left[ + m T_1^s(t) \int_0^{2\pi} \cos^2 \theta d\theta \right] = 0; n = 1, 2, 3 \quad (\text{A.97})$$

Recall:

$$\int_0^{2\pi} \cos^2 \theta d\theta = \pi \quad (\text{A.98})$$

$$\sum_{m=1}^1 \left[ \frac{\partial T_1^c(t)}{\partial t^*}(\pi) \right] + u^* \sum_{m=1}^1 \left[ + m T_1^s(t)(\pi) \right] = 0 \quad (\text{A.99})$$

$$\frac{\partial T_1^c(t)}{\partial t^*} + u^* T_1^s(t) = 0 \quad (\text{A.100})$$

$$\frac{\partial T_1^c(t)}{\partial t^*} = -u^* T_1^s(t) \quad (\text{A.101})$$

$T_1^c(t)$  has been solved for above. Next, the other coefficient will be solved for.

Multiple the entire equation by:

$$\int_0^{2\pi} \sin n\theta d\theta; \quad (\text{A.102})$$

$$\frac{\partial}{\partial t^*} T_0^c(t) \left[ \int_0^{2\pi} \sin n\theta d\theta \right] + \quad (\text{A.103})$$

$$\sum_{m=1}^{\infty} \left[ \frac{\partial T_m^c(t)}{\partial t^*} \cos m\theta + \frac{\partial T_m^s(t)}{\partial t^*} \sin m\theta \right] \left[ \int_0^{2\pi} \sin n\theta d\theta \right] + \quad (\text{A.104})$$

$$u^* \sum_{m=1}^{\infty} \left[ -m T_m^c(t) \sin m\theta + m T_m^s(t) \cos m\theta \right] \left[ \int_0^{2\pi} \sin n\theta d\theta \right] = \quad (\text{A.105})$$

$$-Q \sin \theta \left[ \int_0^{2\pi} \sin n\theta d\theta \right] \quad (\text{A.106})$$

$$\frac{\partial}{\partial t^*} T_0^c(t) \left[ \int_0^{2\pi} \sin n\theta d\theta \right] + \quad (\text{A.107})$$

$$\sum_{m=1}^{\infty} \left[ \frac{\partial T_m^c(t)}{\partial t^*} \int_0^{2\pi} \sin n\theta \cos m\theta d\theta + \frac{\partial T_m^s(t)}{\partial t^*} \int_0^{2\pi} \sin n\theta \sin m\theta d\theta \right] + \quad (\text{A.108})$$

$$u^* \sum_{m=1}^{\infty} \left[ -mT_m^c(t) \int_0^{2\pi} \sin n\theta \sin m\theta d\theta + mT_m^s(t) \int_0^{2\pi} \sin n\theta \cos m\theta d\theta \right] = \quad (\text{A.109})$$

$$-Q \left[ \int_0^{2\pi} \sin n\theta \sin \theta d\theta \right] \quad (\text{A.110})$$

$$\frac{\partial}{\partial t^*} T_0^c(t) \left[ \frac{1}{n} \cos n\theta \Big|_0^{2\pi} \right] + \quad (\text{A.111})$$

$$\sum_{m=1}^{\infty} \left[ \frac{\partial T_m^c(t)}{\partial t^*} (0) + \frac{\partial T_m^s(t)}{\partial t^*} \int_0^{2\pi} \sin n\theta \sin m\theta d\theta \right] + \quad (\text{A.112})$$

$$u^* \sum_{m=1}^{\infty} \left[ -mT_m^c(t) \int_0^{2\pi} \sin n\theta \sin m\theta d\theta + mT_m^s(t)(0) \right] = \quad (\text{A.113})$$

$$-Q \left[ \int_0^{2\pi} \sin n\theta \sin \theta d\theta \right] \quad (\text{A.114})$$

$$\frac{\partial}{\partial t^*} T_0^c(t) \left[ (0) \right] + \quad (\text{A.115})$$

$$\sum_{m=1}^{\infty} \left[ (0) + \frac{\partial T_m^s(t)}{\partial t^*} \int_0^{2\pi} \sin n\theta \sin m\theta d\theta \right] + \quad (\text{A.116})$$

$$u^* \sum_{m=1}^{\infty} \left[ -mT_m^c(t) \int_0^{2\pi} \sin n\theta \sin m\theta d\theta + (0) \right] = \quad (\text{A.117})$$

$$-Q \left[ \int_0^{2\pi} \sin n\theta \sin \theta d\theta \right] \quad (\text{A.118})$$

$$\sum_{m=1}^{\infty} \left[ \frac{\partial T_m^s(t)}{\partial t^*} \int_0^{2\pi} \sin n\theta \sin m\theta d\theta \right] + \quad (\text{A.119})$$

$$u^* \sum_{m=1}^{\infty} \left[ -mT_m^c(t) \int_0^{2\pi} \sin n\theta \sin m\theta d\theta \right] = \quad (\text{A.120})$$

$$-Q \left[ \int_0^{2\pi} \sin n\theta \sin \theta d\theta \right] \quad (\text{A.121})$$

$$\sum_{m=2}^{\infty} \left[ \frac{\partial T_m^s(t)}{\partial t^*} (0) \right] + \quad (\text{A.122})$$

$$u^* \sum_{m=2}^{\infty} \left[ -mT_m^c(t)(0) \right] = \quad (\text{A.123})$$

$$-Q \left[ (0) \right] \quad (\text{A.124})$$

$$0 = 0 \quad (\text{A.125})$$

Note the above equation shows that for  $m \neq n$  the term  $T_m^s(t)$  will disappear, the derivation will continue with  $m = n$ .

$$\sum_{m=1}^1 \left[ \frac{\partial T_1^s(t)}{\partial t^*} \int_0^{2\pi} \sin^2 \theta d\theta \right] + \quad (\text{A.126})$$

$$u^* \sum_{m=1}^1 \left[ -mT_1^c(t) \int_0^{2\pi} \sin^2 n\theta d\theta \right] = \quad (\text{A.127})$$

$$-Q \left[ \int_0^{2\pi} \sin^2 n\theta d\theta \right]; n = 1, 2, 3 \quad (\text{A.128})$$

$$\sum_{m=1}^1 \left[ \frac{\partial T_1^s(t)}{\partial t^*} (\pi) \right] + u^* \sum_{m=1}^1 \left[ -T_1^c(t)(\pi) \right] = -Q \left[ (\pi) \right]; n = 1, 2, 3 \quad (\text{A.129})$$

$$\frac{\partial T_1^s(t)}{\partial t^*} - u^* T_1^c(t) = -Q; n = 1, 2, 3; \quad (\text{A.130})$$

Truncate,  $n = 1$ ;

$$\frac{\partial T_1^s(t)}{\partial t^*} = -Q + u^* T_1^c(t) \quad (\text{A.131})$$

$T_1^s(t)$  has been solved for under the condition that the Fourier series expansion will be truncated for  $n = 1$ . These two coefficients and the momentum equation are shown below.

Note that there are now three variables ( $u^*, T_1^c(t), T_1^s(t)$ ) and three non linear differential equations.

## APPENDIX B

### Linear Stability Analysis using the Routh-Hurwitz Stability Criterion

The following provides a detailed derivations between Equations (3.14) - (3.38).

A linear stability analysis on this toroidal thermosyphon with known heat flux was performed by Pacheco-Vega et. al [10]. In thier work, a linear stability curve graph was developed that accurately predicted what type of behavior would result for any given heat input and tilt angle combination. This analysis is outlined below.

A linear stability analysis using the critical points can be performed, starting with the following equations:

$$x(t) = \bar{x} + x'e^{\lambda t}, \quad (\text{B.1})$$

$$y(t) = \bar{y} + y'e^{\lambda t}, \quad (\text{B.2})$$

$$z(t) = \bar{z} + z'e^{\lambda t}, \quad (\text{B.3})$$

with  $x(t), y(t), z(t)$  as the dimensionless variables,  $\bar{x}, \bar{y}, \bar{z}$  as the steady state solutions, and  $x'e^{\lambda t}, y'e^{\lambda t}, z'e^{\lambda t}$  as the perturbations in the system. As described in Sen et. al [28], these perturbations have an amplitude of  $x', y', z'$  and will either grow and decay depending on the value for  $\lambda$ , particularly if it is positive or negative. Further, the stability of the system will depend on if the lambda values are real, imaginary, or a combination of the two as is solved during this section. Taking the derivative of both sides provides the next

set of equations,

$$\frac{dx}{dt} = \lambda x' e^{\lambda t}, \quad (\text{B.4})$$

$$\frac{dy}{dt} = \lambda y' e^{\lambda t}, \quad (\text{B.5})$$

$$\frac{dz}{dt} = \lambda z' e^{\lambda t}. \quad (\text{B.6})$$

The above equations for  $x, y, z$  and  $dx/dt, dy/dt, dz/dt$  can be substituted in to the three governing Eq's, (3.34 - 3.36), shown below:

$$\lambda x' e^{\lambda t} = -[\bar{x} + x' e^{\lambda t}] + [\bar{y} + y' e^{\lambda t}] \cos \alpha - [\bar{z} + z' e^{\lambda t}] \sin \alpha, \quad (\text{B.7})$$

$$\lambda y' e^{\lambda t} = -[\bar{x} + x' e^{\lambda t}][\bar{z} + z' e^{\lambda t}], \quad (\text{B.8})$$

$$\lambda z' e^{\lambda t} = -Q + [\bar{x} + x' e^{\lambda t}][\bar{y} + y' e^{\lambda t}]. \quad (\text{B.9})$$

Note this is a linear analysis and any nonlinear terms will be neglected. For example, the multiplication of  $x'y'$  will result in an infinitesimally small nonlinear terms so it will be neglected in this analysis. After mathematical reductions, these equations simplify to the following:

$$\lambda x' = -x' + y' \cos \alpha - z' \sin \alpha, \quad (\text{B.10})$$

$$\lambda y' = -x' \bar{z} - \bar{x} z', \quad (\text{B.11})$$

$$\lambda z' = +x' \bar{y} + \bar{x} y'. \quad (\text{B.12})$$

Combining the  $x', y', z'$  terms results in the following equations,

$$-(\lambda + 1)x' + (\cos \alpha)y' + (-\sin \alpha)z' = 0, \quad (\text{B.13})$$

$$(\bar{z})x' + (-\lambda)y' + (-\bar{x})z' = 0, \quad (\text{B.14})$$

$$(\bar{y})x' + (\bar{x})y' + (-\lambda)z' = 0. \quad (\text{B.15})$$

These equation can now be put into matrices to combine the eigen values  $\lambda$ ,

$$\begin{bmatrix} -(\lambda + 1) & \cos \alpha & -\sin \alpha \\ \bar{z} & -\lambda & -\bar{x} \\ \bar{y} & \bar{x} & -\lambda \end{bmatrix} \begin{bmatrix} x' \\ y' \\ z' \end{bmatrix} = \begin{bmatrix} 0 \\ 0 \\ 0 \end{bmatrix},$$

$$-(\lambda + 1) \begin{bmatrix} -\lambda & -\bar{x} \\ \bar{x} & -\lambda \end{bmatrix} - (\cos \alpha) \begin{bmatrix} \bar{z} & -\bar{x} \\ \bar{y} & -\lambda \end{bmatrix} + (-\sin \alpha) \begin{bmatrix} \bar{z} & -\lambda \\ \bar{y} & \bar{x} \end{bmatrix} = 0.$$

Combining like terms and simplifying the equations results in the following polynomial,

$$\lambda^3 + \lambda^2 + \lambda(Q \cos \alpha + \sqrt{\frac{Q}{\cos \alpha}} \sin \alpha) + 2Q \cos \alpha = 0. \quad (\text{B.16})$$

Consider using synthetic division on this polynomial to get a root of  $-1$ . To get an exact root, the last term in the division slot must equal 0, shown below,

$$2Q \cos \alpha - Q \cos \alpha - \sqrt{\frac{Q}{\cos \alpha}} = 0, \quad (\text{B.17})$$

$$Q = \frac{\sin^2 \alpha}{\cos^3 \alpha}. \quad (\text{B.18})$$

This means for the initial eigenvalue polynomial to have a root of  $-1$ , the above must be true. The remainder polynomial can be solved as follows:

$$\lambda^2 + Q \cos \alpha + \sqrt{\frac{Q}{\cos \alpha}} \sin \alpha = 0, \quad (\text{B.19})$$

$$Q = \frac{\sin^2 \alpha}{\cos^3 \alpha}, \quad (\text{B.20})$$

$$\lambda^2 + \left(\frac{\sin^2 \alpha}{\cos^3 \alpha}\right) \cos \alpha + \sqrt{\frac{\frac{\sin^2 \alpha}{\cos^3 \alpha}}{\cos \alpha}} \sin \alpha = 0, \quad (\text{B.21})$$

$$\lambda^2 + 2 \frac{\sin^2 \alpha}{\cos^2 \alpha} = 0, \quad (\text{B.22})$$

$$\lambda = \pm \sqrt{2} i \frac{\sin \alpha}{\cos \alpha}, \quad (\text{B.23})$$

$$Q = \frac{\sin^2 \alpha}{\cos^3 \alpha}; \sqrt{Q \cos \alpha} = \frac{\sin \alpha}{\cos \alpha}, \quad (\text{B.24})$$

$$\lambda = \pm \sqrt{2Q \cos \alpha} i. \quad (\text{B.25})$$

This provides three eigen values:  $(-1, +\sqrt{2Q \cos \alpha} i, -\sqrt{2Q \cos \alpha} i)$ . Next, the Routh Stability Criterion can be applied to check for unstable roots and evaluate stability in a control system. The polynomial is first written in the following structure with  $a$  as the coefficients:

$$a_0 s^n + a_1 s^{n-1} + \dots + a_{n-1} s + a_n = 0, \quad (\text{B.26})$$

$$\lambda^3 + \lambda^2 + \lambda \left( Q \cos \alpha + \sqrt{\frac{Q}{\cos \alpha}} \sin \alpha \right) + 2Q \cos \alpha = 0, \quad (\text{B.27})$$

$$a_0 = 1; a_1 = 1; a_2 = Q \cos \alpha + \sqrt{\frac{Q}{\cos \alpha}} \sin \alpha; a_3 = 2Q \cos \alpha. \quad (\text{B.28})$$

If all the coefficients are positive, the following pattern is set up as follows:

$$\begin{array}{ccccccc}
 s^n & a_0 & a_2 & a_4 & \dots & & \\
 s^{n-1} & a_1 & a_3 & a_5 & \dots & & \\
 s^{n-2} & b_1 & b_2 & b_3 & \dots & & \\
 s^{n-3} & c_1 & c_2 & c_3 & \dots & & \cdot \\
 \vdots & \vdots & \vdots & \vdots & & & \\
 s^1 & d_1 & & & & & \\
 s^0 & e_1 & & & & & 
 \end{array}$$

with the applicable coefficients for  $b$  and  $c$  given as:

$$b_1 = \frac{a_1 a_2 - a_0 a_3}{a_1}, \quad (\text{B.29})$$

$$b_2 = \frac{a_1 a_4 - a_0 a_5}{a_1}, \quad (\text{B.30})$$

$$c_1 = \frac{b_1 a_3 - a_1 b_2}{b_1}. \quad (\text{B.31})$$

Using the values for  $a$  coefficients to find the  $b$  and  $c$  coefficients results in the following pattern,

$$\begin{array}{cccc}
 \lambda^3 & 1 & Q \cos \alpha + \sqrt{\frac{Q}{\cos \alpha}} \sin \alpha & 0 \\
 \lambda^2 & 1 & 2Q \cos \alpha & 0 \\
 \lambda^1 & \sqrt{\frac{Q}{\cos \alpha}} \sin \alpha - Q \cos \alpha & 0 & 0 \\
 \lambda^0 & 2Q \cos \alpha & 0 & 0
 \end{array}$$

If the coefficients in the second column are all positive, the system can be considered stable. This provides two conditions that must be considered. The first conditions must

be:

$$\sqrt{\frac{Q}{\cos \alpha}} \sin \alpha - Q \cos \alpha \geq 0, \quad (\text{B.32})$$

$$Q \leq \frac{\sin^2 \alpha}{\cos^3 \alpha}, \quad (\text{B.33})$$

and the second condition must be:

$$2Q \cos \alpha \geq 0, \quad (\text{B.34})$$

$$\cos \alpha \geq 0, \quad (\text{B.35})$$

$$-90^\circ \geq \alpha \geq 90^\circ. \quad (\text{B.36})$$

A final test is to determine if that system is dissipative, meaning, the right hand side of the governing equations diverge to  $-1$ . This is done by using the nabla operator on the governing equations as shown below: These equations are then put into the form of

$$\dot{x} = Ax + b,$$

$$\begin{bmatrix} \dot{x} \\ \dot{y} \\ \dot{z} \end{bmatrix} = \begin{bmatrix} -1 & \cos \alpha & -\sin \alpha \\ 0 & 0 & -x \\ 0 & x & 0 \end{bmatrix} \begin{bmatrix} x \\ y \\ z \end{bmatrix} + \begin{bmatrix} 0 \\ 0 \\ -Q \end{bmatrix}.$$

The nabla operator is then used on the system to determine if the system diverges,

$$\nabla \cdot (Ax + b) = \begin{bmatrix} \frac{\partial}{\partial x} & \frac{\partial}{\partial y} & \frac{\partial}{\partial z} \end{bmatrix} \begin{bmatrix} -x + y \cos \alpha - z \sin \alpha \\ -xz \\ -Q + xy \end{bmatrix}.$$

Expanding the equation results in the following:

$$\nabla \cdot (Ax + b) = \frac{\partial}{\partial x}(-x + y \cos \alpha - z \sin \alpha) + \frac{\partial}{\partial y}(-xz) + \frac{\partial}{\partial z}(-Q + xy) \quad (\text{B.37})$$

$$\nabla \cdot (Ax + b) = (-1 + 0 + 0) + (0) + (0 + 0) \quad (\text{B.38})$$

$$\nabla \cdot (Ax + b) = -1 \quad (\text{B.39})$$

The divergence to -1 indicates that the system is dissipative. The analysis conducted in this section produces a linear stability curve graph that can predict the stability of this system.

Consider the range  $0 < \alpha < 90^\circ$ ,  $P_1$  is stable while  $Q \leq \sin^2 \alpha / \cos^3 \alpha$ , with  $\alpha \geq 0$  [10].

This linear stability curve is shown below in Figure 3.1 and shows the relationship between fluid flow stability, heat input, and tilt angle variables which provides the foundation for developing a control strategy.

## APPENDIX C

### Custom MATLAB Solver for a Three Equation Dynamical System

```
clc;

clear all;

h=0.1;                % step size

t = 0:h:1000;

x = zeros(1,length(t)); % u, dimensionless
y = zeros(1,length(t)); % T*c, dimensionless
z = zeros(1,length(t)); % T*s, dimesnionless

x(1) = 0;             % initial condition
y(1) = 0;             % initial condition
z(1) = 0;             % initial condition

a = 30; %60 58 50 30 % alpha

q = 5;                % heat input, dimensionless

F_txyz = @(t,x,y,z) -x + y*cosd(a) - z*sind(a); % dx/dt
G_txyz = @(t,x,y,z) -x*z;                        % dy/dt
```

```

H_txyz = @(t,x,y,z) -q + x*y;           % dz/dt
for i=1:(length(t)-1)                   % calc loop

    k_1 = F_txyz(t(i),x(i),y(i),z(i));

    L_1 = G_txyz(t(i),x(i),y(i),z(i));

    m_1 = H_txyz(t(i),x(i),y(i),z(i));

    k_2 = F_txyz(t(i)+0.5*h,x(i)+0.5*h*k_1,y(i)+0.5*h*L_1,...
                z(i)+0.5*h*m_1);

    L_2 = G_txyz(t(i)+0.5*h,x(i)+0.5*h*k_1,y(i)+0.5*h*L_1,...
                z(i)+0.5*h*m_1);

    m_2 = H_txyz(t(i)+0.5*h,x(i)+0.5*h*k_1,y(i)+0.5*h*L_1,...
                z(i)+0.5*h*m_1);

    k_3 = F_txyz((t(i)+0.5*h),(x(i)+0.5*h*k_2),...
                (y(i)+0.5*h*L_2),(z(i)+0.5*h*m_2));

    L_3 = G_txyz((t(i)+0.5*h),(x(i)+0.5*h*k_2),...
                (y(i)+0.5*h*L_2),(z(i)+0.5*h*m_2));

    m_3 = H_txyz((t(i)+0.5*h),(x(i)+0.5*h*k_2),...
                (y(i)+0.5*h*L_2),(z(i)+0.5*h*m_2));

    k_4 = F_txyz((t(i)+h),(x(i)+k_3*h),(y(i)+L_3*h),...
                (z(i)+m_3*h));

    L_4 = G_txyz((t(i)+h),(x(i)+k_3*h),(y(i)+L_3*h),...
                (z(i)+m_3*h));

    m_4 = H_txyz((t(i)+h),(x(i)+k_3*h),(y(i)+L_3*h),...
                (z(i)+m_3*h));

```

```

x(i+1) = x(i) + (1/6)*(k_1+2.*k_2+2.*k_3+k_4)*h; % main eq
y(i+1) = y(i) + (1/6)*(L_1+2.*L_2+2.*L_3+L_4)*h; % main eq
z(i+1) = z(i) + (1/6)*(m_1+2.*m_2+2.*m_3+m_4)*h; % main eq

end

xm(a,:) = x;
ym(a,:) = y;
zm(a,:) = z;

x1 = (15/8)*(exp(-5*t)-2*exp(-3*t)+exp(-t));
y1 = (5/2)*(-exp(-5*t)+exp(-3*t));
z1 = exp(-5*t);

```